SUSTAINABLE SELF-HEALING STRUCTURAL COMPOSITES

by

YONGJING WANG

A thesis submitted to the University of Birmingham for the degree of

DOCTOR OF PHILOSOPHY

Department of Mechanical Engineering

School of Engineering

College of Engineering and Physical Sciences

University of Birmingham

September 2016

Abstract

Self-healing composites are composite materials capable of automatic recovery when damaged. They are inspired by biological systems such as the human skin which are naturally able to heal themselves. Over the past two decades, two major self-healing concepts – based respectively on the use of capsules and vascular networks containing healing agents - have been proposed and material property recovery has been enhanced from 60% to nearly 100%. However, this improvement is still not sufficient to allow self-healing composites to be applied in practice because the healing capability varies with many external factors such as ambient temperatures and damage conditions. The key to the practical application of self-healing composites is to promote the sustainability of healing capacity to make the recovery robust.

The thesis presents various techniques to enhance the healing capacity of fibre-reinforced composites to realise strong recovery regardless of ambient temperatures or material types. It presents the effects of various popular configurations of vascular networks on the flexural properties and healing performances of fibre-reinforced composites. The thesis demonstrates a design enabling recovery at ultra-low temperatures by using hollow vascular networks and porous heating elements. It also presents a new healing mechanism to repair the broken structural carbon fibres by incorporating conventional healing agents with short carbon fibres which could be aligned in an *in situ* electric field. The mechanism was also adopted to enable the restoration of the conductivity of a fibre-reinforced composite incorporating a porous conductive element, a carbon nanotube sheet, which could be used as a heating actuator or a sensing

component. Thus, the development reported in this thesis have contributed to promoting the sustainability of the recovery of self-healing composites.

Acknowledgement

First and foremost I want to thank my supervisor Professor Duc Truong Pham. It has been an honour to be his PhD student. He has taught me, both consciously and unconsciously, how good engineering research is done. I appreciate all his contributions of time and efforts to make my PhD experience productive and stimulating. The joy and enthusiasm he has for his research were contagious and motivational for me, even during tough times in the PhD pursuit. I am also thankful for the excellent example he has provided as a successful professor, a visionary leader and a beloved mentor.

The members in the School of Engineering have contributed immensely to my personal and professional time at Birmingham. The school has been a source of friendships as well as good advice and collaboration. I would like to thank Dr Chunqian Ji and Dr Shizhong Su, without whose support the thesis would not have been possible. My gratitude extends to Dr Mozafar Saadat, my primary assessor, who generously offered a lab where I could accomplish a majority of my experimental works. I am especially grateful for my friends who stuck it out with me since undergraduate study: Mrs Linxue Bai, Mr Hao Fu, Mr Mingyu Xie, Mr Da Si, and Mr Zhongbei Tian. I would like to acknowledge many colleagues in the Department of Mechanical Engineering, Mr Hector De la Torre, Ms Sunan Deng, Mr Jun Huang, Mr Junwei Yan, Dr Xiaogeng Jiang, Dr Maojun Li, Dr Alireza Rastegarpanah, and Mr Amir Mohammad Hajiyavand, whose accompany promote my work from being a toneless solo to an exciting rhapsody. I have had the pleasure to work as a postgraduate teaching associate for Dr Haider Butt, Dr Marco Castellani and Dr Andrew Tobias, who gave excellent examples of lecturing and tutoring. I was fortunate to have Mr Peter Thornton, Mr Carl Hingley, Ms Becky Charles, Mr Brian Thomas, Mr Adam Sheward and Mr Pooria Ghavam, engineers at the Department, to help me with building the lab; Ms Silla Winter and Ms Michelle Worrall whose help eased the burden of arranging experiments and purchasing facilities.

I would also like to thank Mr Jake Edgell, Mr Nathaniel Jackson, Mr Nicholas Graham, Mr Jong How Kiat, Mr Jinjun Li, and Mr Hengkun Liang, UG or PG students at the Department of Mechanical Engineering, whose exceptional experimental works provided invaluable data for my research.

The research based on carbon nanotube sheets discussed in this thesis would not have been possible without the generous supply of the material from the group of Professor Jinsong Leng at Harbin Institute of Technology, China, my alma mater. I have appreciated their collaboration and the impressive fabrication skills.

I would like to thank everyone in Westmere, University Graduate School, where a group of great talents have been keeping me inspired; more notably, Dr Eren Bilgen and Dr Francesco Maria Colacino helped to raise my research profile. I would like to acknowledge whoever in the University showed interests in my research. They are the source of motivation during tough times.

I am also grateful to Professor Kyle Jiang at the University of Birmingham, UK; Professor Francesco Jovane at the Politecnico di Milano, Italy; Professor Zude Zhou at Wuhan University of Technology, China; Dr Dongsheng Wang, Professor Jiecai Han, Professor Mufu Yan, Professor Rengeng Wu and Professor Zhongqi Cui at Harbin Institute of Technology, China, for their emotional support and encouragement.

Lastly, I would like to thank my family for all their love and encouragement. For my parents who raised me and supported me, both mentally and financially, in all my pursuits. And most of all for my loving, wise, and patient wife Linxue Bai whose faithful support since the day we first met here in Birmingham five years ago. Thank you.

Yongjing Wang

University of Birmingham

September 2016

Table of Contents

Chapter 1 - Introduction 1
1.1. Background 1
1.2. Aim, objectives and hypotheses 3
1.3. Outline of the thesis 5
Chapter 2 - Literature review 7
2.1. Introduction to self-healing composites 7
2.2. Capsule-based self-healing structures 9
2.2.1. Mechanisms 10
2.2.2. Fabrication processes 14
2.2.3. Mechanical effects 17
2.2.4. Healing performance analysis 17
2.3. Vessel-based self-healing structures 21
2.3.1. Mechanisms 22
2.3.2. Fabrication process 24
2.3.3. Mechanical effects 35
2.3.4. Healing performance analysis 35
2.4. Trends 38
2.4.1. Shift in development focus and new opportunities 38
2.4.2. Comparison of and future trends in capsule-based and vascular structures 43
2.5. Summary 45
Chapter 3 - Effects of vessel configurations on the flexural properties and healing performances of vessel-based self-healing composites: an experimental study 47
3.1. Preliminaries 47
3.2. Methodology 48
3.2.1. General framework for experiment 48
3.2.2. Definition 49
3.2.3. Fabrication of samples 51
3.2.4. Experimental procedures 52
3.2.5. Assessment methods 53
3.3. Results and discussion 54
3.3.1. Effects of vessel configurations on the flexural properties 54

3.3.2. Effects of network configurations on healing performances. 60
3.3.3. Effects of bending levels on healing performances 62
3.4. Summary 65
Chapter 4 - Sustainable self-healing at ultra-low temperatures in structural composites incorporating hollow vessels and heating elements 67
4.1. Preliminaries 67
4.2. Methods 68
4.2.1. Structure of the composite 68
4.2.2. Fabrication procedure 71
4.2.3. Healing performance assessment and analysis 73
4.2.4. Effects of the conductive sheets on interlaminar properties 75
4.2.5. Double cantilever beam (DCB) test 75
4.2.6. Effects of the conductive sheets on tensile properties 76
4.3. Results and discussion 78
4.3.1. De-icing performance 78
4.3.2. Healing performance 79
4.3.3. Effects of conductive sheets on interlaminar properties 83
4.3.4. Effects of carbon nanotube sheets on tensile properties 84
4.4. Summary 86
Chapter 5 - Towards autonomous restoration of structural carbon fibres in polymer composites using vascular systems and electric alignment 88
5.1. Preliminaries 88
5.2. Methodology 89
5.2.1. Healing mechanism 89
5.2.2. Investigated variables and parameters 91
5.2.3. Fabrication of samples 92
5.2.4. Healing agent composition and synthesis 93
5.2.5. Experimental procedure 93
5.2.6. Healing performance/efficiency 95
5.3. Results and discussion 96
5.3.1. 3.1 Parameters tested 96

5.3.2. Modelling and verifying the effect of electric alignment and additive short fibres on restored strength 97
5.3.3. Effects of electric field intensity on restored strength 101
5.3.4. Investigating the effect of short carbon fibre %wt. on restored strength 102
5.3.5. Investigating the effect of short carbon fibre length/quality on restored strength 104
5.3.6. Investigating the effect of adding dispersant to the healing agent 105
5.3.7. Implementation of a vascular self-healing system 107
5.4. Summary 109
Chapter 6 - Towards autonomous restoration of the electrical conductivity of a polymer composite incorporating a carbon nanotube sheet 110
6.1. Preliminaries 110
6.2. Methodology 112
6.2.1. Healing mechanism 112
6.2.2. Sample fabrication 113
6.2.3. Testing method and procedure 115
6.3. Results and discussion 117
6.3.1. Effect of SCF content on healing performance 117
6.3.2. Effects of electric field intensity/type on healing performance 119
6.3.3. Alternative circuit for alignment method 121
6.3.4. Investigating the effect of silver paste 123
6.3.5. Addition of dispersant to the healing agent 125
6.4. Summary 127
Chapter 7 - Conclusions, contributions and future work 129
7.1. Conclusions 129
7.2. Contributions 132
7.3. Future work 133
References 134

List of Illustrations

Figure 1.1. Schematics of self-healing composites incorporating microcapsules or microvessels [1]. 1
Figure 1.2. Number of academic publications between January 2001 and August 2016 (based on Google Scholar). 2
Figure 1.3. Relationships between aim, objectives and hypotheses. Objective 1 and Hypothesis 1 support the work on healing at low temperatures (Objective 2 and Hypothesis 2) and healing of different materials (Objectives 3 and 4 and Hypotheses 3 and 4) which is aimed at achieving sustainable self-healing. 5
Figure 2.1. Self-healing material examples [8][9]. 7
Figure 2.2. Prototype of capsule-based self-healing composite [2]. 10
Figure 2.3. SEM images of (a) traditional, (b) SWCNT-modified, and (c) nano-alumina-modified microcapsules; wall thicknesses of (d) traditional and (e) modified microcapsules [68]. 16
Figure 2.4. Polymers embedded with hollow fibres containing healing agent [99]. (a, b) Laminating stacking sequence of hollow fibres and reinforcement fibres; (c, d) Outflow of healing agents. 25
Figure 2.5. Fabrication of Scaffolds. (a) 3D printing using nozzles [112]; (b) 3D printing of a bio-mimicking pattern [117]; (c) Self-propagated photopolymer [122]; (d) Fabricated metal interconnected vascular network based on photopolymer [123]. 28
Figure 2.6. Vascular network formed in gelatin by using sacrificial melt-spun shellac fibres [129]. 30
Figure 2.7. Decomposition of PLA fibre [130]. 30
Figure 2.8. Soft lithography for building microfluidics devices [132] 32
Figure 2.9. Replication of a leaf venation [133] 32
Figure 2.10. Electrostatic discharge to fabricate vascular patterns [135]. 33
Figure 2.11. The concept of sustainable self-healing 39
Figure 2.12. Healing potential for multi-cycle healing [107] 44
Figure 3.1. Role of Chapter 3 in the thesis (red area) 48
Figure 3.2. A schematic of S0, an eight-layer glass fibre laminates 50
Figure 3.3. Vessel configurations in S1, S2 and S3 50

Figure 3.4. Fabricated samples. a) Top view of samples; b) cross-section image of a vessel.....52
Figure 3.5. (a) Displacement-load curves; (b) Peak stress 55
Figure 3.6. Transmitting light photography.....57
Figure 3.7. Dark spot on S0 58
Figure 3.8. Dark spot on S1.1 is delamination and debonding on the compression surface 58
Figure 3.9. A combination of debonding and fracture of structural fibres on the compression surface of S2. 59
Figure 3.10. Optical micrograph of damaged specimen after flexure tests 59
Figure 3.11. Healing performances of composites embedded with different vessel configurations. (a) Peak stress; (b) Flexural modulus; (c) Healing efficiency. 61
Figure 3.12. Healed samples under optical microscope 62
Figure 3.13. Healing performances of composites endured different damaged conditions. Bending conditions: (a) 22 mm; (b) 26 mm; (c) 30 mm; (d) 34 mm. 63
Figure 3.14. Healed samples under an optical microscope. (a) Transverse microcracks; (b) Outflowed healing agents from transverse microcracks; (c) Healing of delamination and cracks on the surface; (d) Cross section of a phase-two damaged laminate; (e) Cross section of a phase-three damaged laminate; (f) Top of a phase-three damaged laminate. 64
Figure 4.1. Role of Chapter 4 in the thesis (red area).....68
Figure 4.2. (a) Internal structure of the composites; (b) Damage-bleeding-healing process 70
Figure 4.3. a) Porous copper foam sheet; b) Porous carbon nanotube sheet. 71
Figure 4.4. (a) DCB test of a healed composite specimen incorporating CNS; (b) Composites incorporating CNS and CFS; (c) Fibre-reinforced composite incorporating wave-like micro vessels after DCB test. 74
Figure 4.5. a) Schematic of composite E; b) Schematic of composite C; c) CNT porous sheet; d) Random-discontinuous cotton fibres and CNT sheet; e) Woven carbon fibres and CNT sheet.....77

Figure 4.6. (a) Temperature of the specimen as a function of time and applied voltage; (b) Thermal distribution in the composite heated by CNS in an ultra-low temperature chamber; (c) De-icing of composite with CNS. 79
Figure 4.7. (a) Healing efficiency of composite with and without the conductive layer; (b) Displacement-load curve for a typical sample incorporating CNS. 81
Figure 4.8. Mode I load vs. displacement curve for the laminates with (a) no embedment, (b) a copper foam sheet and (c) a carbon nanotube sheet. Results of DCB testing: (d) fracture energy and (e) peak load. 84
Figure 4.9. Tensile properties of composites with and without carbon nanotube sheets. ..85
Figure 4.10. SEM images of carbon fibre composite incorporating carbon nanotube sheets after tensile tests. SEM image of crack in carbon fibre-reinforced composite incorporating carbon nanotube sheet. a,b) Cross section of a damaged sample; c-e) Delamination of carbon fibres and matrix; f,g) Delamination of carbon nanotube sheet and matrix 86
Figure 5.1. Role of Chapter 5 in the thesis (red area).....89
Figure 5.2. Schematic of the recovery of structural carbon fibres 90
Figure 5.3. Fabrication procedure.....93
Figure 5.4. Topside view of an undamaged (top), damaged (middle) and healed (bottom) specimen. 94
Figure 5.5. An underside view of a damaged (left) and a healed (right) vessel specimen. 95
Figure 5.6. Reconnection of a bundle of fractured carbon fibres 96
Figure 5.7. The effect of SCF addition & alignment 100
Figure 5.8. The effect of voltage on alignment.....101
Figure 5.9. The effect of SCF %wt.....103
Figure 5.10. The effect of changing fibre length/quality 105
Figure 5.11. The effect of adding dispersant to the healing agent 106
Figure 5.12. Comparison of the restored strength of samples with and without using the new healing mechanism 108
Figure 6.1. Role of Chapter 6 in the thesis (red area).....111
Figure 6.2. Schematic of the restoration of a carbon nanotube sheet.....112
Figure 6.3. Fabrication process 115
Figure 6.4. (a) Top view of a specimen; (b) Bottom view of a specimen.....115
Figure 6.5. Experimental procedure.....115

Figure 6.6. Average results for each wt.% 118
Figure 6.7. The averaged results for the samples tested at varying voltages 120
Figure 6.8. Alternative circuit adopted to avoid over heat 122
Figure 6.9. Average results for the two different circuits 123
Figure 6.10. Results for the averages from silver paste experiments 125
Figure 6.11. a) Individual recovery of samples; b) Averaged recovery results 126
Figure 6.12. (a) shows the original undamaged sample, (b) shows the sample being cut, losing its conductivity, (c) shows the sample release HA from vessels, and (d) shows the sample restore its conductivity after 24 hours as SCFs being aligned in an electric field to reconnect the broken CNS 127

List of Abbreviations and Symbols

ATRP: Atom transfer radical polymerisation

CFRC: Carbon fibre-reinforced composites

CFS: Copper foam sheet

CNS: Carbon nanotube sheet

DBTL: Di-n-butyltin dilaurate

DCPD: Dicyclopentadiene

ENB: 5-ethylidene-2-norbornene

FBG: Fibre Bragg Gratings

GFRC: glass fibre-reinforced composite

HA: Healing agent

HOPDMS: Hydroxyl end-functionalised poly (dimethylsiloxane)

MMA: Methylmethacrylate

MUF: Melamine-urea-formaldehyde

PDES: Poly (diethoxy siloxane)

PDMS: Poly (dimethylsiloxane)

PLA: Poly (lactic acid)

PMF: Poly (melamine formaldehyde)

PMMA: Poly (methyl methacrylate)

PUF: Poly (urea formaldehyde)

ROMP: Ring-opening metathesis polymerisation

SCF: Short carbon fibre

SH: Self-healing

VaSC: Vaporisation of Sacrificial Components

WCl_6: Tungsten chloride

Chapter 1 - Introduction

1.1. Background

Self-healing composite materials are artificial materials that can heal after damage. They were originally inspired by the healing processes in natural biological systems. A popular method to make self-healing composites is to incorporate into the host material microcapsules or microvessels filled with a healing agent capable of repairing cracks. When damage to the material causes the capsules or vessels to be ruptured, the healing agent is released to seal the crack, as shown in **Fig. 1.1**. Self-healing composite materials can potentially be employed to make critical systems such as aircraft, satellites and off-shore structures.

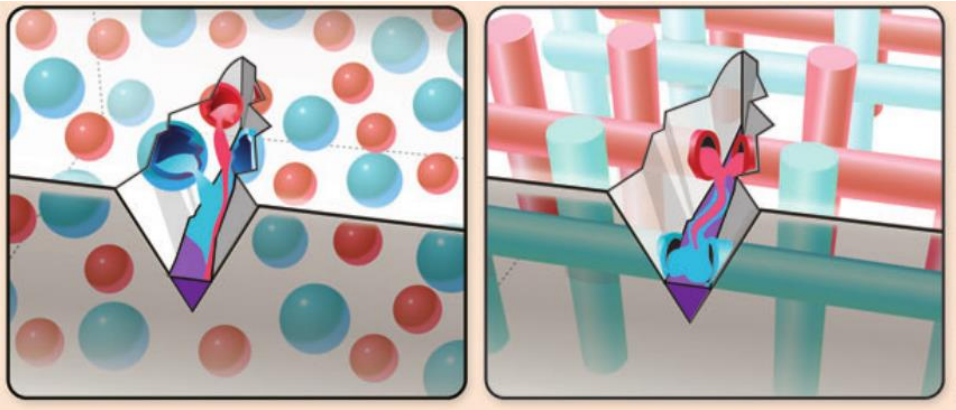

Figure 1.1. Schematics of self-healing composites incorporating microcapsules or microvessels [1].

In the past two decades, developments in self-healing materials have enabled some of the challenging areas within self-healing materials to be overcome. When self-healing materials were first proposed, the reported percentage of recovery was only 60% after a 48h curing period [2]. Nowadays, the recovery has been raised to near 100% and even

over 100% as can be seen in many academic review papers [3], [4]. The time required for curing has also decreased from 48 h to a few seconds due to the employment of newly synthesised healing agents [5]. The vessel-based design enables the refilling of healing agents so that recovery from large-scale damage [6] and multi-cycle damage [7] becomes possible. **Fig. 1.2** presents the number of academic articles (indexed by Google Scholar) published each year starting from 2001, indicating a strong growth in the research intensity in the field.

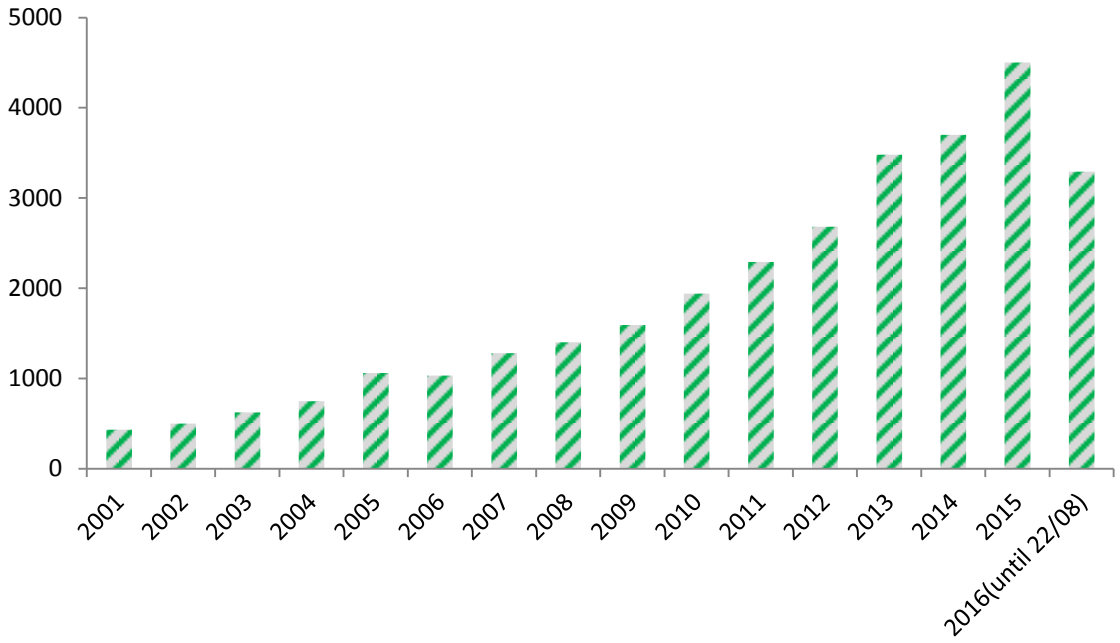

Figure 1.2. Number of academic publications between January 2001 and August 2016 (based on Google Scholar).

However, self-healing composite materials are not yet applicable in practice. The most significant barrier is inconsistent healing performance. For example, damage to fibre-reinforced composites, which are widely adopted in critical systems such as airplanes and satellites, is of two general types: debonding and fracture of structural fibres. Established self-healing mechanisms can cure debonding, as it is the fracture of the matrix, which

could be repaired by polymer healing agents. However, when fracture of structural fibres is the primary type of damage, established healing agents are no longer effective. Also, in almost all studies where strong recovery was achieved, good conditions for the healing processes such as suitably high temperatures were adopted. However, such conditions are not realistic in practice. For example, airplanes need to endure temperatures as low as -60 ºC, at which almost all healing agents would be frozen and cannot be activated. Therefore, the key to the practical application of self-healing composites is the sustainability of healing capacity, which is discussed in **Chapter 2**.

1.2. Aim, objectives and hypotheses

The aim of the research was to promote the sustainability of healing capacity by developing novel healing mechanisms or new composite structures so that strong recovery is achievable regardless of ambient conditions and material types. Fibre-reinforced composites will be the main study objects, but similar designs can be applied to other host materials.

The objectives of the research are structured as follows:

Objective 1 (OBJ. 1). Investigate popular vessel configurations to reveal the effects of vessel configurations on healing performances and flexural properties of host materials.

Objective 2 (OBJ. 2). Propose and verify a new design to enable sustainable self-healing at ultra-low temperatures.

Objective 3 (OBJ. 3). Propose and verify a new healing mechanism to enable the recovery of structural carbon fibres.

Objective 4 (OBJ. 4). Propose and verify a new healing mechanism to enable the recovery of conductive elements.

The above objectives will be achieved if the following hypotheses hold:

Hypothesis 1 (HO. 1). Healing performance and flexural properties can be altered by using various vessel configurations because the coverage of vessels and the volumes of voids introduced are different.

Hypothesis 2 (HO. 2). Materials are able to recover at ultra-low temperatures if they can generate heat internally to maintain their temperatures in a range where healing agents are active.

Hypothesis 3 (HO. 3). Broken structural carbon fibres could be repaired if short carbon fibres could be delivered to the crack and be aligned autonomously to reconnect the broken fibres.

Hypothesis 4 (HO. 4). Fractured conductive elements could be repaired if suitable conductive particles could be delivered to the crack and be aligned autonomously in the gap to reconnect the conductive elements.

The relationships between objectives, hypotheses and the overall aim are shown in **Fig. 1.3**

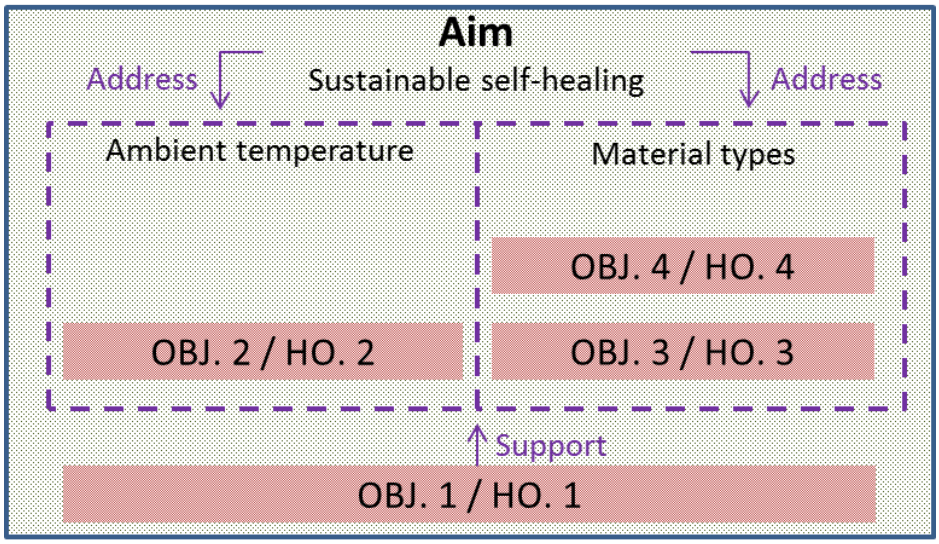

Figure 1.3. Relationships between aim, objectives and hypotheses. Objective 1 and Hypothesis 1 support the work on healing at low temperatures (Objective 2 and Hypothesis 2) and healing of different materials (Objectives 3 and 4 and Hypotheses 3 and 4) which is aimed at achieving sustainable self-healing.

1.3. Outline of the thesis

Chapter 1 presents a general introduction to self-healing composites and highlights key barriers in practice. The aim and objectives of the project are given and explained.

Chapter 2 gives a detailed literature review on self-healing composite materials, in which established healing mechanisms and fabrication techniques are summarised. The concept of sustainable self-healing is proposed and its importance explained.

Chapter 3 reports on an experimental investigation into the effects of vessel configurations on the healing performance and flexural properties of fibre-reinforced composites. The results obtained indicate that, when the composites are designed using a correct vessel configuration, the vessels only have a minor effect on the flexural properties, and more than 100% healing efficiency is achievable. Otherwise, the healing efficiency can

be very poor. Thus, in this study, **Objective 1** is accomplished and **Hypothesis 1** is verified. The results of the study are used to guide the research reported in **Chapters 4-6**.

Chapter 4 presents a new self-healing material incorporating vascular networks and heating elements so that sustainable self-healing at temperatures as low as -60 ºC can be achieved. The effects of the heating element on the interlaminar and tensile properties are experimentally investigated. In this work, **Objective 2** is accomplished and **Hypothesis 2** is verified.

Chapter 5 describes a carbon fibre composite that can repair its structural fibres and restore its mechanical properties after it has been subjected to damage by using an embedded vascular self-healing system. Damage is healed through the application of an epoxy-based resin containing short carbon fibres that can reconnect the fractured carbon fibres upon electric alignment and curing. In this study, **Objective 3** is accomplished and **Hypothesis 3** is verified.

Chapter 6 presents a polymer composite incorporating a carbon nanotube sheet (CNS) as a conductive element. The composite can inherently restore its electrical conductivity after damage. Hollow vessels are embedded in the composite to deliver a healing agent containing short carbon fibres (SCFs) to the damaged areas to repair broken CNS. Experimental results demonstrate that an average recovery of 54% is achievable, and recovery as high as 100% has been observed. **Objective 4** is accomplished and **Hypothesis 4** is verified in this work.

Chapter 7 summarises the conclusions and contributions of the research and suggests directions for further work.

Chapter 2 - Literature review

2.1. Introduction to self-healing composites

For centuries, man has been searching for and creating tougher and more durable structural materials. However, from the perspective of other natural creatures, protection and defence are not fulfilled only by their hard coats or shells, but also adaptively as in the healing of the human skin and the regeneration of the lizard's tail. Inspired by this design, intelligent material systems defined as self-healing composites have been developed. Two examples are shown in **Fig. 2.1**. The left picture presents a specimen recovered from a puncture by delivering healing agents to the crack through microvessels. The right picture shows the 'bleeding' in a sample incorporating microcapsules. The crack causes the microcapsules to burst to release the healing agents. They are capable of automatic recovery and adaptation to environmental changes in a dynamic manner, unlike traditional tough and static composites. Through self-healing, it is expected that safety and reliability will improve, the cost of maintaining artificial composites will decrease and material life will be extended. This area has rapidly developed for near two decades and seen a number of significant achievements.

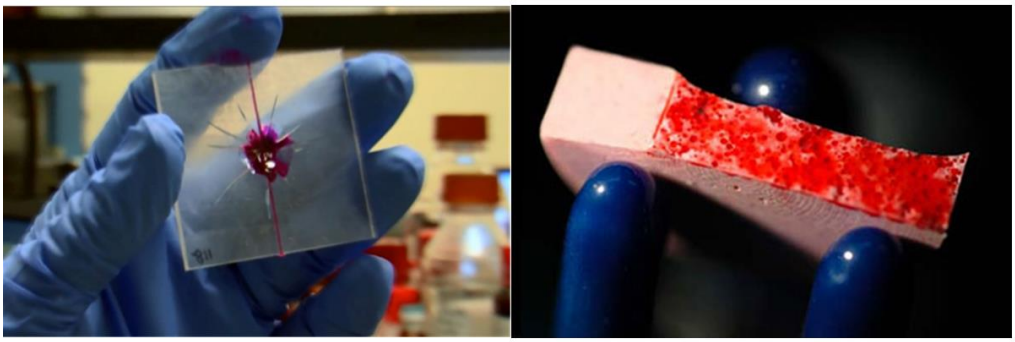

Figure 2.1. Self-healing material examples [8][9].

Current self-healing composites can be categorised into three groups: capsule-based, vessel-based and intrinsic self-healing materials [3], [10]. In capsule-based self-healing materials, small capsules containing a liquid able to fill and close cracks are embedded under the material surface. When the material is damaged, cracks cause some capsules to rupture, releasing the liquid and closing the gap. For vessel-based self-healing materials, the capsules are replaced by a vascular structure similar to a tunnel network, in which various functional liquids flow. These functional liquids will also fill the gap when a crack occurs and breaks the vascular network. The material contained inside a capsule or a vascular network is called a healing agent. The mechanism and behaviour of healing agents are fundamental to the recovery process and restoration of mechanical properties. Intrinsic self-healing materials heal through inherent reversibility of chemical or physical bonding instead of structure design [11], such as the swelling of shape memory polymers [12], the melting and solidification of thermoplastic materials [13], and increasing viscosities of pH-sensitive micro-gels [14]. Consequently, the healing mechanisms of intrinsic self-healing materials are fundamentally different from those of capsule-based and vessel-based self-healing composites.

Since the first review of self-healing materials in 2007 [15], a number of articles have summarised and analysed this field [3], [4], [10], [16]–[26]. A gap has emerged between capsule-based/vascular self-healing composites and intrinsic self-healing materials in recent years. For capsule-based/vascular designs, research is generally focused on not only healing agents, but also the rupture process, mixing process and microstructure fabrication techniques. In comparison, most research about intrinsic self-healing composites still concentrates on developing new healing mechanisms to achieve higher healing strength. This is because for both capsule-based and vascular designs, not

only healing mechanisms, but also structural factors (e.g. size, shape and pattern) and dynamic factors (e.g. flow, pressure and mixing) have significant effects on healing performance. On the other hand, for intrinsic self-healing materials, the healing mechanism is purely the reversibility of the material itself. Moreover, in capsule-based/vascular self-healing composites, the development focus has shifted from healing strength to the sustainability of healing capacity.

This chapter reviews the development of self-healing materials, especially that of self-healing composite structures. The healing and mechanical performances of the established self-healing composites are discussed, as well as related fabrication techniques. For clarity, the chapter concentrates on polymer materials, but similar concepts can also be applied to other material systems, such as concrete and ceramics.

The remainder of the chapter is organised as follows. Mechanisms, fabrication methods, mechanical effects and healing performance for capsule-based and vascular self-healing composites are reviewed in **Section 2.2** and **Section 2.3** respectively. **Section 2.4** analyses historical and future trends in self-healing composite systems, highlighting key barriers and potential solutions. Finally, a brief summary is given in **Section 2.5**.

2.2. Capsule-based self-healing structures

In the natural biological world, the unit that carries out self-healing is the cell, in which different liquids accomplish specific functions. Inspired by this design, small artificial capsules capable of bridging gaps when a crack occurs have been developed using encapsulation techniques, as shown in **Fig. 2.2**.

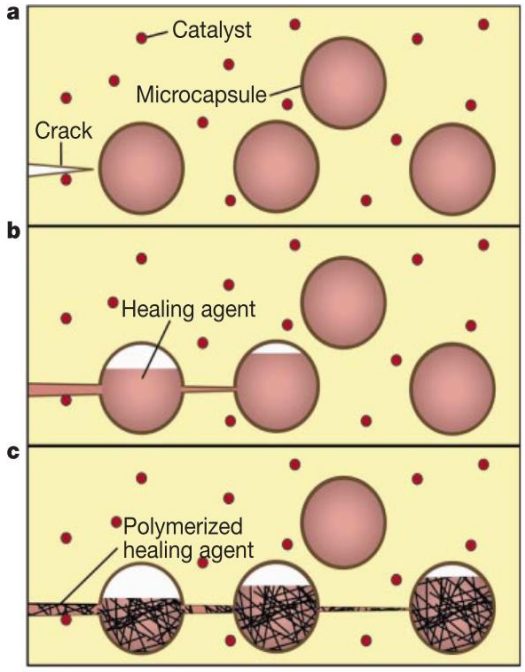

Figure 2.2. Prototype of capsule-based self-healing composite [2].

2.2.1. Mechanisms

I. Ring-Opening Metathesis Polymerisation (ROMP)

The University of Illinois at Urbana-Champaign presented a prototype capsule-based self-healing material [2]. In the prototype, cell-like capsules containing dicyclopentadiene (DCPD) and Grubbs' catalyst were dispersed in a polymer matrix during material formulation. When the material is damaged and a crack occurs, the healing agent contained in the capsules will be released due to the fracture of the poly (urea-formaldehyde) (PUF) capsule shell. The healing agent floods the crack and clots under the ring-opening metathesis polymerisation (ROMP) of DCPD catalysed by Grubbs' catalyst. ROMP is a chain growth polymerisation process where a mixture of cyclic olefin is converted to a polymeric material by opening the strained rings in monomers and reconnecting them to form long chains. As a result, almost 75% toughness can be

recovered in 48 hours at room temperature. This technology was later applied to fibre-reinforced composites to produce self-healing fibre-reinforced composites by curing the host material that contained the healing-agent-filled capsules. Kessler *et al*. developed capsules loaded with DCPD and embedded inside fibre-reinforced composites to repair delamination and extend material life [27], [28] and Brown *et al*. also used the same method to heal fatigue cracks in fibre-reinforced composites [29]. In addition to mixing the capsules with host materials, Blaiszik *et al*.[30] and Jones *et al*. [31], [32] described the integration of capsules onto surfaces of reinforcement fibres thus enabling healing of interfacial bonding between the fibres and the matrix.

Capsule-based self-healing materials can be improved in a number of respects, among which the healing mechanism is the most fundamental. In the case of capsule-based materials, this means using more advanced healing agents. For DCPD and Grubbs' catalyst, there are several drawbacks. The stability of Grubbs' catalyst is weak because of its low melting point at 153 ^{0}C [33] and its reactivity is also influenced by prolonged exposure to oxygen and moisture [34]. Additionally, its application is also limited by its toxicity and high price [35]. As for DCPD, it also has a low melting point and requires large amounts of catalysts for rapid reaction [36]. To increase the stability of the healing process, Kamsphaus *et al*. [33] tested tungsten chloride (WCl_6) as an alternative ROMP catalyst because of its relatively high melting point at 275 ^{0}C and lower cost at the same time. In another work [37], the DCPD healing agent was replaced by the cost-effective material 5-ethylidene-2-norbornene (ENB) which is known for much faster ROMP reaction. However, the main disadvantage of ENB is that the formed crossed-link structure is less strong than the polymerised linear chain structure created by using DCPD [36]. To produce a balanced result, Liu *et al*.[38] introduced a blending plan in which DCPD and ENB were both

encapsulated, as DCPD reactivity built tough and reliable bonds and ENB reactivity provided immediate aid. Afterwards, Huang *et al*. [39] tested a number of the factors including blend ratio, healing temperature and healing time that affected healing performance and proposed an improved blending plan.

Other kinds of catalysts were also taken into consideration [40], such as Grubbs' second-generation catalyst, Hoveyda–Grubbs' first generation catalyst, and Hoveyda–Grubbs' second generation catalyst. These new catalysts allow a cure temperature up to 170 ^{0}C without becoming deactivated and showed high levels of healing efficiency. The establishment of alternative healing agents and catalysts provides more options in the application of ROMP-reaction-based self-healing materials when higher operating temperatures and lower costs are required.

II. Polycondensation

Polycondensation is a chemical condensation to formulate a polymer by linking single or multiple kinds of monomers to form long chains and releasing water or a similar simple substance. Cho *et al*. [41] developed a polycondensation-based mechanism by using di-n-butyltin dilaurate (DBTL) as the catalyst and a mixture of hydroxyl end-functionalised poly(dimethylsiloxane) (HOPDMS) and poly(diethoxy siloxane) (PDES) as the healing agent. The new mechanism had a lower efficiency compared to that of DCPD and Grubbs' catalyst. However, it is more resistant to deactivation by air, water and the vinyl ester matrix and has a lower cost, expanding its application fields and making it more suitable for real use [35]. Self-healing coatings [42] and woven fibre reinforced composites [43] had been developed based on this mechanism and it was claimed that the healing efficiency had been increased to achieve a nearly full recovery.

III. Epoxy-based system

Epoxy-based healing reactions have gained popularity in recent years. In an epoxy-hardener system the epoxy resin and hardener are separately encapsulated and embedded inside the composite matrix. When a crack occurs, both kinds of capsules rupture and the outflowing epoxy resin and hardener are mixed to heal the crack [34], [44]–[47]. In addition, solvent and epoxy-solvent capsule healing systems were also developed for polymer composites [48]–[50]. When the encapsulated solvent is released, it locally swells and entangles the matrix across the plane and heals the crack. Epoxy resin can also be added into capsules with solvent, promoting crosslinking reaction. Epoxy-based mechanisms have become the most popular compared to ROMP-reaction-based and polycondensation-based mechanisms as they are easily accessible. Capsules containing different kinds of amines for anti-corrosion of steel sheets were developed by Choi *et al*. [51]. The characterisation for epoxy-based coating healing performance was analysed and summarised by Liao *et al*. [52] and Liu *et al*. [53]. More information about epoxy-amine mechanisms for self-healing can be found in the reviews by Zhang *et al*. [54], [55].

IV. Others

In addition to polymeric composites, capsule-based structures have been adopted in other areas such as construction [56], [57]. Dry *et al*. [58] made use of cylindrical glass capsules filled with cyanoacrylate to heal cracks in concrete and a two-part epoxy system was also used in self-healing cementitious composite materials [59]. Related research to increase the stability of bitumen [60] has also evolved to a very detailed level. More information can be found in the review by Van Tittelboom *et al*. [61].

2.2.2. Fabrication processes

Fabrication of capsule-based self-healing composites normally involves two processes: encapsulation of healing agents and integration of capsules with matrix materials. Existing encapsulation techniques, which have already been widely employed in the food industry and medical applications, can also be used for the encapsulation of healing agents.

Currently, *in situ* polymerisation in an oil-in-water emulsion is the most popular and effective method for developing capsules containing healing agents. With this method, the polymerisation of shell monomers is carried out on the surface of core materials. In the work of Brown *et al*. [62], poly (urea-formaldehyde) (PUF) was used as shell material to encapsulate DCPD healing agents and the process of *in situ* polymerisation in an oil-in-water emulsion was presented in their paper in a very clear and detailed fashion. Liu *et al*. [63] followed a similar method to encapsulate ENB using melamine-urea-formaldehyde (MUF) as shell materials. For two-part epoxy, PUF [45], [48] Poly (melamine-formaldehyde) (PMF) [46] and Poly (methyl-methacrylate) (PMMA) [64], [65] have all been used to build shell walls by different groups around the world. During *in situ* polymerisation in an oil-in-water emulsion, agitation is critical to the size of capsules and the size of the produced capsules follows a Gaussian distribution. Zuev *et al*. [66] presented a statistical analysis of the size of the produced capsules. For smaller capsules, Blaiszik *et al*. [67] used ultra-sonication to assist nano-capsule generation and created nano-capsules with a diameter as small as 220 nm. In addition, shell materials for capsules can be incorporated with nanoparticles to improve capsule quality. Fereidoon *et al*. [68] improved the morphology, thermal properties and water resistance of microcapsules by introducing either single-walled carbon nanotubes or aluminium oxide nanoparticles into the wall material, UF resin,

as shown in **Fig. 2.3**. The microcapsules were synthesised via *in situ* polymerisation in an oil-in-water emulsion. After the emulsion had stabilised, formaldehyde mixed with the particles were added to the emulsion, which was then heated, cooled, rinsed, filtered and dried in sequence to produce the new capsules. Test results proved that the introduction of nanoparticles to the shell wall could reduce the surface roughness and size of the microcapsules, and the thermal stability was also improved. Yang *et al*. developed microcapsules loaded with ethyl phenylacetate (EPA) and the PU/PMF shell walls were incorporated with silica nanoparticle [69]. SiO_2 nanoparticles can be absorbed at the interface between oil and water to stabilise the emulsions, and the size of the produced microcapsules can be altered depending on the concentration of SiO_2 nanoparticles [69]. The shell made of hybrid materials makes a rough exterior surface for capsules and promote their thermal conductivities and dispersion stability.

In addition, other encapsulation techniques have also been employed to fabricate capsule-based self-healing materials to suit various material properties such as solubility and viscosity. Rule *et al*. [70] encapsulated Grubbs' catalyst with wax shell by rapidly cooling hot and stirred wax mixed with the catalyst. Cho *et al*. [41] and McIlroy *et al*. [71] used interfacial polymerisation to encapsulate DBTL and amine for epoxy-based self-healing systems. Chen *et al*. [72] described the self-assembly phenomenon of Poly (acrylate amide) shells, containing Polystyrene as core under the principle of atom transfer radical polymerisation (ATRP). Zhang *et al*. [73], [74] created a fabrication method to build etched glass bubbles as healing agent containers as they would be more brittle and easy to rupture, by using diluted hydrofluoric acid in a specially designed mixer. Furthermore, the shell can also be formed of more than one kind of materials. Jin *et al*. [75] developed a two-layer capsule shell so that the thermal stability of the capsule can be improved without

influencing the rupture performance. More information about encapsulation techniques can be found in the work of Jyothi *et al*. [76].

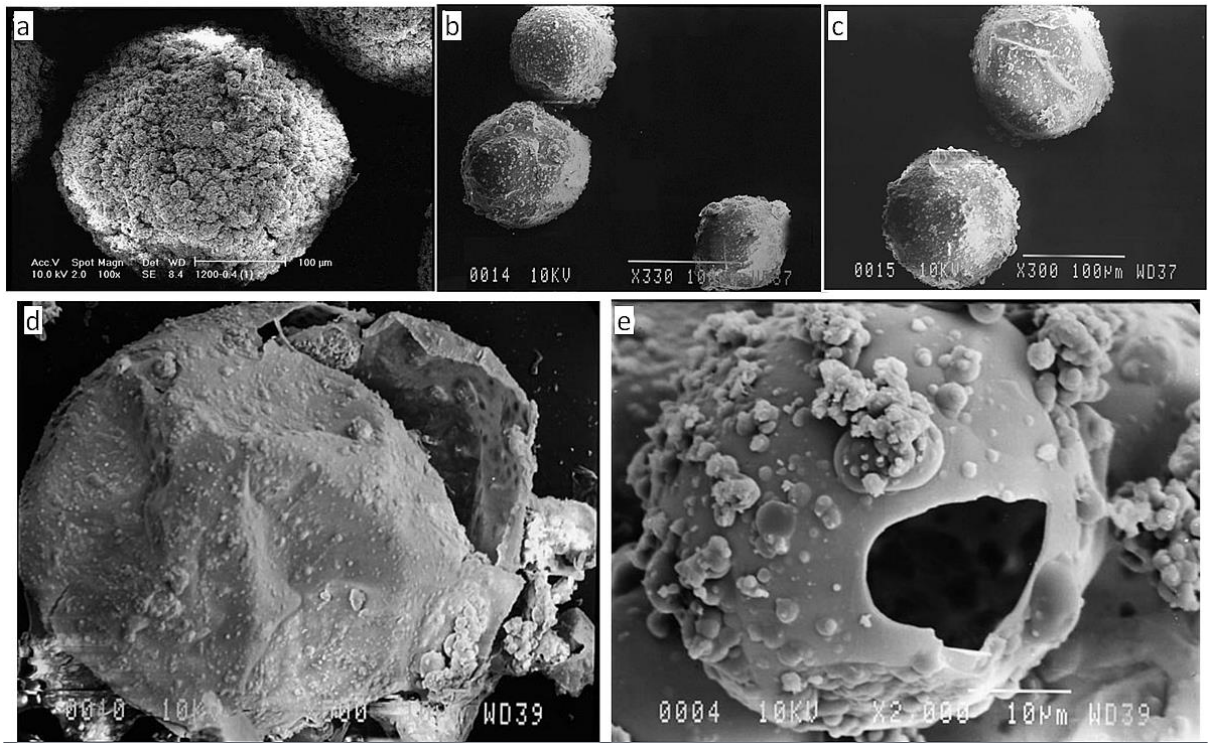

Figure 2.3. SEM images of (a) traditional, (b) SWCNT-modified, and (c) nano-alumina-modified microcapsules; wall thicknesses of (d) traditional and (e) modified microcapsules [68].

The integration of capsules into matrix materials is another process that affects the healing quality. Sometimes, when a capsule-based material cracks, the capsules simply detach from the matrix material instead of rupturing, resulting in no healing agent outflows. Most of the recent investigations into unsatisfactory releasing of healing agents tend to investigate the influence of the encapsulation process on the quality of the capsules and the triggering of the release of healing agents. However, integration techniques and

integration quality, especially mechanical properties of the interface between shells and matrix materials, are yet to be systematically studied.

2.2.3. Mechanical effects

Several researchers have investigated the influence of capsules on the overall mechanical properties. Zhang *et al*. [77] tested glass fibre-reinforced composite with embedded capsules and concluded that the tensile strength and elastic modulus would decrease. The fracture toughness of epoxy embedded with capsules containing DCPD was found to increase compared to that of pure epoxy [78]. However, for epoxy adhesives, the fracture toughness is reduced by the addition of capsules [79]. The size of the capsules also has effects on the fracture toughness of FRC and the interlaminar fracture toughness is higher with a smaller capsule size [80]. Regarding the effects of different kinds of capsules, it was demonstrated numerically that the carrying capacity almost unrelated to Young's modulus of the microcapsules [81]. Also, the microcapsule shell wall material did not play any significant role in defining the mechanical properties of the composites [82].

2.2.4. Healing performance analysis

A summary of the main capsule-based self-healing materials and their healing performances is shown in **Table 2.1**. It is worth noting that a particular healing performance cannot be guaranteed even if the same mechanism and healing conditions are adopted due to differences in application areas, host material properties and manufacturing techniques. The point of the table is to describe the range of possible

outcomes that may be achieved by using a certain mechanism, and to provide a general idea of the potential of capsule-based self-healing composites.

Table 2.1. Summary of healing performance of capsule-based self-healing materials

Mechanism	Recovery rate	Healing Time	Healing Condition	Host Material	References
DCPD+Grubbs	75-100%	10-48 h	Room Temperature (RT)	Epoxy	[2], [83]–[85]
DCPD+Grubbs	~30%	24 h	RT	Epoxy vinyl ester	[86]
DCPD+Grubbs	67-100% (depending on the extent of damage)	48 h	RT	Epoxy+CFRC	[27], [87], [88]
DCPD+WCl_6	20-64.9%	24 h	22 ^{0}C – 50 ^{0}C	Epoxy	[33], [89]
ENB + Grubbs	45% and 80%	48 h	RT and 80 ^{0}C	Epoxy	[37]
ENB/DCPD + Grubbs	85%	48 h	RT	Epoxy	[38]
ENB + Hoveyda Grubbs	95%	2 h	170 ^{0}C	Epoxy	[40]
HOPDMS and PDES	24%	24 h	50 ^{0}C	Epoxy vinyl ester	[41]
HOPDMS and PDES	100%	48 h	150 ^{0}C	Epoxy+FRC	[43]
Epoxy and Solvent	82-100%	24 h	RT	Epoxy	[49], [50], [67]
Epoxy and Solvent + scandium (III) triflate	> 80%	48 h	80 ^{0}C	Epoxy	[34]
Epoxy+ CuBr(2)(2-MeIm)(4)	111%	1 h 30 min	130 ^{0}C – 180 ^{0}C	Epoxy	[44], [90]
Epoxy + mercaptan	104%	24 h	20 ^{0}C	Epoxy	[46]
Epoxy + MBM tetrathiol	121%	5 days	25 ^{0}C	Epoxy	[35]
Epoxy + antimony pentafluoride	71%	15-20 s	RT, 0.2Mpa pressure	Epoxy	[5]

Capsule-based self-healing materials have the ability to heal small and moderate fractures in one single healing cycle. The original ROMP reaction of DCPD facilitated by Grubbs' catalyst as the basic mechanism has a healing efficiency of 75% in 48h [2]. Brown *et al*. [83] explained that the healing efficiency depended largely on the concentration of catalyst. Full healing is achievable when the concentration of Grubbs' catalyst: DCPD is higher than 10:1. However, it is obvious that this will significantly increase the cost. Also, the mechanical properties of the overall composite system can be greatly affected with an increased number of capsules inside the host material. WCl_6, as an alternative to Grubbs' catalyst, has a relatively low healing efficiency at room temperature [33], [91]. As for ENB, it is powerless when used alone [37], but the healing efficiency rises significantly when it is blended with DCPD [38]. Increasing the temperature combined with using Hoyeyda-Grubbs' catalyst will also greatly improve healing strength and save healing time [40].

Apart from ROMP-reaction-based healing mechanisms, HOPDMS and PDES with DBTL as catalysts have demonstrated great potential when the healing temperature is high [41], [43]. Epoxy-solvent self-healing systems and epoxy-hardener systems have a high applicability considering their high healing efficiency and mild healing conditions. Yuan *et al*. [47], Billiet *et al*. [35] and Yin *et al*. [90] all developed epoxy-based self-healing systems able to achieve a healing efficiency higher than 100%. Ye *et al*. [5] demonstrated an ultra-fast epoxy-hardener system, in which healing could be activated instantly and healing time was shortened to tens of seconds. All of these healing mechanisms have added significant diversity to this field and brought new possibilities to smart material design.

However, as seen in **Table 2.1**, the healing performance is not entirely determined by the mechanisms. The temperature and healing time play a critical role in the healing

process, which is often ignored in the discussion of healing performance. These factors can be generally divided into two categories: structural factors and dynamic factors.

Structural factors:

- Capsule size, capsule shell thickness and roughness

The size of capsules and the thickness of the capsule shells directly influence rupture and the triggering of healing reactions. With larger capsule sizes, more healing agents are contained and larger cracks could be healed. Also, with a thinner shell wall, the capsule can rupture more easily. The integration quality is also related to the roughness of the capsule outer shell. In general, to secure a successful healing process, the capsule shell should be thin and rough, and the size should be suitably large to provide sufficient healing agents.

- Dispersion of capsules

The capacity of healing agents also depends on the amount of capsules dispersed inside the matrix. Generally, with more locally dispersed capsules, more healing agents will be available and local healing will be more effective.

- Ratio of different parts of a healing mechanism

For two-or-multiple-parts healing agents, the ratio of different parts directly influences the healing efficiency. For example, the maximum healing efficiency of the Epoxy+latent CuBr(2)(2-MeIm)(4) catalyst system was achieved only when the concentrations of epoxy and hardener were 10 wt.% and 2 wt.% respectively (Yin *et al*., 2008; Yin *et al*., 2007).

Dynamic factors:

- Temperature, pressure and healing time

With higher temperature, higher pressure and longer healing time, the healing performance will improve. For example, HOPEMS and PDES based healing systems can only achieve a healing efficiency of 24% when the specimen is exposed to 50 ^{0}C for 24h compared to 100% healing efficiency when the temperature is 150 ^{0}C and the exposure time is 48h.

- Ageing and fatigue

The healing performance does not stay constant. For example, Neuser and Michaud (Sam Neuser & Michaud, 2013; S. Neuser & Michaud, 2014) tested the effect of ageing and established that the healing efficiency reduced from 77% for fresh samples to 13% for samples aged at room temperatures for 77 days.

Structural and dynamic factors as well as healing agents decide healing performance. At the same time, there are concerns about the effects of introducing capsules on mechanical properties. If the capsule structure significantly reduces the mechanical properties of the host material and makes it no longer able to meet the mechanical requirements, then the self-healing function has no real value. The conflict between healing and mechanical performance fundamentally determines future research trends, which will be analysed in **Section 2.4**.

2.3. Vessel-based self-healing structures

If capsule-based self-healing composites mimic the natural healing process on a cellular level, then vascular self-healing materials emulate, on a macro level, healing by the

vascular and circulation systems in animals. With a circulation system, the healing agent can be refilled, providing the potential for continuous healing agent delivery and flow control.

2.3.1. Mechanisms

In the 1990s, Dry *et al*. [92]–[94] pioneered the development of hollow glass tubes as containers preloaded with an epoxy-based healing agent. In their research, when the hollow glass tubes cracked, the loaded healing agent filled the cracked surface and solidified. These hollow fibres can be regarded as 1D vessels. Bleay *et al*. [95] fixed hollow glass fibres with an external diameter of 15 μm and an internal diameter of 5 μm into a glass fibre reinforced composite. It was found that negative effects on the mechanical properties of the host materials can be decreased [21], [25] by reducing the size of the vessels. Vacuum-assisted capillary action filling was used to inject the healing agent into the small fibres [25]. Pand and Band [96], [97] filled 60 μm diameter hollow glass fibres with a mixture of healing agents and UV fluorescent dye so that the ‘bleeding process’ could be observed. These researchers constructed prototypes of 1D self-healing material structures based on hollow fibres, which are not only a healing agent container, but also a part of the reinforcing material.

In 2007, 3-dimensional vascular self-healing materials were developed by Toohey *et al*. [98]. The healing mechanism was ROMP reaction of DCPD enabled by Grubbs’ catalyst and the healing efficiency varied from 30% to 70% in different healing cycles. Even though the healing efficiency was lower compared to the capsule-based healing

mechanisms available then, this was the first time a self-healing composite capable of multi-cycle healing was demonstrated.

Healing mechanisms for vascular self-healing composites are similar to those for capsule-based self-healing composites. For one-dimensional vascular networks based on hollow fibres, the healing agent can be a one-part adhesive like cyanoacrylate [95] or a two-part epoxy resin [21], [99], [100]. On the other hand, for 3-dimensional networks, ROMP reaction based on DCPD and Grubbs' catalyst was initially developed [98]. Afterwards, Toohey *et al*. also developed a two-part epoxy-based self-healing microvascular network [101]. They were the first to build two isolated 3D vascular networks embedded in the same host materials, each containing a different liquid. White *et al*. [6] developed a two-stage chemistry, involving a gel stage for gap-filling scaffolds and a polymer stage for restoration of structural performance, so that a damaged area up to 35mm in diameter on a PMMA specimen can be healed. To secure good fluidity and stability, the selection of healing agents is more rigorous and should consider a number of new factors such as surface wettability and viscosity [10]. Such a selection also in turn affects the design and development of the vascular network.

The vascular structure has been applied in developing self-healing fibre-reinforced composites. William *et al*. have focused on embedding hollow glass fibres and forming vasculatures inside fibre reinforced composites, especially for sandwich structures [100], [102]. Nademi *et al*. also carried out similar research in FRCs containing hollow glass fibres [103]. Chen *et al*. [104] considered inserting vascular layers to form a sandwich-like structure as an alternative to embedding vasculatures. A two-part polyurethane was also used in polymeric foam healing systems [105], and for mitigation of fatigue in an epoxy

matrix [106]. ROMP based on DCPD and Grubbs' catalyst was also investigated for its potential in coating technology [107].

Cementitious materials with self-healing properties are another area where the vascular self-healing function is popular. Material designs have included a single vessel containing cyanoacrylate [108], [109] and multi-channels based on three-part MMA [93]. More information can be found in the review by Van Tittelboom *et al*. [61].

2.3.2. Fabrication process

Even though vascular self-healing composites share similar mechanisms with capsule-based self-healing composites, research on this topic has been developing slowly due to immature fabrication techniques. As small vessel diameters, large network coverage, high vessel strength and high network interconnectivity are all required at the same time, developing suitable fabrication techniques becomes difficult. In fact, as opposed to capsule-based self-healing materials research where most of the effort has been on developing new mechanisms to improve healing efficiencies, work on vascular self-healing materials has concentrated on fabrication processes. In this section, popular fabrication methods are categorised and analysed.

I. Hollow fibres

Installing tubes containing the healing agent inside is one method to fabricate vascular self-healing fibre reinforced composites [96], [97], [99], as shown in **Figure 2.4**. The hollow fibres act as an isolating layer between the healing agent and the matrix. When the material is damaged, some fibres rupture and release the healing agent. The process of integrating hollow fibres with the host matrix is similar to that for a normal fibre-reinforced

material (i.e. covering fibres with uncured epoxy resins followed by curing). When the hollow fibres are aligned parallel to the reinforcement fibres, the mechanical effect of the hollow fibres on the host composite is small (Kousourakis & Mouritz, 2010). However, the main drawback of using hollow fibres is that the design cannot yield interconnected networks and refilling is difficult.

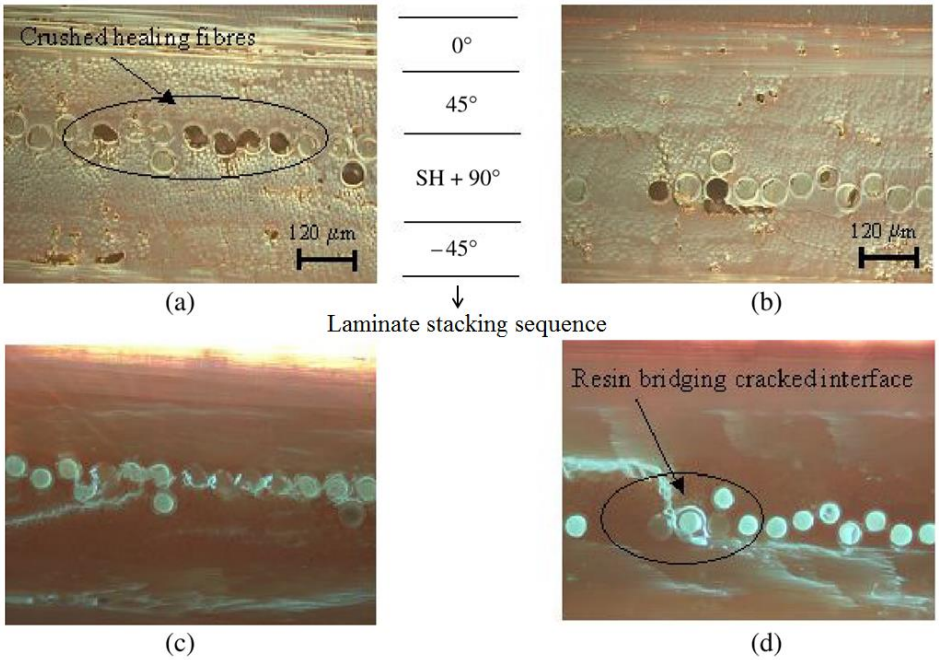

Figure 2.4. Polymers embedded with hollow fibres containing healing agent [99]. (a, b) Laminating stacking sequence of hollow fibres and reinforcement fibres; (c, d) Outflow of healing agents.

II. Sacrificial fibres/scaffolds

Sacrificial fibres/scaffolds are a three-dimensional structure formed of materials easy to remove, dissolve or degrade. Such a structure is integrated inside the polymeric host material and should be able to survive the process of curing the host material. After the polymeric system is fully cured, the sacrificial fibres/scaffolds are removed manually, or simply by increasing the temperature or changing the pH of the environment to modify the

state of the embedded sacrificial materials. This leaves a hollow microvascular network inside the host material. For example, to build single-line channels, straight steel wire [110] or nylon fibres [111] were placed inside the uncured host materials. After it was fully cured, the wire or the fibre has a weak bond with the host materials and can be removed manually, leaving hollow channels. However, this method can only be used to build 1-D hollow structures inside composites and the sacrificial-wire/fibre-removing process may introduce invisible damage. To build complex 3-D structures, the following methods have been adopted.

- 3D printing of sacrificial scaffolds

A fugitive-ink 3D direct-write method to develop sacrificial microvascular networks was first developed by Therriault, *et al*. [112] and Lewis, *et al*. [113] who used a robotic deposition apparatus in a layerwise scheme to print paraffin-based organic ink in three dimensions, as shown in **Fig. 2.5a**. After the integration of scaffold and polymeric host material, the system was heated up to 60 °C under a light vacuum to remove the melted sacrificial materials, leaving a hollow microvascular network inside. This technique was claimed to be able to produce a scaffold with a diameter ranging from 10 to 300 μm with a root-mean-square (r.m.s.) surface roughness of 13.3±6.5 nm. Other fugitive inks were also considered, such as a composition of 60 wt.% petroleum jelly and 40 wt.% microcrystalline wax [98]. However, it is difficult to remove the melted sacrificial materials from vascular networks and residues always exist when the diameters of vessels are small and liquids are locked inside the vessels due to viscous force.

Poly (lactic acid) (PLA) is a good option for sacrificial materials as it will turn into gas after thermal depolymerisation at high temperature. 3D-printed PLA has been used to build sacrificial structures [114]. However, the high temperature during the sacrificial-

materials-removing process may be harmful to the host material. Dong *et al*. [115] discovered a catalytic reaction system based on catalysts such as tin(II) oxalate that improved the reaction rate of PLA depolymerisation from 1 wt.%/hr (weight percent per hour) to 25 wt.%/hr, lowering the depolymerisation temperature approximately 100 ^{0}C. It is worth noting that the heat distribution on samples to remove the sacrificial PLA component must be even. Otherwise, the locally depolymerised monomers are possible to be locked inside the composites and introduce high air pressure that may damage the samples. Afterwards, the mixture of PLA and the catalyst was 3D-printed to form sacrificial structures [116]. In addition, recent research has also improved the printed pattern from a simple uniform pattern to a biomimetic pattern similar to a leaf venation [117], [118], as shown in **Fig. 2.5b**. The varying diameter of the network was achieved by changing the pressure inside the printing nozzle. To improve the printing efficiency, Hansen *et al*. [119] developed a multi-nozzle array to print multiple lines simultaneously. The mechanical properties of hollow channel structures were improved by integrating halloysite nanotubes with sacrificial fibres as the nanotubes covered the inner surface of the microvascular network after dissolving the fibres and provided structural reinforcement [120].

In addition to using nozzles, light-triggered solidification based on photopolymers can also be employed to 3D-print sacrificial components. Jacobsen *et al*. [121], [122] fabricated interconnected photopolymer waveguides based on self-propagation and generated open-cellular micro-truss structures (**Fig. 2.5c**). This technique was further developed to produce metallic vascular networks [123] (**Fig. 2.5d**) and bicontinuous fluid networks [124].

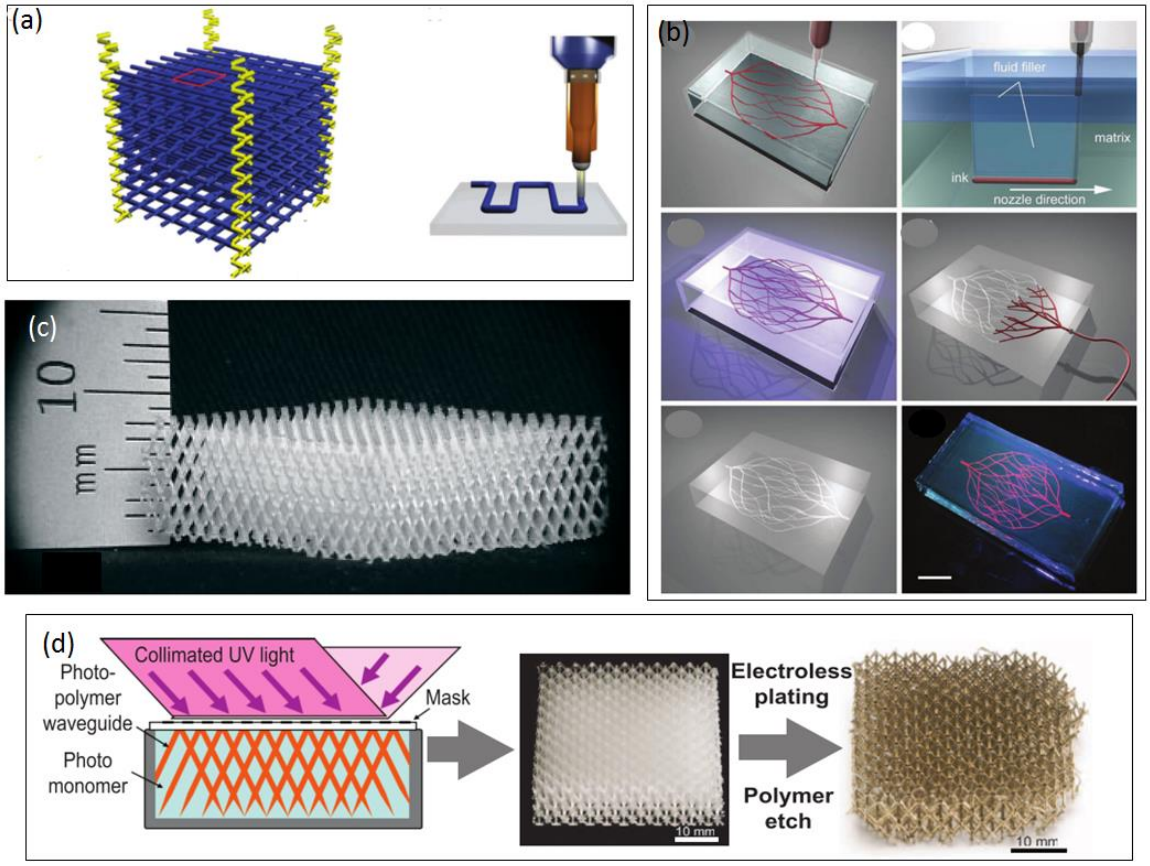

Figure 2.5. Fabrication of Scaffolds. (a) 3D printing using nozzles [112]; (b) 3D printing of a bio-mimicking pattern [117]; (c) Self-propagated photopolymer [122]; (d) Fabricated metal interconnected vascular network based on photopolymer [123].

- Melt-spinning and Electro-spinning

Melt-spinning and electro-spinning generate fibres from liquids and the processes are similar to the generation of cotton candy. In fact, the original equipment for melt-spinning sacrificial fibres was simply a cotton candy machine [125]. After the sugar fibre was fabricated, it was placed in a Teflon mould. Degassed uncured PDMS mixed at a resin: hardener ratio of 10: 1 was then poured over the sugar, followed by 24h curing at room temperature. Afterwards, the devices were placed in a bath of water and ethanol at 70°C for several days to dissolve away the sugar structure, leaving a micro channel network

inside the PDMS matrix. A similar method was applied to form vascular networks inside gelatin by using shellac as sacrificial fibres, as shown in **Fig. 2.6**. Shellac is a kind of natural material that exhibits pH-sensitive solubility in aqueous solutions and has an appropriate melt temperature and viscosity.

Electro-spinning can be used to produce similar sacrificial fibres. Gualandi *et al*. [126] used Pollulan as the fibre material and integrated the fibres with diameters as small as 3μm inside an epoxy matrix. Afterwards, the Pollulan degraded when heated up to 250°C. In addition, electro-spinning has the potential to build core-shell structures directly as a vascular network, skipping the sacrificial fibre degradation process and healing agent injection steps. This method was proposed by Gualandi *et al*. [126] and developed by Wu *et al*. [127]. The DCPD healing agent was contained directly inside polyacrylonitrile shells during electro-spinning. With the fibres embedded, when a crack occurred, the rupture of the polyacrylonitrile shells released the DCPD healing agent to repair the damage.

The spun fibres can also be chemically or physically treated to improve the performance of the sacrificial-material-removing process. As the authors mentioned, the thermal depolymerisation of the PLA impregnated can be accelerated by using suitable catalysts. Dong *et al*. [115] developed a technique to integrate PLA fibres with the catalyst tin(II) oxalate to lower its depolymerisation temperature, as shown in **Fig. 2.7**. To build a microvascular network inside fibre-reinforced composite, PLA sacrificial fibres can be wound with reinforcement fabrics [7], [128] followed by heat treatment.

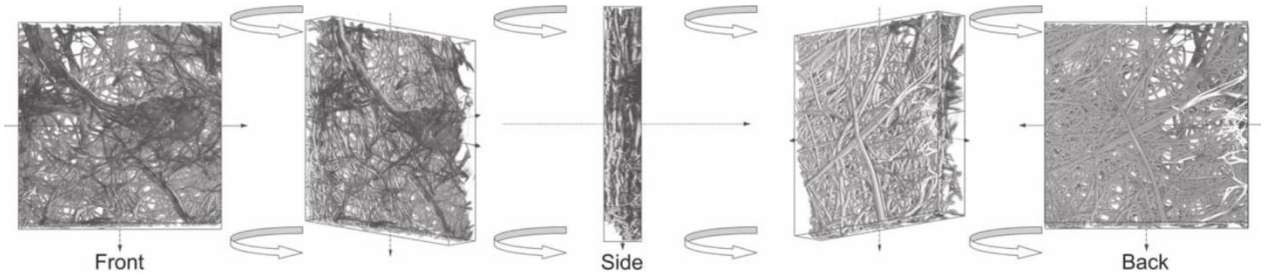

Figure 2.6. Vascular network formed in gelatin by using sacrificial melt-spun shellac fibres [129].

By using melt-spinning and electro-spinning, the fabrication process to produce small diameter fibres is simple and fast. However, this method is only used to generate single sacrificial fibres and the installation of the fibres into a designed pattern can only be done manually. Other advanced positioning techniques have not yet established. Core-shell fibres are convenient for producing self-healing materials. However, this method cannot be used to build interconnected networks and the healing agent cannot flow inside the vessels and refilling is not possible. In this case, the material acts more like an improved capsule-based self-healing material than a vascular self-healing material.

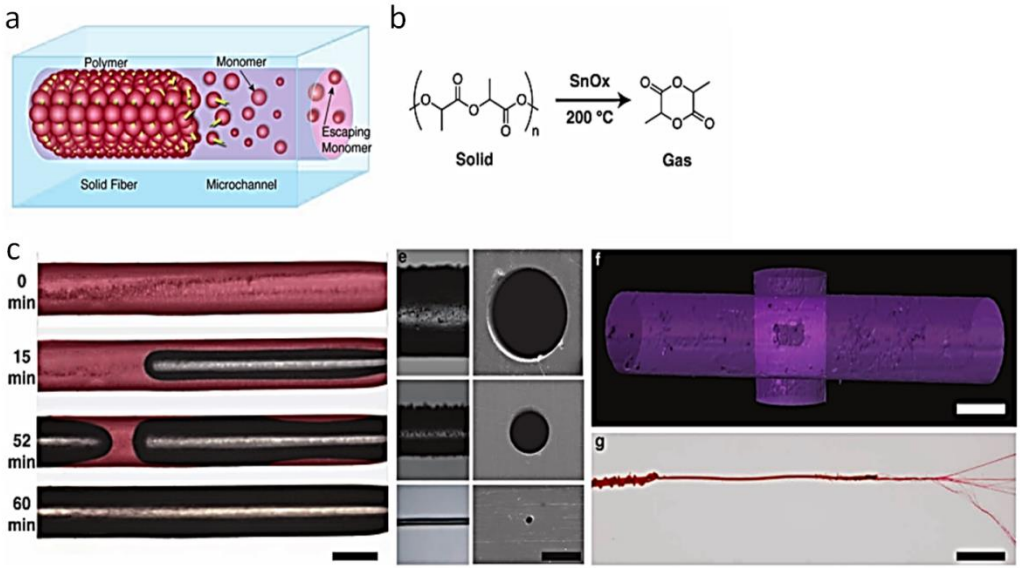

Figure 2.7. Decomposition of PLA fibre [130].

- Replication of existing patterns

Soft lithography is a powerful tool for fabricating micro-fluidics networks [131] and a similar method can also be applied to fabricate microvascular networks for self-healing material systems. Golden *et al*. [132] described a method using gelatin as sacrificial material to form a hexagon beehive structure, as shown in **Fig. 2.8**. This method started with building the pattern of a vascular network followed by replicating the pattern using a substrate made of glass or pre-oxidised PDMS, forming a 'negative' version of the structure on the substrate. The gelatin then filled up the cavity in the substrate. When the gelatin became solid, it was removed from the substrate and integrated inside hydrogel, which was later heat treated. After the molten gelatin was removed, a microvascular network in the pattern was left inside the hydrogel. The diameter of the channels can be as small as 6 μm. Many natural systems also have suitable structures that can be replicated directly using PDMS. He *et al*. [133] adopted a similar method to replicate the leaf venation to build interconnected vascular networks, as shown in **Fig. 2.9**.

The replication of existing patterns can also be combined with other fabrication methods. Bellan *et al*. [134] employed a melt-spinning technique to fabricate small diameter fibres and used soft lithography to produce primary vessels.

The replication of existing patterns is suitable for mass production as it is a fast way to copy large and complex networks precisely. However, this process is complex and inefficient when only one item is to be produced.

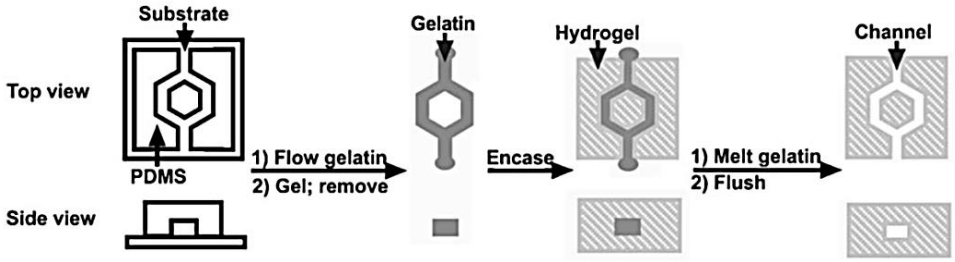

Figure 2.8. Soft lithography for building microfluidics devices [132]

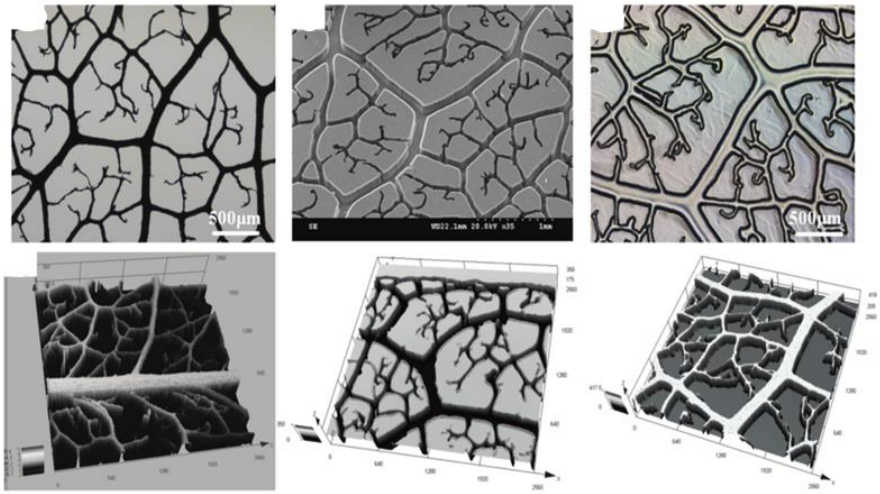

Figure 2.9. Replication of a leaf venation [133]

III. Electrostatic discharge

Electrostatic discharge is likely to be the most rapid fabrication method to build microvascular networks following natural designs (e.g. Murray's law). Huang *et al*. [135] irradiated PMMA with an electron beam, causing electrical charges to accumulate inside the material. The specimen was then connected to the ground and a process of rapid discharge similar to lightning occurred, creating a tree-shape branched microvascular network inside the specimen block, as shown in **Fig. 2.10**. Alternatively, a defect was introduced on the surface of the block prior to irradiation that became a nucleation site

allowing spontaneous discharge upon exposure to the electron beam. The diameter of the vessels ranged from 10 to 500 μm.

This method is suitable for building vascular networks of any size rapidly and efficiently. However, the generated pattern is not controllable, resulting in uncertain quality of the network. Thus, this method still needs further investigation, especially as regards the performance and property of the discharge process.

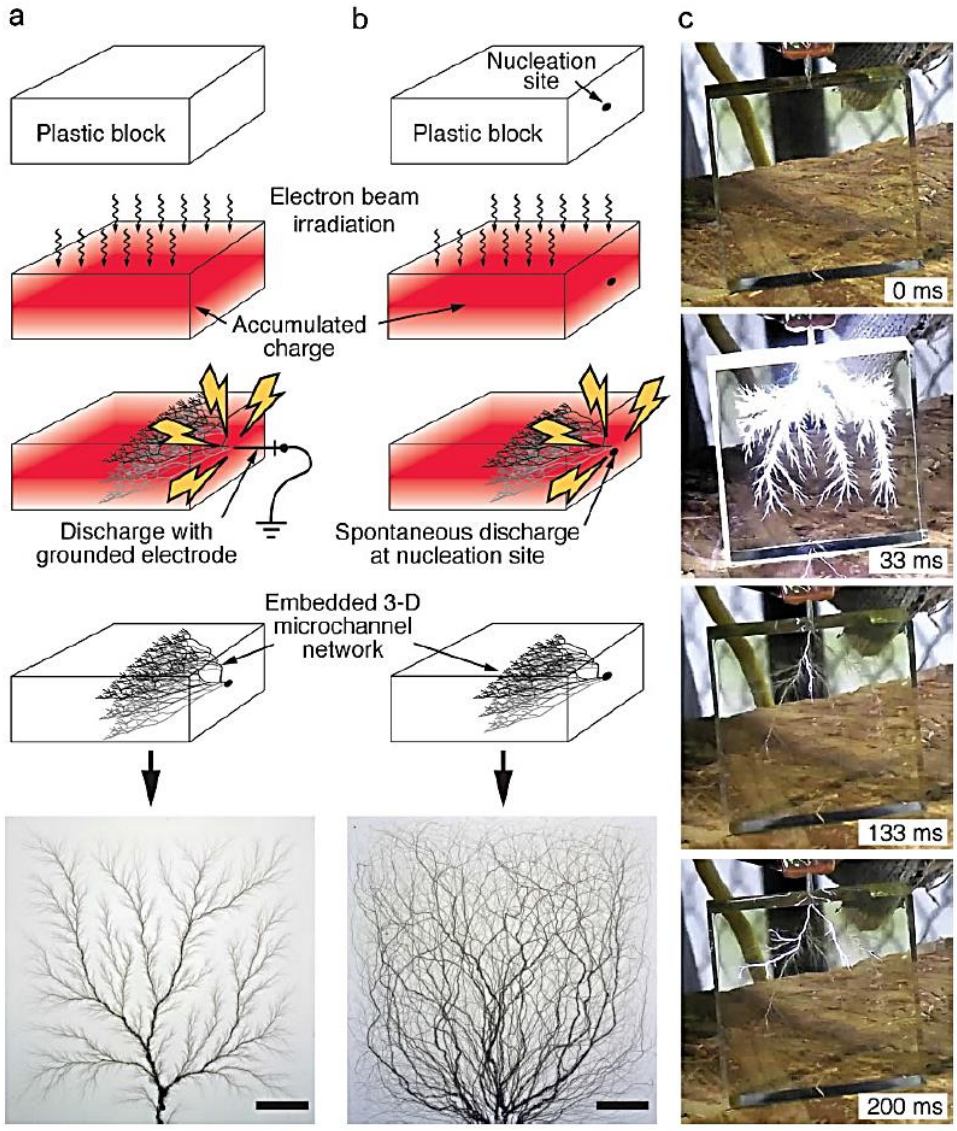

Figure 2.10. Electrostatic discharge to fabricate vascular patterns [135].

IV. Laser direct-write

Laser direct-write techniques have been applied to fabricate channels in microfluidics devices. These channels could act as vessels in vascular systems. Lim *et al*. [136] used high-brightness diode-pumped Nd:YAG slab laser to manufacture microchannels on a PDMS block. Lasers can be used to fabricate very complex 2D patterns directly on polymeric materials. However, it is difficult to produce 3D structures by using lasers and more work is needed to achieve this.

Table 2.2. Features of fabrication techniques for vascular networks

	1D Hollow Fibres	**Sacrificial fibres/scaffold**				**Electrostatic discharge**	**Laser direct-write**
		Straight wire/fibre	**3D printing**	**Spinning**	**Replication**		
1D vessels	Yes	Yes	Yes	Yes	Yes	Not predictable	Yes
2D vessels	No	No	Yes	Yes	Yes	Not predictable	Yes
3D vessels	No	No	Yes	Yes	Yes	Not predictable	No
Interconnection	No	No	Yes	Yes	Yes	Yes	Yes
Refill	Possible but difficult	Possible but difficult	Easy	Possible but difficult	Easy	Easy	Easy
Size	10~ 500 µm	10~ 500 µm	10~ 500 µm	5~300 µm	Depends on the pattern to be replicated	20~300 µm	Depends on the size of the laser beam
Fabrication time	Short	Short	Medium	Medium	Long	Short	Short
Large-scale fabrication	Yes	Yes	Possible but inefficient	Possible but inefficient	Yes	Yes	Possible but inefficient
Possibility of damage	Low	High	Low	Low	Low	High	Low
Surface roughness	Good	Good	Good	Good	Depends on the pattern to be replicated	Good	Bad

2.3.3. Mechanical effects

For vascular systems, Coppola *et al*. [128] tested the tensile strength of fibre-reinforced composites with a wave-shaped vascular network architecture inside formed by using PLA sacrificial fibres and found that vascular channels have a minimal effect on tensile behaviour when fibre alignment is unaltered and the reinforcement fibre architecture is not distorted. Zhou *et al*. [137] numerically showed the influence of microvessels on the structural properties of laminated composites especially on stress concentration around vessels and delamination cracking. Work by Kousourakis *et al*. [138] showed that hollow fibres located along the mid-thickness plane of the composite material caused no change to or a small reduction (less than a few percent) in the in-plane elastic modulus. The tension and compression strengths did not change when hollow fibres were aligned to the loading direction, but strength decreased when the fibres were normal to the load. Nguyen *et al*. [139] did a similar work and highlighted fibre waviness angle as a key geometrical parameter for structural performance. Norris *et al*. [140] found the compressive strength of FRC embedded with hollow one-dimensional vessels reduced between 13% and 70% with different vessel dimensions. Similar research has been reported by Huang *et al*. [141].

2.3.4. Healing performance analysis

There are two original motivations to build vascular structures: 1) giving self-healing capability to fibre-reinforced composites, and 2) achieving multi-cycle self-healing. After approximately 10 years of development, research along these two different paths has largely converged and should be considered together and compared. A summary of the main designs in this field and their healing performances is shown in **Table 2.3**.

Table 2.3. Summary of healing performance of vessel-based self-healing materials

Mechanism	Healing Efficiency	Healing Condition	Healing Cycle	Host Material	References
DCPD + Grubbs' catalyst	70%	12 h 25 ^{0}C	7	Epoxy	[98], [107]
Epoxy resin+Hardener	60-90%	48 h 30 ^{0}C	30	Epoxy	[101], [142]
Epoxy resin+Hardener	74% and 27%	6h 70 ^{0}C and 30 ^{0}C	1	Epoxy	[143]
Epoxy resin+Hardener	87%-100%	Normally higher than RT	1	FRC	[7], [19], [21], [97], [99], [100], [110], [144], [145]
Two-stage chemistry	62%	20 min to fill impacted regions, 3h to restore mechanical function, 125 ^{0}C	1	PMMA	[6]

For vascular self-healing composites, healing efficiency is less than 80% under most circumstances. This is relatively low compared to capsule-based self-healing composites where a number of researchers have achieved a healing efficiency higher than 100 %. As seen from the table, different healing mechanisms did not make significant differences to the healing efficiency. Other structural and dynamic factors, as categorised as follows, have made a significant impact on healing performance.

Structural factors:

- Vessel size and roughness.

The vessel size and the roughness of the vessel's inner surface determine the efficiency of liquid flow inside the vascular system [146]. A large size vessel is able to efficiently provide adequate healing agents when a large-scale crack occurs.

- Vascular network pattern.

The healing behaviour is triggered by the rupture of the vascular network. Thus, in order to create a high possibility of releasing the healing agent, the pattern of the network should have a high coverage. However, a large volume of hollow structures inside composites brings uncertain impact on mechanical properties. Thus, a balance between acceptable pattern coverage and a compact pattern structure is required [147]–[150].

Dynamic factors:

- Temperature and healing time.

For two-part epoxy systems, suitably high temperatures and long healing time normally result in high healing efficiency. For example, given the same healing time, Hansen *et al*. [143] found that healing efficiency increased to 74% from 24% as the temperature increased to 70 ^{0}C from 30 ^{0}C. Temperature is a common factor for both capsule-based healing systems and vascular healing systems.

- Hydraulic pressure and mixing process.

The applied hydraulic pressure inside the vascular network not only determines the amount of healing agents outflow, but also the mixing quality of the multiple-parts healing

agents. With a suitably high hydraulic pressure inside vessels, continuous delivery of healing agent to the crack location is possible. More importantly, when two-part-epoxy healing agents are applied and epoxy resin and hardener contact at the crack location, the mixing only takes place at the interfaces of those two viscous liquids and the mixing ratio of the different parts is hard to control. By applying a suitable pumping strategy according to the mixing process of viscous liquids, it is possible to enhance healing efficiency from 50% to almost 100% [111].

- Other environmental factors.

Other factors like moisture and oxygen can also influence the healing performance. A number of researchers have considered the effects of the environmental factors on capsule-based healing systems. These factors should also be valid for vascular self-healing composites but this is yet to be demonstrated.

As with capsule-based materials, structural and dynamic factors as well as healing agents determine healing performance. However, the effects of vessels on mechanical performance could be more significant compared to those of capsule-based structures. Such concerns fundamentally determine future trends, which will be analysed in **Section 2.4**.

2.4. Trends

2.4.1. Shift in development focus and new opportunities

Although researchers may claim to have greatly improved the healing performance of self-healing composites, these products have yet to be used in practical applications owing to

uncertainties in their performances. Some self-healing composites heal well only when conditions are favourable and the damage is minor. For self-healing products to be practically useful, it is essential that the material is able to achieve 'sustainable healing'. This means that healing can effectively carry on regardless of environmental conditions and the size of the damage.

Sustainable healing consists of 3 main aspects: healing efficiency (healing strength), healing rate and healing capability, as shown in **Fig. 2.11**. Healing rate and efficiency represent the rate of curing and the strength of the repaired material, respectively. Healing capability relates to the size of the damaged area and the range of materials that can be healed. For example, vascular self-healing composites have a larger healing capability than capsule-based self-healing composites, as vascular systems can heal larger areas, although the types of healable materials are similar in both cases. In addition, sustainable healing implies the ability to undergo multiple healing cycles and, ideally, means that the healing rate, healing efficiency and healing capability remain unchanged throughout.

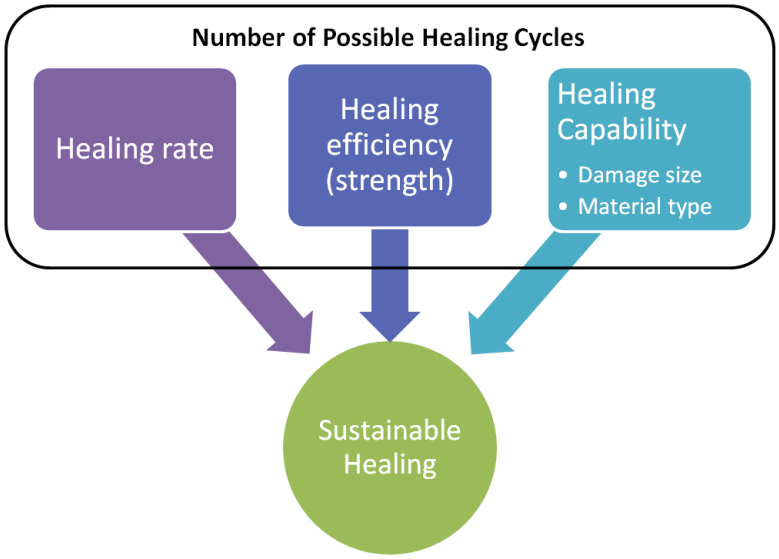

Figure 2.11. The concept of sustainable self-healing

The past ten years have seen great improvements in healing efficiency (strength). Whether in capsule-based or vascular healing systems, when the size of the damage is small or moderate and appropriate healing conditions are adopted, healing efficiencies of more than 60% and sometimes even higher than 100% can be achieved. Thus, healing strength is no longer an issue. By comparison, advances in healing rate and capability are less obvious. To achieve sustainable healing, the healing rate must be controllable and the healing capability must be improved to ensure that large damage sizes and a wide variety of types of materials can be healed. Hence, the research focus will shift from healing efficiency to healing rate and healing capability, as they have become the key barriers to sustainable healing. New research opportunities are discussed below.

I. Healing rate

There are potentially a number of methods to increase healing rate, such as employing advanced healing agents, increasing the healing temperature and adopting better mixing strategies. On the other hand, the healing rate cannot be too high in some applications. For example, one-part healing agents must have a medium healing rate to avoid solidifying inside vascular networks. Fundamentally, once the type of healing mechanism has been confirmed, the healing rate in a particular environment is intrinsically determined as well. For sustainable healing, the healing rate must be controllable and kept in an appropriate range regardless of environmental conditions. However, this has yet to be achieved.

Having a controllable healing rate means that the healing rate can be accelerated or decelerated according to the situation. This will be a significant step towards sustainable healing. As the healing rate is fundamentally determined by the energy provided, it becomes controllable as long as a suitable energy delivery component able to supply

energy to healing agents is available. Chu *et al*. and Zhang *et al*. [151] developed a carbon nanotube paper for de-icing that is able to heat up a composite surface from -22 ^{0}C to 150 ^{0}C, which is an ideal temperature for accelerating reaction in two-part-epoxy systems. Fehrman *et al*. [152] developed a method to deliver acoustic energy to certain target defect locations. All of these techniques have the potential to provide energy in self-healing composites. Vascular systems can be more easily actuated by controlling the pressure and temperature of the liquids inside the network. Research on this topic will be strongly related to studies of the characteristics and the design of vascular networks.

However, to achieve a controllable healing rate, it is not enough to have an energy delivery component. A sensing system is also necessary. The sensing system is particularly critical to the application of structural materials working in extreme environments.

The devices studied include Brillouin distributed fibre sensors [153], Fibre Bragg Gratings (FBG) , inkjet-printed sensors [154], carbon nanotubes based sensors [155], and acoustic emission sensors [156]. Some of these sensing systems have been adopted for detection of cracks in self-healing materials [36], [157], [158]. For example, Hong *et al*. [159] designed a multifunctional healing and monitoring system based on the vascular model by introducing conductive carbon powders and metallic micro-wires inside micro-tubes. However, researchers have mainly focused on gathering crack information and the feedback loop has not been built to guide healing process in real time.

Overall, through combining energy delivery control and sensing, it is possible to achieve a controllable healing rate. The former is to ensure that the rate is in an

appropriate range, while the latter is to obtain crack and environmental information to determine the appropriate energy control strategy.

II. Healing capability

There have been two significant improvements regarding the healing scale: the establishment of vascular self-healing composites to achieve multi-cycle healing and moderate-scale healing [98], and the development of multi-phase healing mechanisms for large-scale healing [6]. The authors believe that, ultimately, the healing size would be infinite which means the damage can be healed regardless of its size. This situation might be referred to as self-regeneration, a process similar to the regeneration of a lizard's tail which has yet to be artificially accomplished.

Regarding the types of materials able to self-heal, there have been no obvious advances since the establishment of capsule-based self-healing composites. In any composite formed of more than one substance, different parts have different functions. Once a certain component in a composite has failed and cannot be healed, the corresponding functions disappear. For example, the recovery in self-healing fibre-reinforced composites can only be effective when the structures of the reinforcement fibres remain intact. To restore all functions, it is essential that all types of materials can be repaired or replaced by newly generated parts that are able to fulfil the same functions. However, this is still not achievable at the moment. A new opportunity is to develop mechanisms for healing reinforcement fibres, and other materials used in composite systems.

2.4.2. Comparison of and future trends in capsule-based and vascular structures

As mentioned previously, the two main topics in the area of self-healing composites are healing performance and mechanical properties. As for healing performance, in most cases, a capsule-based self-healing composite can only cope with very small cracks due to the limited amount of healing agent contained inside the capsules. So this is especially suitable for dealing with delamination and other kinds of damage to the micro level, which is a common issue when using layered composites. Even though capsule-based structures can provide higher healing strength compared to vascular structures, thanks to the dispersion of capsules providing wide coverage, the key advantages of the vascular structure are its capability for multi-cycle healing and large area healing, both of which are essential to sustainable healing. As for large scale damage, capsule-based self-healing structures become powerless while vascular self-healing composites can heal relatively large gaps when healing agent refill and multi-phase healing are effective [6]. A multi-phase healing mechanism can build a semi-solidified surface for later epoxy curing or solid healing, just like the multi-phase healing behaviour in biological systems. **Fig. 2.12** shows the performance of multi-cycle healing, comparing vascular networks with micro-capsules. Considering that the sustainability of healing behaviour becomes increasingly important, the development of vascular structures is likely to be the focus of research in the future.

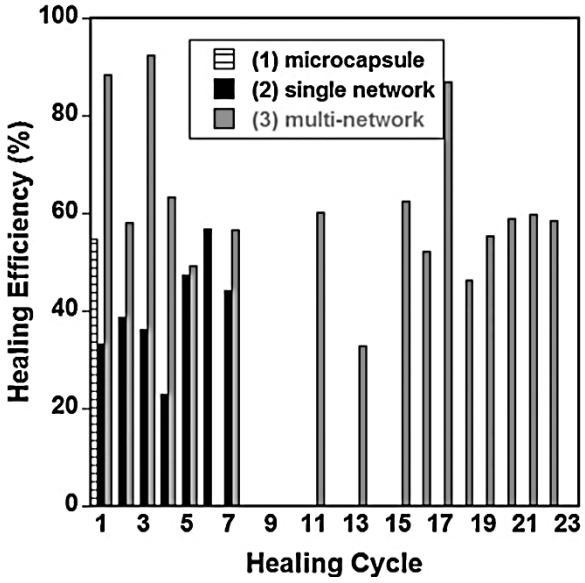

Figure 2.12. Healing potential for multi-cycle healing [107]

Regarding the mechanical properties of capsule-based and vascular structures, the size of the capsule and vessel makes a large difference to the mechanical properties of the overall composite. Smaller sizes tend to introduce less effect on the host material. On the other hand, smaller containers generally cannot provide adequate amounts of healing agents. In order to minimise the mechanical effects of capsules and optimise the capacity of healing agents, the crack location can be predicted [160] from the perspective of structural optimisation and the location and number of capsules can be designed and planned instead of being random. However, an upper limit of the capacity of healing agents still exists and the conflict between having enough healing agent and satisfying mechanical performance requests remains for capsule-based structure. The potential to refill a vascular structure makes this problem solvable, and also makes vascular structure more competitive in this regard.

Even though a vascular structure has more advantages, it still cannot totally replace capsule-based structure. Actually, in biological systems, healing is fulfilled by both cells and vascular networks in combination. As the capsule-based structure is more suitable for healing small crack and the vascular structure is more suitable for healing medium and large crack, these two structures can be combined and used simultaneously to develop sustainable healing systems to cope with all kinds of damage conditions.

2.5. Summary

Main developments in self-healing materials in the past decades have been reviewed in this chapter. Capsule-based and vessel-based self-healing structures are the main routes to building autonomous self-healing structures. Healing mechanisms, healing performance and fabrication techniques for producing capsules and building vascular networks have been summarised and analysed. Capsule-based self-healing materials are able to heal small cracks while vascular systems are more suitable for healing larger damaged areas. The healing performance varies from 24% to 121% depending on the types of healing agents, different healing and damage conditions.

Future work in this area will still follow historical trends: (i) improvement of healing performance and (ii) investigation of effects on mechanical properties. It is worth noting that the development focus has been shifting from healing strength to the sustainability of healing ability. Sustainability requires significant improvement on healing capability to enable fast and robust recovery regardless of ambient conditions, material types and damage size. As the vessel-based design enables recovery from extensive damage, the

vessel-based design was adopted in this research. **Chapters 3** to **6** report various new designs and mechanisms promoting the sustainability of healing ability.

Chapter 3 - Effects of vessel configurations on the flexural properties and healing performances of vessel-based self-healing composites: an experimental study

3.1. Preliminaries

The aim of the chapter is to answer some fundamental and common questions in the design of vessel-based self-healing fibre-reinforced composites. First, what are the flexural properties of composites incorporating complex vascular networks? Fibre-reinforced composites become popular because of their exceptional strength and light weight. Hence, they are favoured in applications where large-scale structural beams sustaining bending in dynamic environments are required, such as aeroplane wings and wind turbine blades. However, the influence of the embedded vascular networks on bending strength has yet to be investigated. Second, what would be the effects of vessel configurations on the recovery of the flexural properties? In the past 15 years, vessel configurations have evolved from one dimension to three dimensions. However, whether the change of configuration can significantly improve the healing performance remains unanswered.

The goal of this research is to investigate the effects of vessel configurations on the flexural properties of host materials and healing performances, and to provide guidance on how to design strong self-healing composites able to recover reliably. As the composites sustain bending, damage conditions (debonding, delamination, and fracture of reinforcement fibres) can be different. The study also reveals the effects of damage conditions on healing performance to highlight what should be further improved in the application of vessel-based self-healing fibre-reinforced composites. The role of the chapter in the thesis is shown in **Fig. 3.1**.

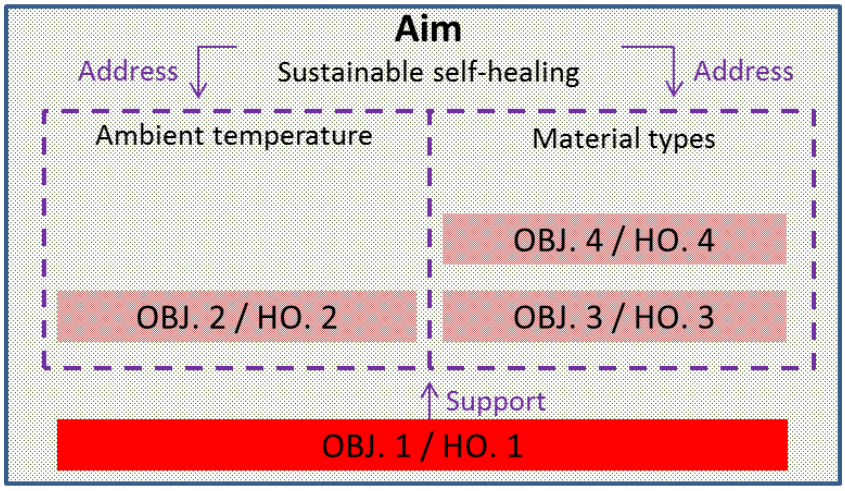

Figure 3.1. Role of Chapter 3 in the thesis (red area)

3.2. Methodology

3.2.1. General framework for experiment

The research has three stages. The first stage aims to examine the flexural properties of vascular fibre-reinforced laminates. Three vessel configurations were tested: straight channels in single layer, wave-like channels in multiple layers and herringbone-and-wave-like channels in multiple layers. A standard glass fibre-reinforced composite (GFRC) was also tested as a reference.

In the second stage, samples incorporating vessels of different configurations were damaged in a standard way, followed by injecting a pre-mixed healing agent, the 'blood' of the material, into the vessels to allow the samples to cure. Afterwards, the recovery was assessed to reveal the effects of vessel configurations on healing performances. Based on the test results from Stage 1 and Stage 2, the most suitable vessel configuration can be experimentally confirmed.

In the third stage, the effects of damage conditions were investigated. Samples incorporating identical vessels were damaged by different bending strategies which caused different levels of damage. The samples cured under the same healing conditions and were re-assessed after healing to measure the percentage of the flexural strength restored.

3.2.2. Definition

In the first and second stage, four types of composites were used. S0 was a standard 8-layer glass fibre-reinforced composite with no vascular network inside (**Fig. 3.2**). Testing this type aimed to assess the strength and understand the damage process of a standard fibre-reinforced laminates without vessels.

S1 contained hollow channels incorporated into a single layer of woven glass fibre (**Fig. 3.3a**). In the 8-layer structure, the layer containing vascular networks was the seventh layer from the bottom up, creating an asymmetric structure inside composites. As the layer was very thin, the vessels were straight, similar to a tunnel. The configuration has been a typical design in various established results [140], [161], [162]. S2 was embedded with wave-like vessels placed in the four layers of the core as shown in **Fig. 3.3b**. The vessels in S3 were in a herringbone-and-wave-like configuration (**Fig. 3.3c**). Both configurations in S2 and S3 have been proposed and become popular because they enable satisfactory recovery from Mode I fracture [7], [130].

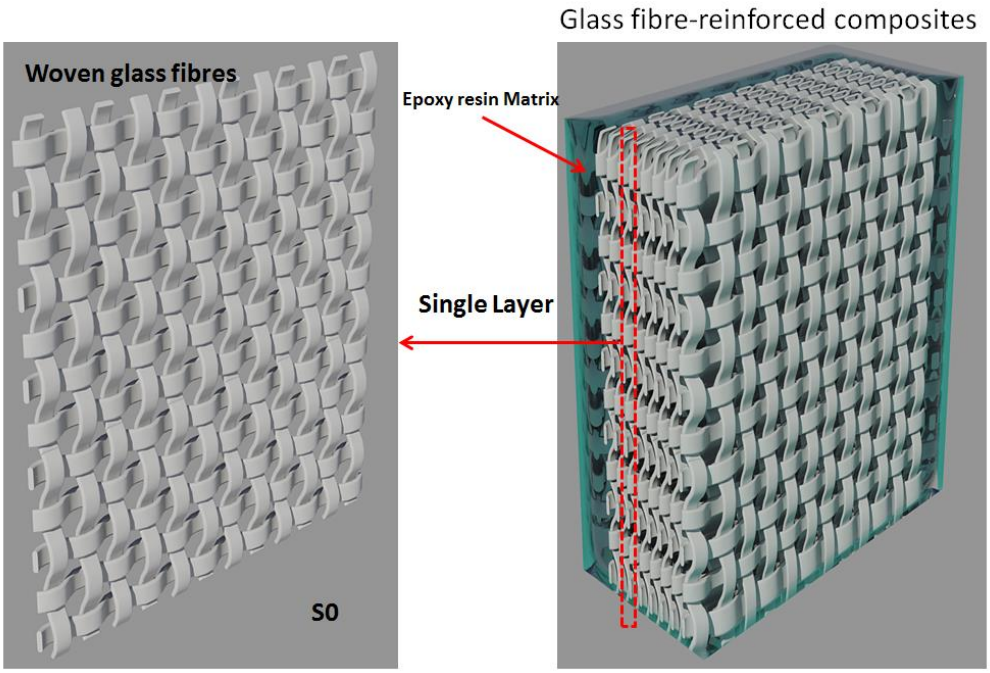

Figure 3.2. A schematic of S0, an eight-layer glass fibre laminates

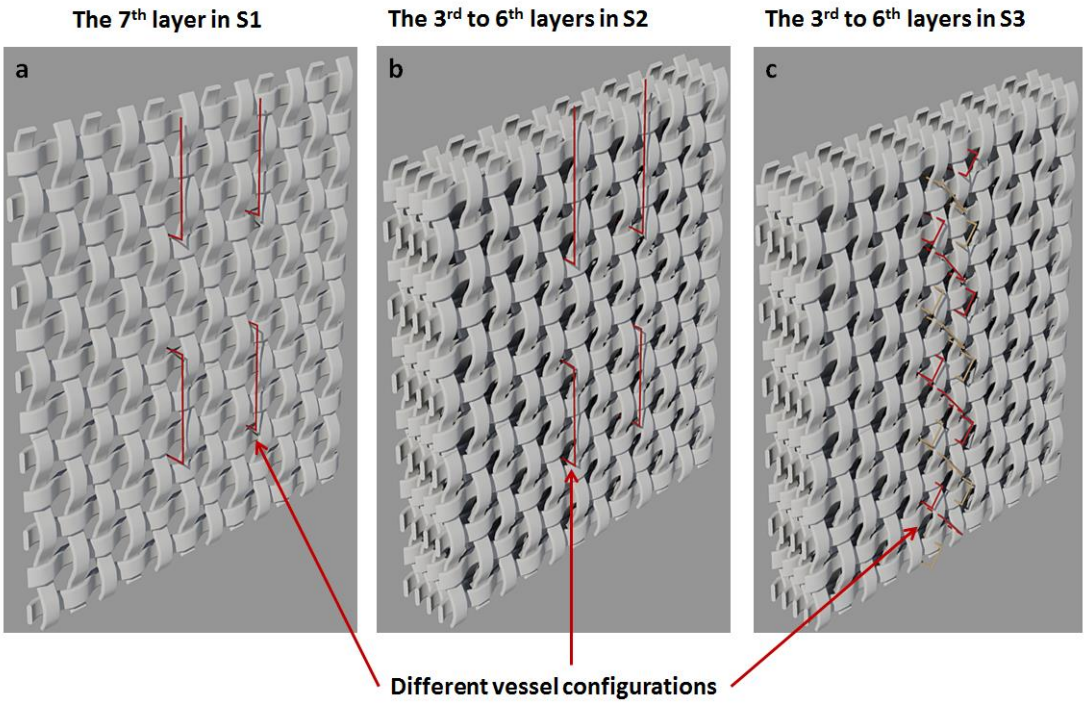

Figure 3.3. Vessel configurations in S1, S2 and S3

In the first stage, the flexural properties of S1, S2 and S3 were compared to that of S0 to measure the reduction of strength caused by different vessel configurations. In the second stage, S1, S2 and S3 were damaged following a standard criteria and be injected with the same amount of healing agents for curing. In the third stage, the candidate with the best performance in Stage 1 and Stage 2 was tested to understand the effects of damage conditions on healing performances.

3.2.3. Fabrication of samples

To fabricate the samples, resin infusion techniques and the vaporisation of sacrificial components (VaSC) [7], [115], [116], [130], [163] were employed to make fibre-reinforced composites embedded with hollow vessels. Glass-fibre fabrics ready for incorporating sacrificial components (single layer for S1 and four layers for S2 and S3) were fixed on a needlework frame (Q-Snap 11”×11”) to prevent the distortion of the woven architecture. PLA sacrificial fibres (300μm, CU Aerospace Ltd.) were manually incorporated into the woven glass fibre. Afterwards, the fabrics incorporated with sacrificial components and other unprocessed fabrics were placed on a PVA releasing agent (PVA-02, Easy Composites Ltd.) covered polypropylene table and sealed in vacuum bagging film. Prior to resin infusion process, the vacuum space was left for 1 hour and it was found no vacuum drop, confirming its airtightness. Epoxy resin and hardener (EP-HTL, Easy Composites Ltd.) were mixed at 100:35 parts by weight (pbw) and degassed at 35 ºC for 30 minutes in a vacuum chamber (DRK616A-1, Drick Instruments co., Ltd.). The epoxy resin was cured for 36 h at room temperature followed by post-cure heating cycles at 40 ºC, 60 ºC, 80 ºC, 100 ºC and 120 ºC each for one hour, and 140 ºC for 3 hours.

After the curing and the post-cure heating cycles, the specimens were cut into rectangular shape 180 mm × 21 mm × 2 mm using a grit saw and polished with a sanding paper. The cutting and polishing processes followed a high-speed-low-force strategy to avoid possible damage. The final step was to remove the sacrificial fibres from the composites and to generate hollow vessels. The specimens were given a heating treatment at 200 ºC in a vacuumed chamber for 24h. After the PLA sacrificial components had been fully depolymerised, hollow vessels were generated with no residue, as in **Fig. 3.4**.

The healing agents were the mixed and degassed IN2 Epoxy Infusion Resins (EP-IN2-S-1, Easy Composites Ltd.), dyed in red colour (Signal Red, Epoxy pigment paste, West & Senior Ltd.).

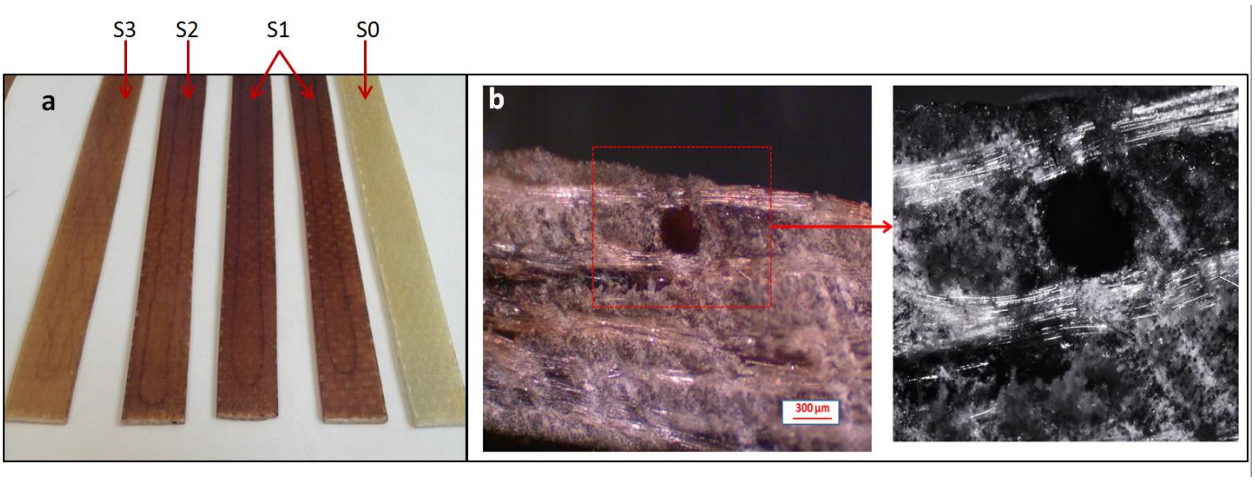

Figure 3.4. Fabricated samples. a) Top view of samples; b) cross-section image of a vessel.

3.2.4. Experimental procedures

Flexural properties were assessed based on a three-point bending test carried out on a MTS Criterion Model 43 machine (MTS Criterion® Series 40 Electromechanical Universal

Test Systems). The support span in the three-point bending fixture was fixed at 125 mm. All the mechanical tests took place at room temperature with a displacement-control mode such that the loading rate of 3 mm/min was applied.

In the first stage, the test started with reaching a displacement of 7.81mm, and the collected data was used to calculate flexural modulus. The specimens were removed from the fixture and observed using transmitting light photography and an optical microscope to collect crack information. Afterwards, specimens were loaded again to reach peak stress, creating large-scale cracks which were also observed. It is worth noting that the test on S1 was different compared with the tests on S2 and S3. S1 specimens were grouped into S1.1 and S1.2. The aim of the test on S1.1 was to understand the response of specimens when vessels were near to the compression surface, close to the loading pin. While in the test on S1.2, vessels were near to the tension surface, close to the supporting span.

In the second stage, bending did not stop until peak load. Afterwards, 1 ml healing agents were injected into the vessels using an analogue adhesive dispenser and the samples self-healed at room temperature for 24h. Afterwards, the healed specimens were tested again to measure the healing efficiency.

In the third stage, four groups of identical samples were tested separately by different bending levels: 22mm, 26mm, 30mm and 34 mm. Different bending levels caused various damage conditions. Afterwards, the samples recover and be re-assessed as in Stage 2.

3.2.5. Assessment methods

The peak stress flexural moduli are calculated using **Eq. 3.1** and **Eq. 3.2** respectively.

$$\sigma = \frac{3FL}{2bd^2} \quad (3.1)$$

$$E = \frac{L^3 m}{4bd^3} \quad (3.2)$$

where F=Peak load, L=Support span, b=Width of tested beam, d=Depth of tested beam and m=The gradient of the initial straight-line portion of the load deflection curve

Healing efficiency is calculated using **Eq. 3.3**:

$$\eta = \frac{f_{Healed} - f_{damaged}}{f_{virgin} - f_{damaged}} \times 100\% \quad (3.1)$$

where f refers to the property of interest (peak stress or flexural modulus).

3.3. Results and discussion

3.3.1. Effects of vessel configurations on the flexural properties

The flexural properties of samples incorporating different vessel configurations are shown in **Fig. 3.5**. As expected, S0, the fibre-reinforced laminates with no incorporated vessels are the strongest materials among all samples. Only S2 could have flexural modulus on the similar level of S0, while the others are poorer than S0 regarding both peak stress and modulus. The reduction in peak stress varies from 11.8% to 31.7%, and that in flexural modulus is in the range -10.02% to 29.8% (in fact, S2 presents a higher averaged flexural modulus than S0). The comparison of S1.1 and S1.2 suggests that the location of the vessels could cause differences in the flexural properties of the overall structures. Another interesting observation is that although the increase in the complexity of vessel

configurations brings more void into the structure, this does not cause more reduction in flexural properties. As can be seen, even if S2 and S3 have the most sophisticated vessel configurations, they are significantly stronger than S1.1 and S1.2. To explain the phenomenon, damage conditions need to be looked into.

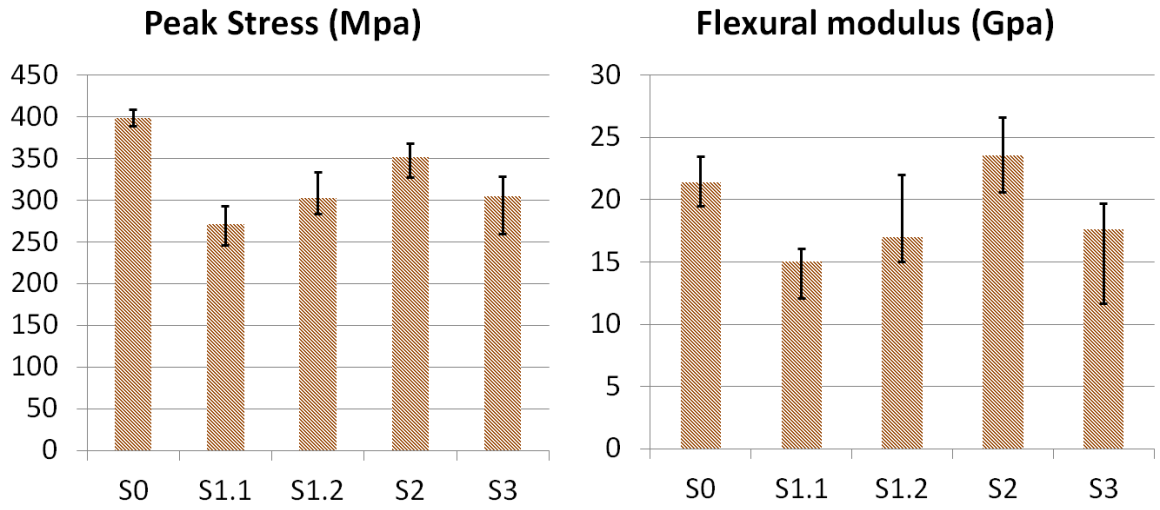

Figure 3.5. (a) Displacement-load curves; (b) Peak stress

For fibre-reinforced laminates, there are three popular types of crack: fine cracks on a surface, debonding, and fracture of structural fibres. Fine cracks on a surface typically happen on the tension surface of the matrix. Debonding is the separation of the polymer matrix and structural fibres. When materials sustain bending, fine cracks on a surface may propagate and reach the structural fibres, causing local fibres to debond. A special case in debonding is delamination meaning a large area of structural fibres in one layer or several layers leave their adjacent matrix, which usually occurs when the shear force is greater than the interlaminar toughness. Fracture of structural fibres can be the most severe damage in fibre-reinforced composites as the structural fibres buried in the matrix are the

primary loading component. To explain the results in **Fig. 3.5**, different types of cracks need to be identified for different samples.

Transmitting light photographs showing damage progression in S0, S1, S2 and S3 are given in **Fig. 3.6**. In the initial stage of bending S0, there were sounds of microcracks, suggesting the emergence of fine cracks on a surface. There were no obvious cracks on S0 until the samples reaching failure. The dark spot is a debonding of matrix and reinforcement fibres on the compression surface observed under an optical microscope, shown in **Fig. 3.7**. For S1, it could be seen that with an increasing bending, transverse fine cracks can be observed on the tension surface of S1.1 and S1.2. It can be seen a large scale of delamination and debonding occurred near the compression surface of S1.1, shown in **Fig. 3.8**. Even though S1.1 and S1.2 had internal hollow vessels, the location of damage is on the surface of the composites, and internal damage remained on an invisible scale. Delamination and debonding occurred on the compression surface and the density of transverse micro cracks on the tension surface increased with bending. As discussed in the last paragraph, the most possible reason for the reduction in flexural properties is delamination. When vessels are placed close to a compression surface, the voids can greatly increase the possibility of delamination near the compression surface. This could be the reason that S1.2 has better flexural properties than S1.1.

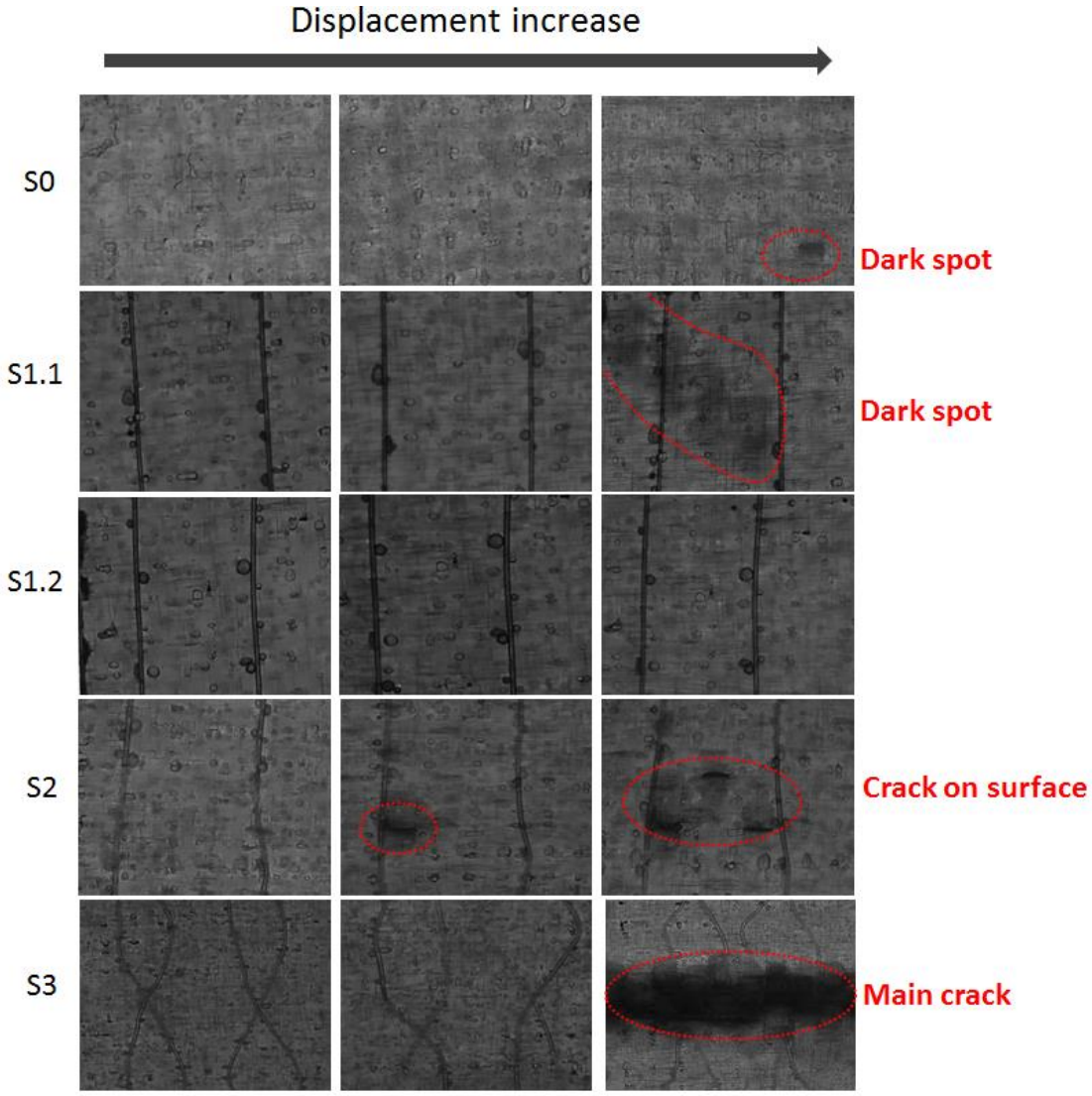

Figure 3.6. Transmitting light photography

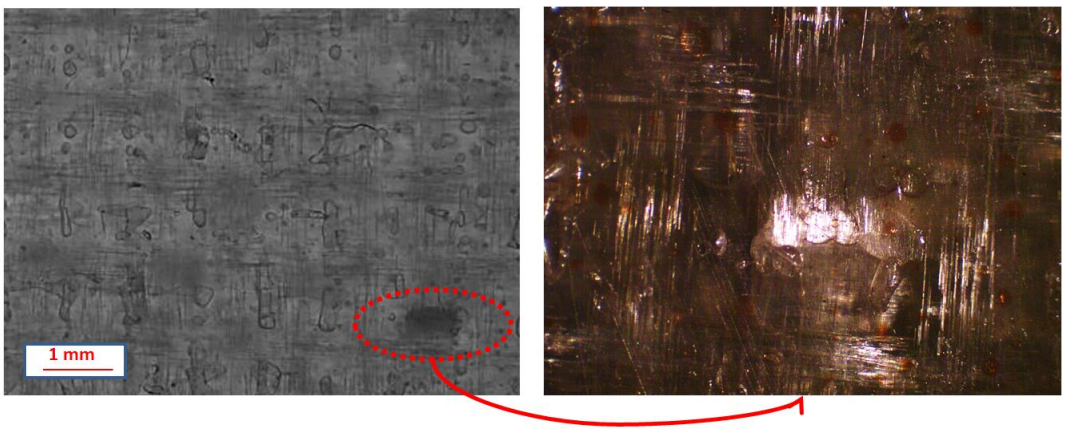

Figure 3.7. Dark spot on S0

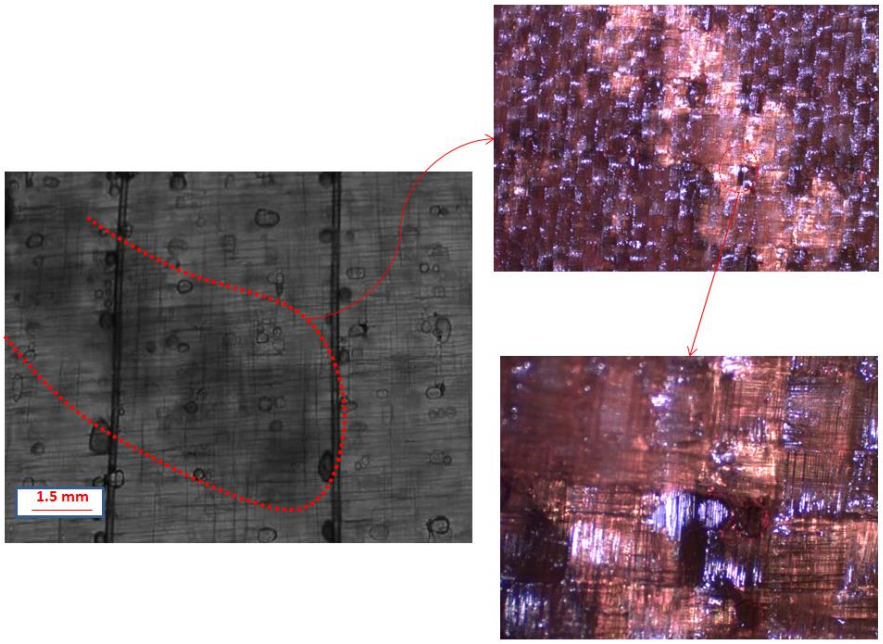

Figure 3.8. Dark spot on S1.1 is delamination and debonding on the compression surface

For S2, it could be seen in **Fig. 3.6** that there is only one dark spot in the second picture but the number increases to three in the third picture. The crack is the fracture of structural fibres that observed near the compression surface, as shown in **Fig. 3.9**. Compared to S0, S2 has more cracks on the compression surface and the crack is a combination of debonding and the fracture of structural fibres instead of single debonding. For S3, there is no obvious major cracks in the second picture, but a very deep and large scale damage can be seen in the third picture, as shown in **Fig. 3.6**. The detail of the big damage is shown in **Fig. 3.10**. Obvious fracture of fibres made the layer on the surface not capable of enduring loads. The cross section image indicates that damage occurred

mainly on the surface of the composites, while the core of the composites was not greatly deformed.

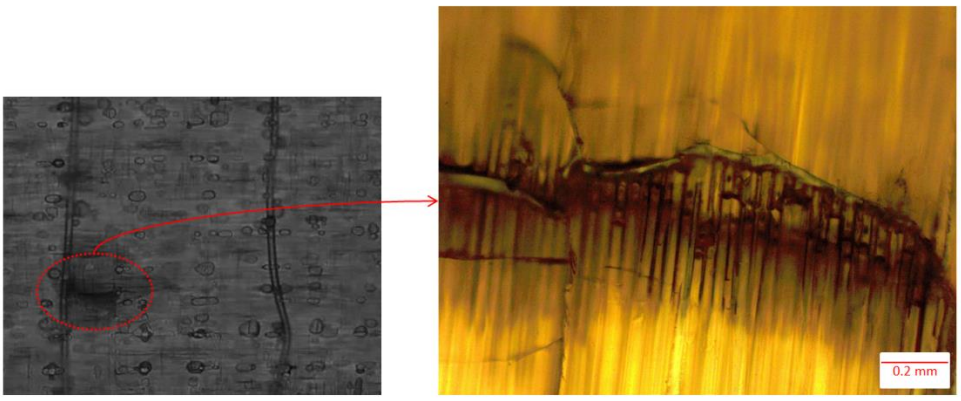

Figure 3.9. A combination of debonding and fracture of structural fibres on the compression surface of S2.

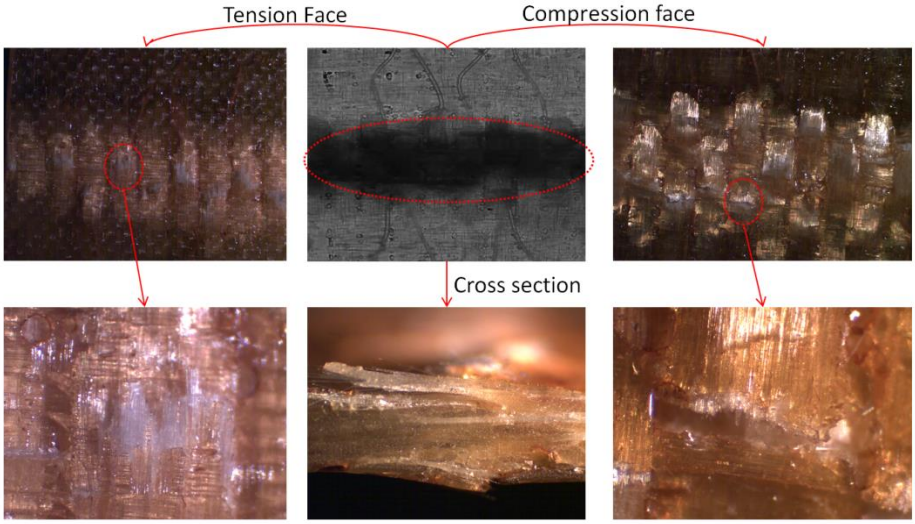

Figure 3.10. Optical micrograph of damaged specimen after flexure tests

The results in **Fig. 3.5** can be explained as follows. When vessels are placed near to a compression or tension surface, as in S1, the voids introduced could cause severe debonding near the surface as shown in **Fig. 3.8.** This is the primary reason to explain the

reduction of flexural properties observed in S1. When the vessels are placed in the core of the composites, as in S2 and S3, the voids are in the core only, and the delamination near the core is not worsened (**Fig. 3.9** and **3.10**). The final failure mode is the fracture of structural fibres on the surface layers, instead of delamination, meaning a larger threshold before the composites reaching the peak stress. Therefore, the S2 is significantly stronger than S1. The comparison of S2 and S3 proves that the flexural properties of the composites could be negatively influenced by the volume of voids in the core of the composites. When the configuration is complex resulting in more introduced voids, the material is weakened.

3.3.2. Effects of network configurations on healing performances.

After the materials are damaged by the bending, they recover for 24h, and healing performances are shown in **Fig. 3.11**. S1 has the lowest healing efficiency in terms of both peak stress and flexural modulus, compared to those of S2 and S3. The recovery of peak stress in S2 and S3 is significantly higher than in S1. S3 has the best healing performance, with the recovery of peak stress and flexural modulus near 50% and 150% respectively. It could be concluded that network configuration adopted in S3 is able to provide the best healing performance.

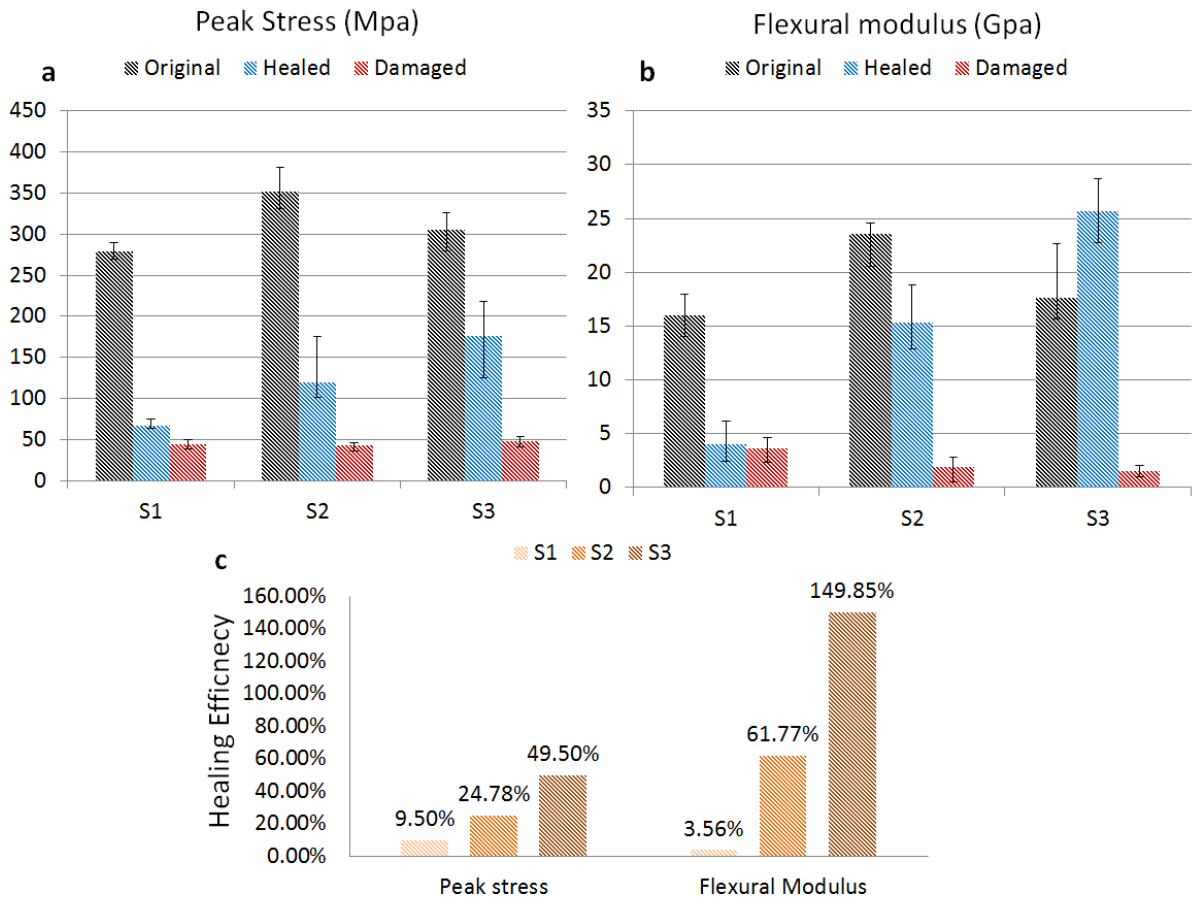

Figure 3.11. Healing performances of composites embedded with different vessel configurations. (a) Peak stress; (b) Flexural modulus; (c) Healing efficiency.

Fig. 3.12 shows healed samples under an optical microscope. In S1, the released healing agents were not obvious, except for an inconspicuous ‘bruises’ near one vessel. As vessels in S1 existed in only one layer, the outflowed healing agents cannot reach other layers, resulting in a weak recovery. Regarding S2 and S3, adequate healing agents were released and filled the gaps between different layers as the vessels pass through multiple layers. At the same time, healing agents could also reach the surfaces. Compared to S2, the red area on S3 is larger, indicating healing agents covered more cracks than that in S2. The results prove that the vessel configuration adopted in S3 is able to provide a larger coverage of healing agents. As a result, S3 presents the best healing performance.

Overall, it could be summarised that network configurations have a large effect on healing performances. To restore flexural properties, it is essential that vessels have a large coverage, which consists of coverage in interlaminar plane and in multiple layers.

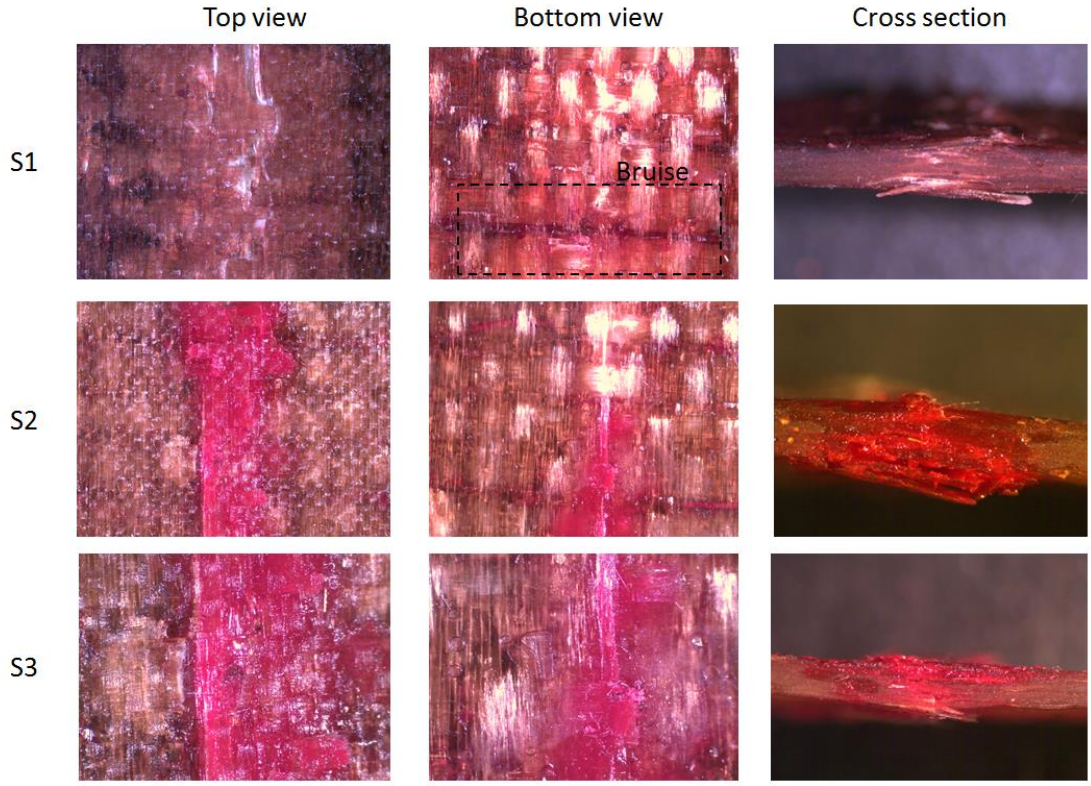

Figure 3.12. Healed samples under optical microscope

3.3.3. Effects of bending levels on healing performances

Considering that S2 presented minor effects on mechanical properties (**Section 3.3.1**), and good level of healing performance (**Section 3.3.2**), this design was employed in this section. The flexural responses of undamaged composites, damaged composites, and healed composites are given in **Fig. 3.13**.

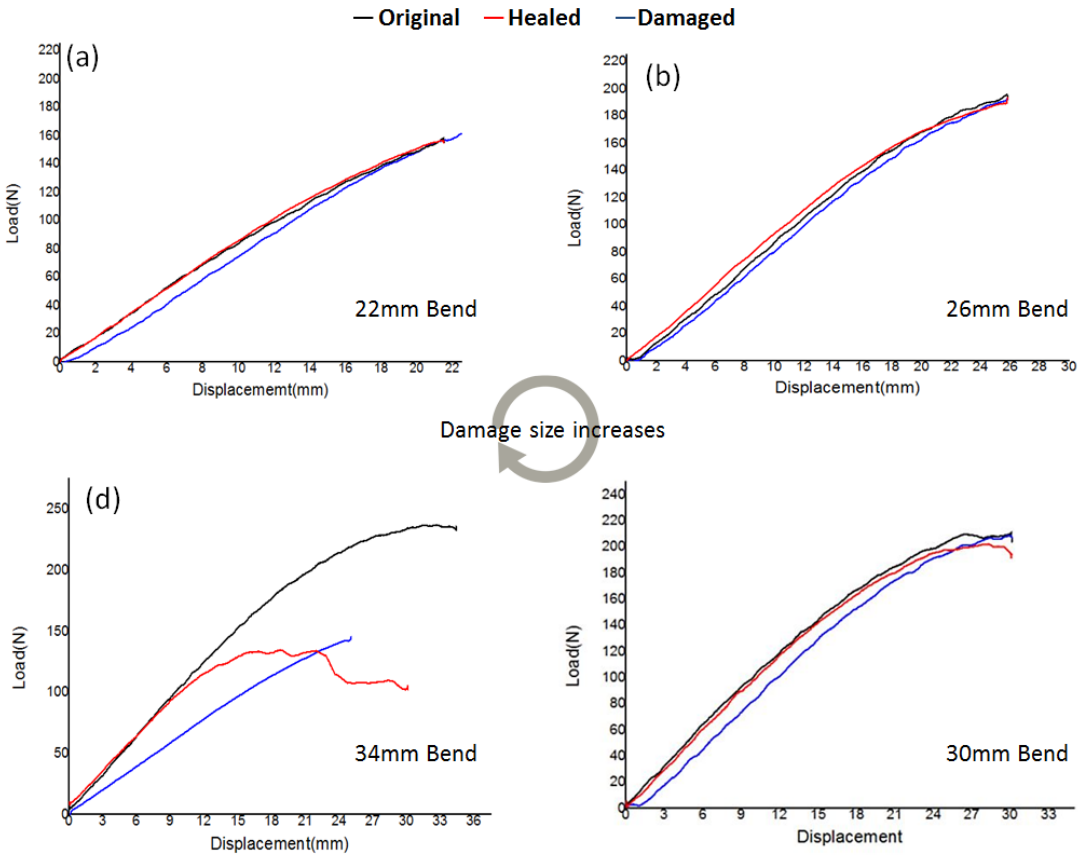

Figure 3.13. Healing performances of composites endured different damaged conditions. Bending conditions: (a) 22 mm; (b) 26 mm; (c) 30 mm; (d) 34 mm.

As can be seen, healing performances decreased significantly when bending reaches 34 mm. Cracks in fibre-reinforced laminates are in different phases owing to various bending levels. In the first phase (**Fig. 3.13a and 3.13b**), which is the mildest one, transverse micro cracks on the surface are the primary cracks (**Fig. 3.14a**). With an increasing bending force and displacement, the cracks propagate into the core and reach vessels to cause the outflow of healing agents. Healing agents flow through the transverse cracks to reach the surface (**Fig. 3.14b**). In this phase, composites can fully recover as long as the healing agents could be released from the vessels. Therefore, it is essential that vessels have a large coverage so that cracks have a large possibility to trigger the

release. In the second phase (**Fig. 3.13c**), debonding starts to emerge, accompanied with minor ruptures of structural fibres. During this phase, material could still achieve satisfactory recovery, as healing agents can reach the gaps and solidify (**Fig. 3.14c and 3.14d**). Although parts of the reinforcement fibres have been damaged which cannot be healed, the main architecture remains undamaged. When it comes to the third phase (**Fig. 3.13d**), in which bending forces entirely break the reinforcement structure, although healing agents can still fill the gaps, the healing performance is poor as the polymer healing agents cannot recover structural fibres (**Fig. 3.14e and 3.14f**). This result calls for the development of new healing agents or mechanisms to recover structural fibres.

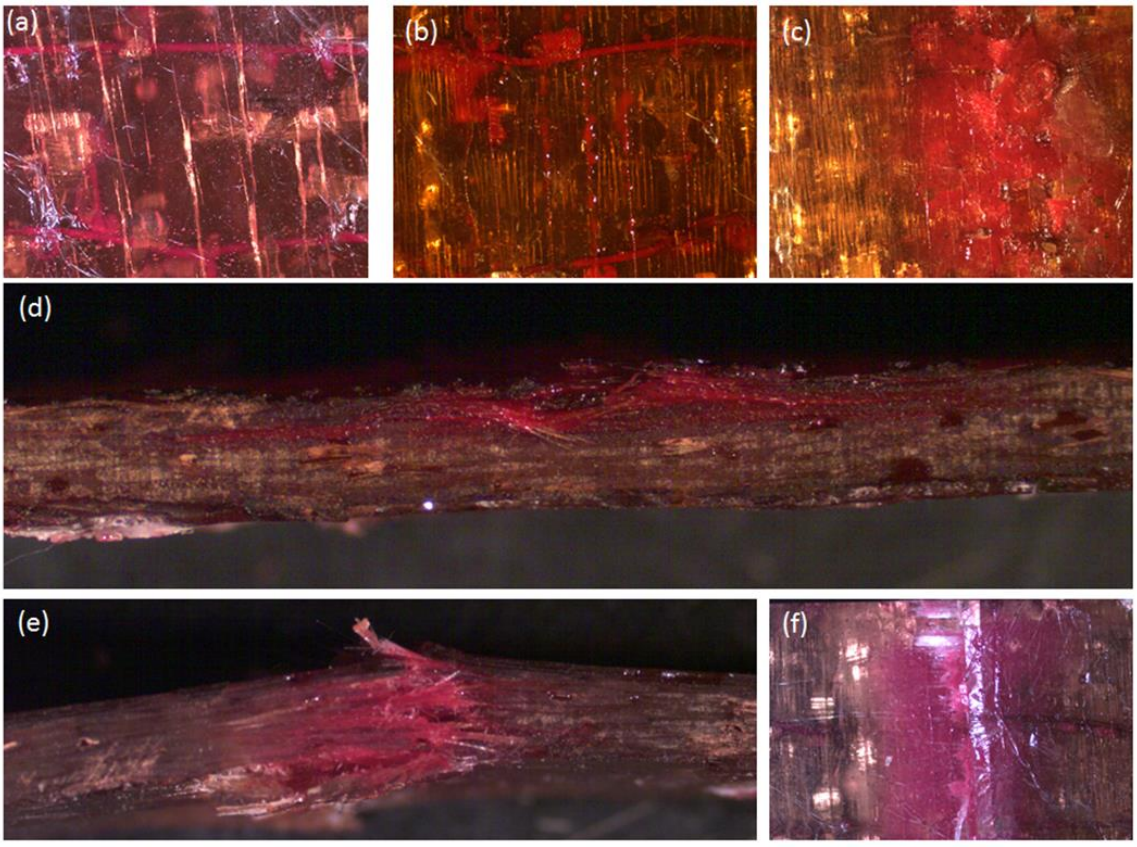

Figure 3.14. Healed samples under an optical microscope. (a) Transverse microcracks; (b) Outflowed healing agents from transverse microcracks; (c) Healing of delamination and cracks on the surface; (d) Cross section of a phase-two damaged laminate; (e) Cross section of a phase-three damaged laminate; (f) Top of a phase-three damaged laminate.

In conclusion, vessel-based self-healing composites can only heal debonding or any other types of damage to the matrix. Cracks in composites initialise with transverse micro cracks, and develop into debonding, delamination, and minor fracture of fibres on the surface layer. In these cases, the composites are capable of full recovery. However, when the bending continues and the damage thoroughly breaks the reinforcement fibres, the composites can no longer recover.

3.4. Summary

The chapter investigated the effects of vessel configurations on the flexural properties and healing performances of a 3D orthogonally woven glass/epoxy composite. The studied vessel configurations were of three popular types: straight vessels in one layer, wave-like vessels in multiple layers and herringbone-and-wave-like vessels in multiple layers. The vessels were produced by the vaporisation of sacrificial PLA fibres. The following key points can be concluded based on the experimental results.

1. Different vessel configurations can cause different levels of reduction in the flexural properties of fibre-reinforced composites. Placing the vessels near the tension or compression surface resulted in obvious reduction in flexural properties. In comparison, when they were in the core, the modest decreases in strength and modulus were statistically insignificant. However, the reduction became greater with the amount of voids introduced.
2. Vessel configurations can significantly affect the healing performances. When vessels only existed in one layer of the laminates, healing agents could not reach

other layers to cure delamination/debonding, resulting in poor healing performances. When vessels penetrated multiple layers, the healing performances improved significantly. In addition, vessels having larger in-plane coverages could also promote the recovery.

3. The healing efficiency of materials recovering from various levels of bending damage can be different, although the same vessel configuration is employed. When the damage was minor, mainly consisting of debonding and delamination, the composites were able to achieve a high healing efficiency, even a full recovery. However, when the place where structural fibres fractured became the primary crack, the healing performance was poor. The result suggests that there is a need for a new healing agent or mechanism to repair not only the matrix but also the structural fibres.

The above principles should be taken into consideration when designing vessel-based self-healing laminates. When the correct vessel configuration is adopted, the voids can have minor effects on flexural properties, and a healing efficiency higher than 100% is achievable as long as the damage does not break the structural fibres. Otherwise, healing performance can be unsatisfactory.

Chapter 4 - Sustainable self-healing at ultra-low temperatures in structural composites incorporating hollow vessels and heating elements

4.1. Preliminaries

The good healing performances reported so far were attained only when there were favourable healing conditions, such as a suitably high ambient temperature or an appropriate radiation treatment, which is often impossible to ensure in practical applications. For instance, composites used on an aircraft may endure temperatures as low as -60 ^{0}C, at which almost all healing liquids would be frozen and cannot be activated. This has become one of the main barriers to the wider adoption of self-healing composites, prompting efforts to develop systems that can self-heal regardless of environmental and damage conditions. A few researchers have been trying to do this by employing new healing liquids, and have reported healing agents able to heal at temperatures as low as 10^{0}C [164], [165]. The effects of ultra-low temperatures on a typical healing agent have also been investigated [166]. However, real high-efficiency healing at very low temperatures (-40 ^{0}C to -80 ^{0}C) is still impossible.

This chapter reports a design to enable self-healing in fibre-reinforced composites at ultra-low temperatures. With the proposed approach, healing was fulfilled by two components: 3D vessels and a thin layer of conductive material. The vessels were embedded inside the structural composites with the purpose of delivering and releasing healing agents. The thin layer was to supply heat internally from the composites to cause de-icing and provide a suitable temperature for healing. The vessel-based design instead of a capsule-based design was selected because the former is capable of recovery from

large-area damage, as healing agents can be continuously pumped into the vessels. Furthermore, the vessel network would in general only have minor effects on the tensile properties of the composites [128]. The fabricated composites are able to recover from severe delamination with average efficiencies around 100% at ultra-low temperatures. It is also discussed the effects of the conductive sheets on interlaminar and tensile properties of the laminates. The experimental results in this chapter indicate that the sheets reduced interlaminar strength but increased tensile properties. The role of the chapter in the thesis is shown in **Fig. 4.1**.

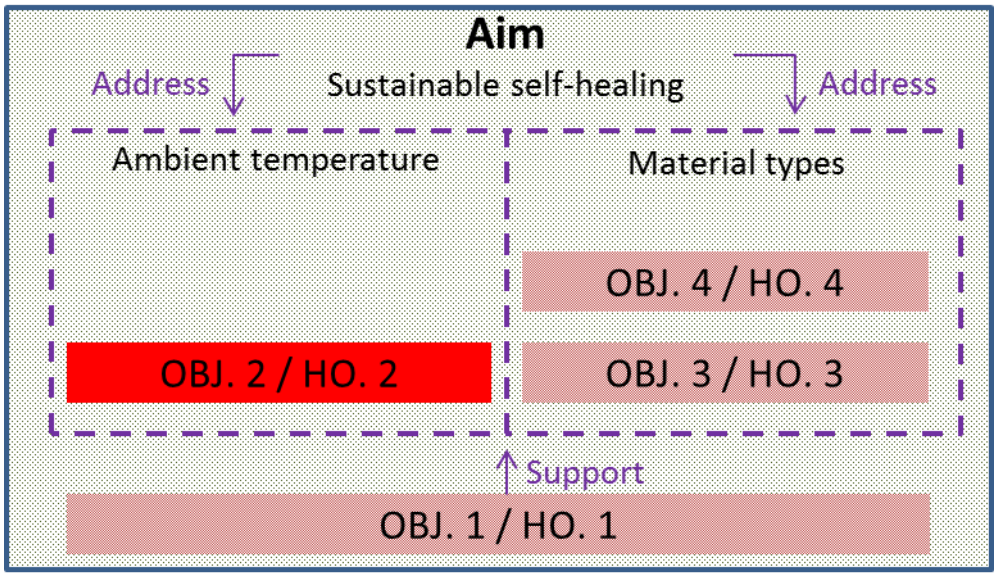

Figure 4.1. Role of Chapter 4 in the thesis (red area)

4.2. Methods

4.2.1. Structure of the composite

The composite is a glass fibre-reinforced laminate embedded with wave-like hollow vessels and conductive sheets, as shown in **Fig. 4.2a**. When delamination occurs at low

temperature, cracks can propagate and break the vessels. Heat could be generated internally through electrical heating to defrost, releasing liquid healing agents into the cracks. Solidification of the agents could also be accelerated by the internal heat. The healing process is shown in **Fig. 4.2b**. Here, we discuss the wave-like hollow vessels and conductive sheets separately.

- Wave-like hollow vessels in the core

The wave-like configuration was proposed by Patrick *et al*. [7] who were the first to use it as well as a herringbone configuration for self-healing in FRCs. The hollow vessels can be made by the vaporisation of sacrificial components (VaSC) incorporated in the material with the reinforcement fibres. PLA sacrificial fibres 300μm in diameter were selected as sacrificial components as they left little residues, greatly reducing the risk of blocking the channels [7], [115], [116], [130]. Other methods to fabricate internal hollow structures include using hollow fibres [97], [161], electrostatic discharging [135] and laser direct-writing [136]. However, only VaSC can produce large-scale 3D vascular networks following an accurate pre-designed pattern.

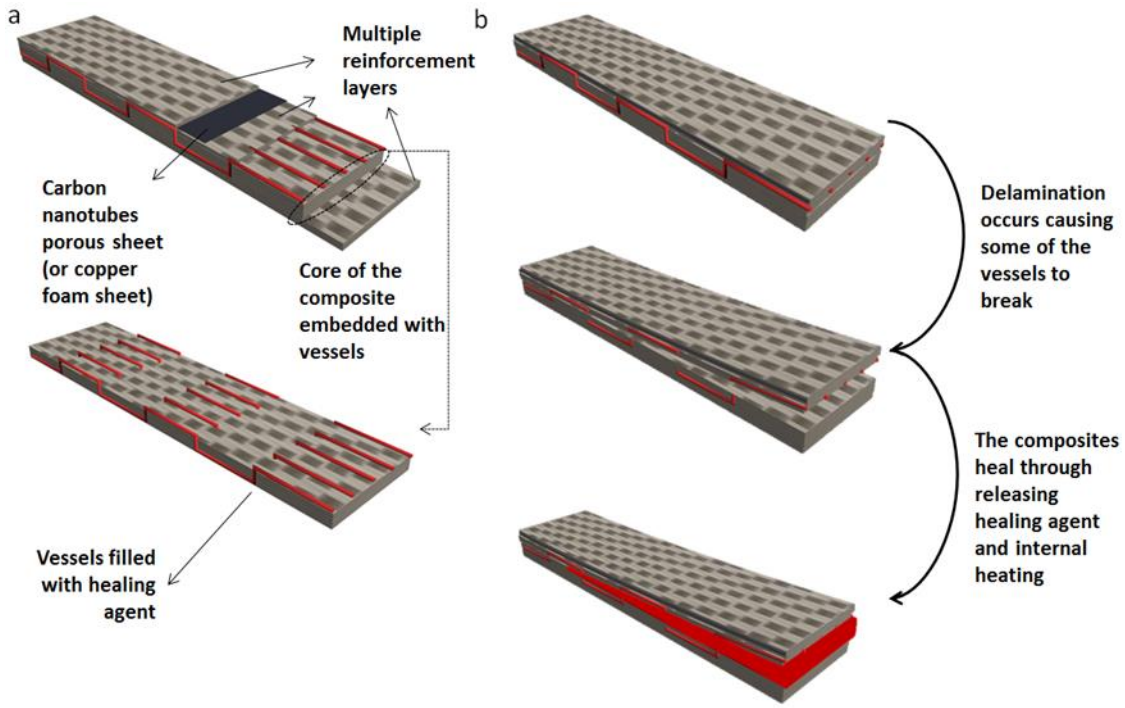

Figure 4.2. (a) Internal structure of the composites; (b) Damage-bleeding-healing process

- Conductive porous sheets

The conductive layer must satisfy two requirements: good electrical conductivity and good thermal conductivity. To fabricate this conductive layer, two types of conductive sheet were selected: porous copper foam sheet (CFS) and porous carbon nanotube sheet (CNS). Metal foam has already been applied in batteries [167], heat exchange devices [168] and energy absorbers [169]. The CFS (see **Fig. 4.3a**) had a thickness of 0.5 mm and a porosity of 96~98%. It had a thermal conductivity around 10 $W \cdot m^{-1} \cdot K^{-1}$, very high electrical conductivity (around 3.9×10^6 S/m) and a large area of contact with the host material. The other conductive sheet (see **Fig. 4.3b**), CNS, with a thickness of 40 μm, had a stable electrical conductivity of $1.25 \sim 1.38 \times 10^{-4}$ Ω·m and a thermal conductivity estimated to be in the range 100~1000 $W \cdot m^{-1} \cdot K^{-1}$. The thermal conductivity was measured by using the

method in the work of Wang *et al*. [170]. The CNS was fabricated by multiple steps of single wall carbon nanotubes (SWCNTs) dispersion and suspension filtration [151].

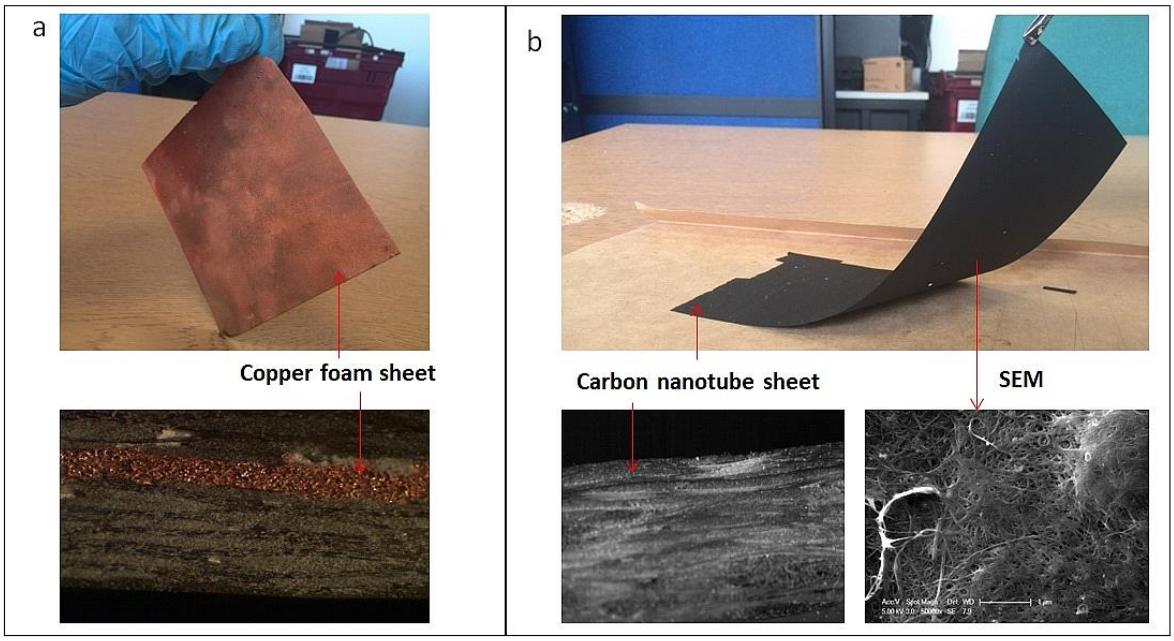

Figure 4.3. a) Porous copper foam sheet; b) Porous carbon nanotube sheet.

4.2.2. Fabrication procedure

1) **Fabrication of the core of the laminates**. The core of the laminates (eight layers of reinforcement fibres in the middle) was incorporated with PLA sacrificial fibre in a wave-like configuration by needle stitching. To install the PLA sacrificial fibres, eight layers of woven glass fibres (area density of 290 g/m2 for each layer) were fixed on a needlework frame to prevent the distortion of the woven architecture. The PLA sacrificial fibres (300μm VascTech fibres, CU Aerospace Ltd.) were manually embedded into the layers of woven glass fibres in a square-wave-like configuration.

2) **Resin Infusion preparation**. A polypropylene table ready for resin infusion was covered with PVA releasing agent to prevent damage during de-moulding. The releasing agent became completely dry in 30 min at room temperature. The incorporated reinforcement fibres and other untreated reinforcement fibres as well as the conductive sheets were deposited layer by layer in the following sequence: Bottom – Four layers of normal glass fibres – Eight layers of glass fibres with the sacrificial components – two layers of normal glass fibres – conductive sheet – two layers of normal glass fibres – Top. A nylon sheet was placed at the mid-plane position and offset 30 mm from one of the edges. The sheet served as a crack created during the fabrication of the composite. The laminates were covered with a peel ply, resin infusion mesh and infusion spiral before sealing with sealant tape and vacuum bagging film.
3) **Resin infusion**. Air was extracted from the sealed space by using a vacuum pump and a PVC vacuum hose to reach a vacuum level of 17 kPa. After the vacuum pump was turned off, the sealed space was left for 1 hour to ensure no pressure drop. Epoxy resin and hardener (Very High Temperature Epoxy, Easy Composites Ltd.) were mixed at a ratio of 100:35 parts by weight and degassed at 35 ^{0}C for 30 minutes in a vacuum chamber. Afterwards, the mixture was infused into the sealed space.
4) **Curing.** After infusion, the mixture was cured for 36 h at room temperature and then put through post-cure heating cycles at 40 ^{0}C, 60 ^{0}C, 80 ^{0}C, 100 ^{0}C and 120 ^{0}C each for one hour, and 140 ^{0}C for 3 hours, as suggested by the supplier.
5) **Cutting.** After the resin was fully cured, the composite was cut into identical specimens. The fully cured composite which had a thickness of 4 mm was cut into 180 mm × 25 mm pieces using a grit saw and polished with sand paper. The cutting and polishing

followed a high-speed-low-force strategy to avoid damage. The cross-section of the samples are shown in **Figs. 4.3a** (FRCs + CFS) and **4.3b** (FRCs + CNS).

6) **VaSC.** The specimens were heated up to 200 ^{0}C in the vacuum chamber for 24h to remove the sacrificial components. This left a hollow vascular network inside the composite in a wave-like configuration.
7) **Injection of healing agents.** After the fabrication of the hollow vessels, the healing agent, which was a pre-mixed two-part epoxy (RT151, ResinTech Ltd.) dyed in red, was injected into the vessels with a controllable liquid dispenser.

4.2.3. Healing performance assessment and analysis

The mechanical strength of the samples was assessed using the double cantilever beam (DCB) test, as shown in **Fig. 4.4a**, following the procedure described in **Section 4.2.5**. For each sample, a total of three DCB tests were conducted. The first test was to measure the original interlaminar strength and to break the sample. Afterwards, the broken sample was loaded again for the second test to reveal the residual strength. Then it was given a 24h rest to heal at -60 ^{0}C before taking the third test to assess the healing performance. The healing process started with a continuous injection of healing agents into the vessels, followed by the specimens being placed in an ultra-low temperature (-60 ^{0}C) chamber. During healing, the conductive layer was electrically heated. The power used was 7 W and 9.45W for CFS and CNS respectively. A thermometer was attached to the specimen to monitor its temperature. The cross-section of the healed sample is shown in **Fig. 4.4b**. During the test, cracks propagated and traversed the wave-like vessels as in **Fig. 4.4c.**

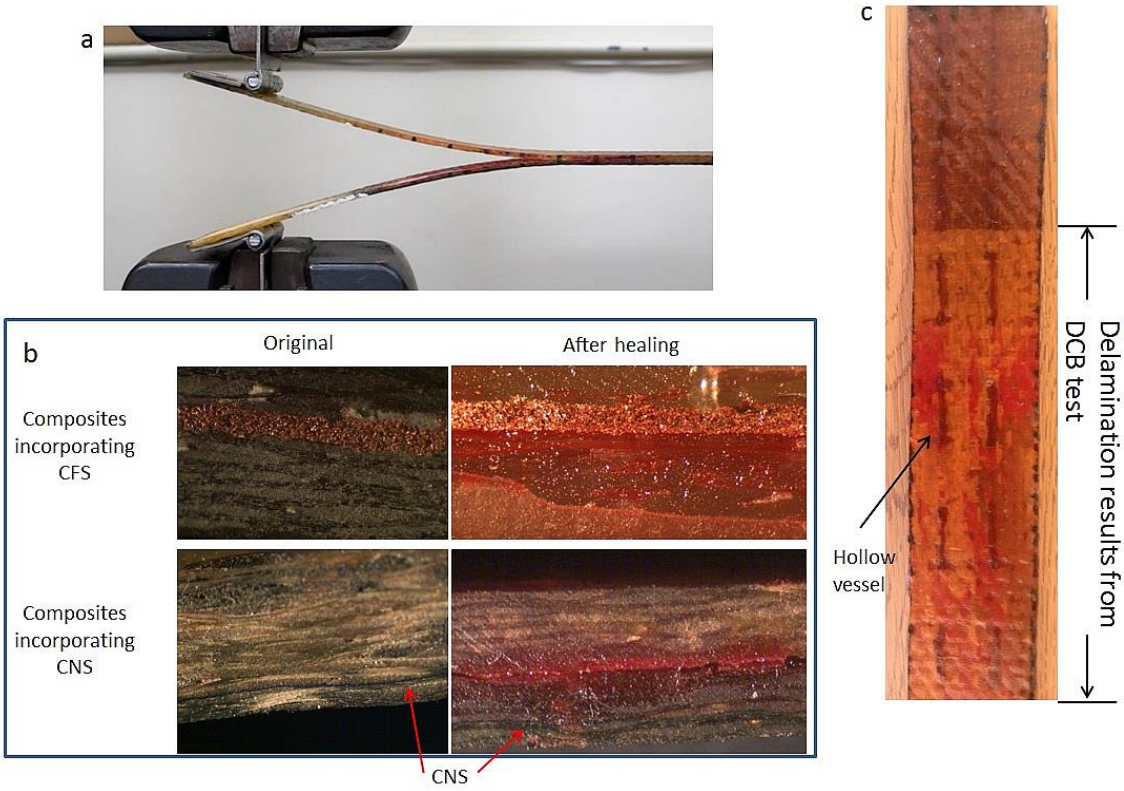

Figure 4.4. (a) DCB test of a healed composite specimen incorporating CNS; (b) Composites incorporating CNS and CFS; (c) Fibre-reinforced composite incorporating wave-like micro vessels after DCB test.

- Calculation of healing efficiency

The healing efficiency in relation to peak load (η_1) was calculated as [7], [171]:

$$\eta_1 = \frac{L_{Healed}}{L_{Virgin}} \times 100\% \quad \textbf{(4.1)}$$

where L_{Virgin} is the achieved maximum load before damage and L_{Healed} is the maximum load after the specimen has recovered from a 80 mm mode-I fracture.

The healing efficiency in relation to fracture energy (η_2) was calculated as [7]:

$$\eta_2 = \frac{U_{I,Healed}}{U_{I,Virgin}} \times 100\% \quad \textbf{(4.2)}$$

where $U_{I,Healed}$ and $U_{I,Virgin}$ are the fracture energies of a specimen before damage and after recovery respectively, derived from first principles as the area under the load–displacement trace at a particular crack length.

4.2.4. Effects of the conductive sheets on interlaminar properties

The introduction of a conductive sheet created a new layer inside the laminates. The effects of having this layer on interlaminar properties were revealed using DCB tests to compare samples with and without the sheets.

Three groups of samples, each containing 5 specimens, were made using the techniques described in **Section 4.2.2**. In the first group, specimens were fibre-reinforced laminates with the carbon nanotube sheet in the middle layer. In the second group, the carbon nanotube sheet was replaced by the copper foam sheet. Specimens in the third group were ordinary fibre-reinforced laminates. All specimens were 120 mm in length, 20 mm in width and 4mm in thickness, and had 20 mm deep pre-crack on one edge. DCB tests followed the procedure outlined in **Section 4.2.5**.

4.2.5. Double cantilever beam (DCB) test

Aluminium piano hinges were attached onto the specimen using a structural adhesive (Loctite 330 Glue and Activator Multibond Kit). After heating for six hours at 60 ^{0}C, the adhesive was fully cured and testing was carried out on a MTS Criterion Model 43 machine. The specimens were loaded through the bonded hinges in quasi-static tension to induce mode-I fracture propagation along the mid-ply interlaminar region until the crack

reached 80 mm. The displacement-controlled crosshead speed was 5 mm/min during loading.

4.2.6. Effects of the conductive sheets on tensile properties

The effects on two types of composites were investigated: random-discontinuous cotton-fibre-reinforced composites (type E) and woven carbon-fibre-reinforced composites (type C), as in **Fig. 4.5**. E contained four layers of cotton breather cloth and C had four layers of woven carbon fibres. As the fillers are different, E and C have different bearing strengths, representing weak and strong polymer composites respectively.

E and C are further divided into two sub groups (E1/E2 and C1/C2) as shown in **Table 4.1**. The effects of the CNT layer can be revealed through comparing E1 (or C1) to E2 (or C2).

Table 4.1. Details of the sub-groups of composites

Sub-group code	Description	Number of Specimens
E1	Random-discontinuous cotton fibre composites	5
E2	Random-discontinuous cotton fibre composites embedded with porous CNT layer	5
C1	Woven carbon fibre composites	5
C2	Woven carbon fibre composites embedded with porous CNT layer	5

The porous CNT layer was fabricated inside E2 and C2 by embedding a carbon nanotube sheet using the techniques described in Section 2.2. After the resin was fully

cured, the composites were cut into 100 mm × 9 mm × 2 mm specimens. The specimens were placed in a chamber at 50 C for 12h to release internal strain. A MTS Criterion testing machine (MTS Criterion Model 43 Electromechanical Universal Test System) was used to collect data. Each specimen was subject to tension parallel to its long edge whose effective length is 15mm. The loading rate was 0.5mm/min. After tensile testing, the samples were observed under optical and electron microscopy to reveal cracking patterns and the nature of the fracture.

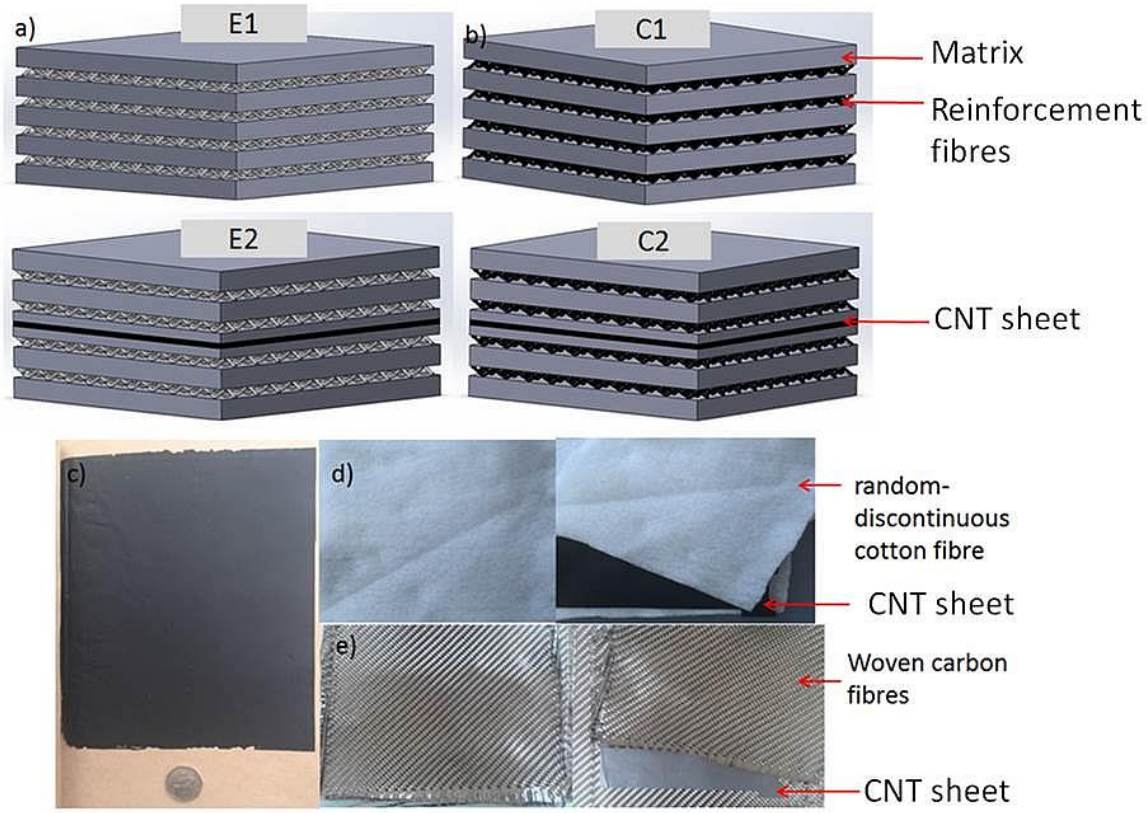

Figure 4.5. a) Schematic of composite E; b) Schematic of composite C; c) CNT porous sheet; d) Random-discontinuous cotton fibres and CNT sheet; e) Woven carbon fibres and CNT sheet

4.3. Results and discussion

4.3.1. De-icing performance

Fig. 4.6a shows the temperature of a sample incorporating CNS under electrical heating. With the applied voltage maintained between 10V and 16V, the steady-state temperatures of the specimens remained in the range 20^{0}C to 85 ^{0}C (**Fig. 4.6a**), which was sufficiently high to enable curing in 24h (**Fig. 4.6b**). There was no severe heat concentration due to the use of a relatively low electrical current (200 mA) and its good thermal conductivity. The composite was able to be fully de-iced in 90s (**Fig. 4.6c**) which also demonstrates the efficiency of CNS.

The composite with CFS was able to keep the temperature in the range 5 ^{0}C to 20 ^{0}C. However, for the design using CFS, it was found that although the healing agent was still active in the temperature range, 24h was not long enough for it to cure fully. Increasing the electrical power to raise the internal temperature may seem a solution to this problem. However, this was almost impossible as the copper foam had an extremely low resistivity, and so a very large electrical current – 55 A in this case – was required to generate the heat necessary to keep the healing agent active. Such a high electrical current might generate extremely high temperature at the points of contact between the sample and the power supply and may cause local melting. In our experiments, although four of the five samples tested successfully healed themselves, there was still one that failed due to heat concentration. Therefore, although increasing the supplied power will raise the internal temperature, it also heightens the risk of local overheating as a side effect.

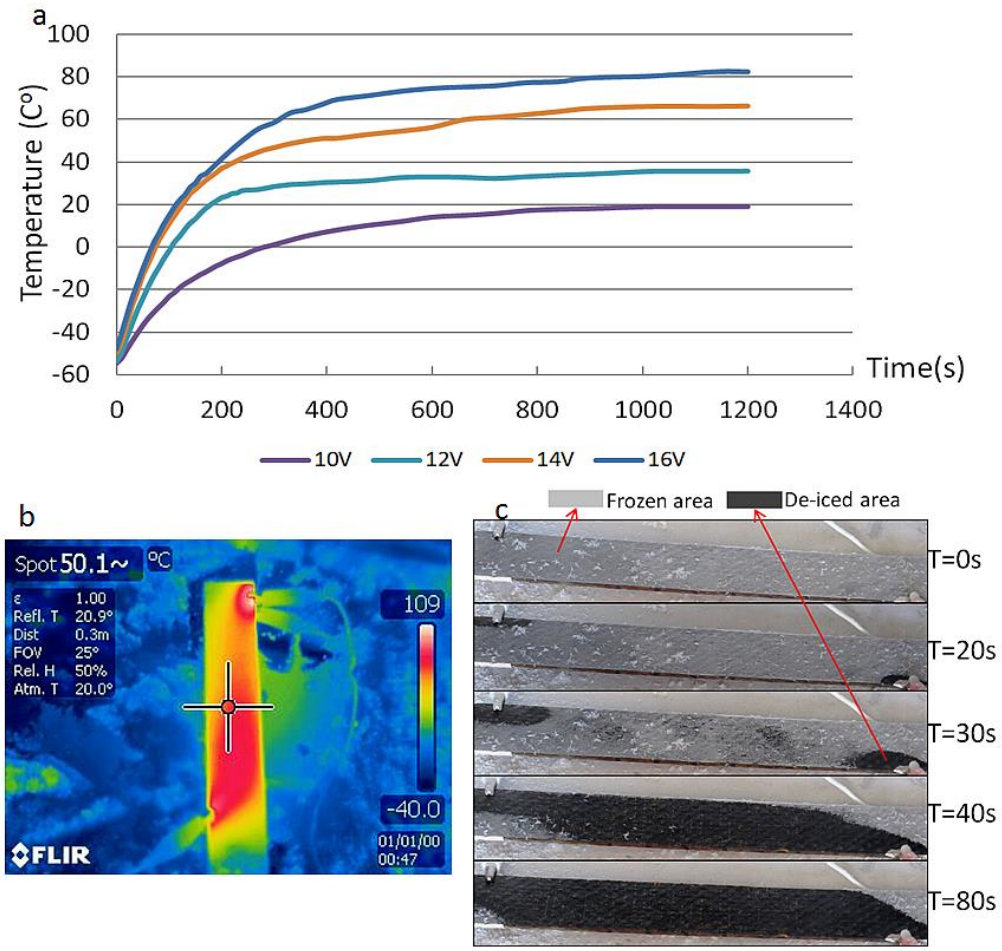

Figure 4.6. (a) Temperature of the specimen as a function of time and applied voltage; (b) Thermal distribution in the composite heated by CNS in an ultra-low temperature chamber; (c) De-icing of composite with CNS.

4.3.2. Healing performance

After 24 h of healing at -60 ^{0}C, the recovered mechanical properties of the samples are given in **Table 4.2** and **4.3** and **Fig. 4.7**.

For the composite with CNS, an average healing efficiency of 108% for fracture energy and 96% for peak load was achieved. The maximum healing efficiency for fracture energy was 141%.

Four samples of the composites with CFS out of five successfully recovered from damage with an average healing efficiency of 63% for fracture energy and 59% for peak load. The maximum healing efficiency for fracture energy was 128%.

Table 4.2. DCB tests results quantifying healing performances

GFRC+CNS						
Specimen No.	Original peak load (N)	Recovered peak load (N)	Original fracture energy (N·mm)	Recovered fracture energy (N·mm)	Healing efficiency for peak load	Healing efficiency for fracture energy
1	31.5	32.5	1544.2	2077.4	103%	135%
2	30	29.8	1437.5	728.8	99.30%	50.70%
3	31.2	26.6	1356.8	1329	85.30%	98%
4	28	26.44	1586.5	2238	99.40%	141%
5	32.3	30.4	1565.35	1783.5	94.10%	114%
GFRC+CFS						
Specimen No.	Original peak load (N)	Recovered peak load (N)	Original fracture energy (N·mm)	Recovered fracture energy (N·mm)	Healing efficiency for peak load	Healing efficiency for fracture energy
1	65	40	3484.8	3298.4	61.50%	94.70%
2	62	45	2978.6	1837.3	72.60%	61.70%
3	58	30	3610.2	1141.7	51.70%	31.60%
4	51	55	2564.3	3284.1	108%	128%
5	55	N/A	3024.5	N/A	0%	0%

Table 4.3. Healing efficiency summary

	Number of samples	**Max. healing efficiency for fracture energy**	**Min. healing efficiency for fracture energy**	**Ave. healing efficiency for fracture energy**	**Max. healing efficiency for peak load**	**Min. healing efficiency for peak load**	**Ave. healing efficiency for peak load**
GFRC+CNS	5	141%	50.7%	107.7%	103%	85.3%	96.22%
GFRC+CFS	5	128%	0%	63.2%	108%	0%	58.8%

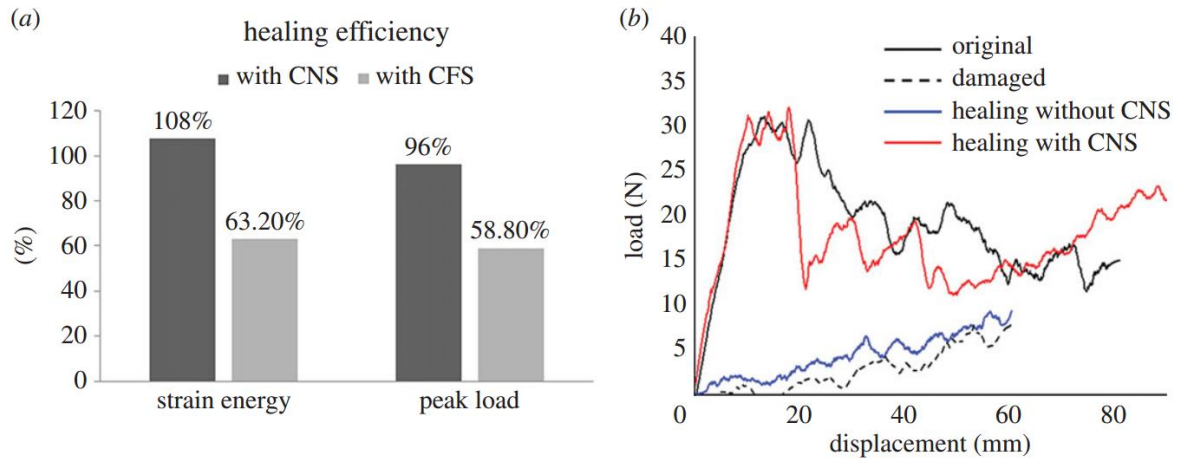

Figure 4.7. (a) Healing efficiency of composite with and without the conductive layer; (b) Displacement-load curve for a typical sample incorporating CNS.

The results indicate that the composite materials with either CFS or CNS are able to self-heal at ultra-low temperatures. Furthermore, CNS is the better of the two types of conductive layer. The electrical resistivity of CFS was too low and therefore a very high electrical current was required to generate heat, causing potential overheating for everything connected in series with the composite, especially at the contact points. Such a high current may locally generate temperatures approaching 500 ^{0}C. Also, the thermal conductivity of CFS is not high enough to allow heat transfer to other areas. This caused parts of the composite to be damaged by heat concentration, while the rest remained so cold that the healing agents could not function properly. As a result, the composite only achieved an average healing efficiency no greater than 70%. CNS, on the other hand, had an electrical resistivity which was much higher than that of CFS. Thus, only a small electrical current was sufficient to generate the required heat. The thermal conductivity was also sufficiently high to enable heat to flow rather than concentrate at local hot spots.

To achieve satisfactory healing performances, another important factor was how well the healing agent covers the composite materials. There have been concerns that the wave-like design in which the vessels penetrate multiple layers cannot ensure a large coverage and might be less effective than that adopted in straight hollow-fibre-based self-healing composites [97], [135], [161]. However, the high healing efficiency proved that a large coverage was achievable.

It might be possible to achieve self-healing at ultra-low temperatures using new healing agents. However, it is worth noting that any healing agent will have an active temperature range, out of which the healing process cannot take place. All established healing agents so far have narrow active temperature ranges, and none of them is suitable when a high healing efficiency over a wide temperature range, such as -60 ^{0}C to 100 ^{0}C, is required. Even if a new healing agent can be developed for that temperature range, it would become ineffective as soon as the operating temperature fell outside the range. Thus, the development of new healing agents is not an effective way to achieve sustainable self-healing. The essence of our approach is that there is no limitation relating to types of healing agents and composites - all established composites that self-heal in certain temperature ranges can be modified based on the design presented here to achieve self-healing at ultra-low temperatures. By tuning the power provided to the conductive layer, the internal temperature of composites can be altered regardless of the ambient temperature to provide suitable conditions for any healing agent.

4.3.3. Effects of conductive sheets on interlaminar properties

The mode I load vs. displacement curves for composites with and without conductive sheets are shown in **Figs. 4.8a** to **4.8c**. Each figure displays the load–displacement curves for 5 tested specimens. Comparison of composites with and without conductive sheets (**Figs. 4.8d** and **4.8e**) indicates obvious reductions in fracture energy and peak loads. The adoption of a porous sheet was to form a short-fibre-reinforced layer inside the composite so that the layer could bond strongly to the host material. The results might be explained by the possibility that the resin had not fully infiltrated the porous layer and that the conductive sheet should have a very rough surface to strengthen the interface bonding with the host material. A potential solution might be to optimise the surface pattern of the sheet to help preserve the interlaminar strength while ensuring heating efficiency. Techniques similar to those used with vascular networks for vessel-based self-healing materials could be adopted as the same potential issue with delamination exists there also [172]–[174].

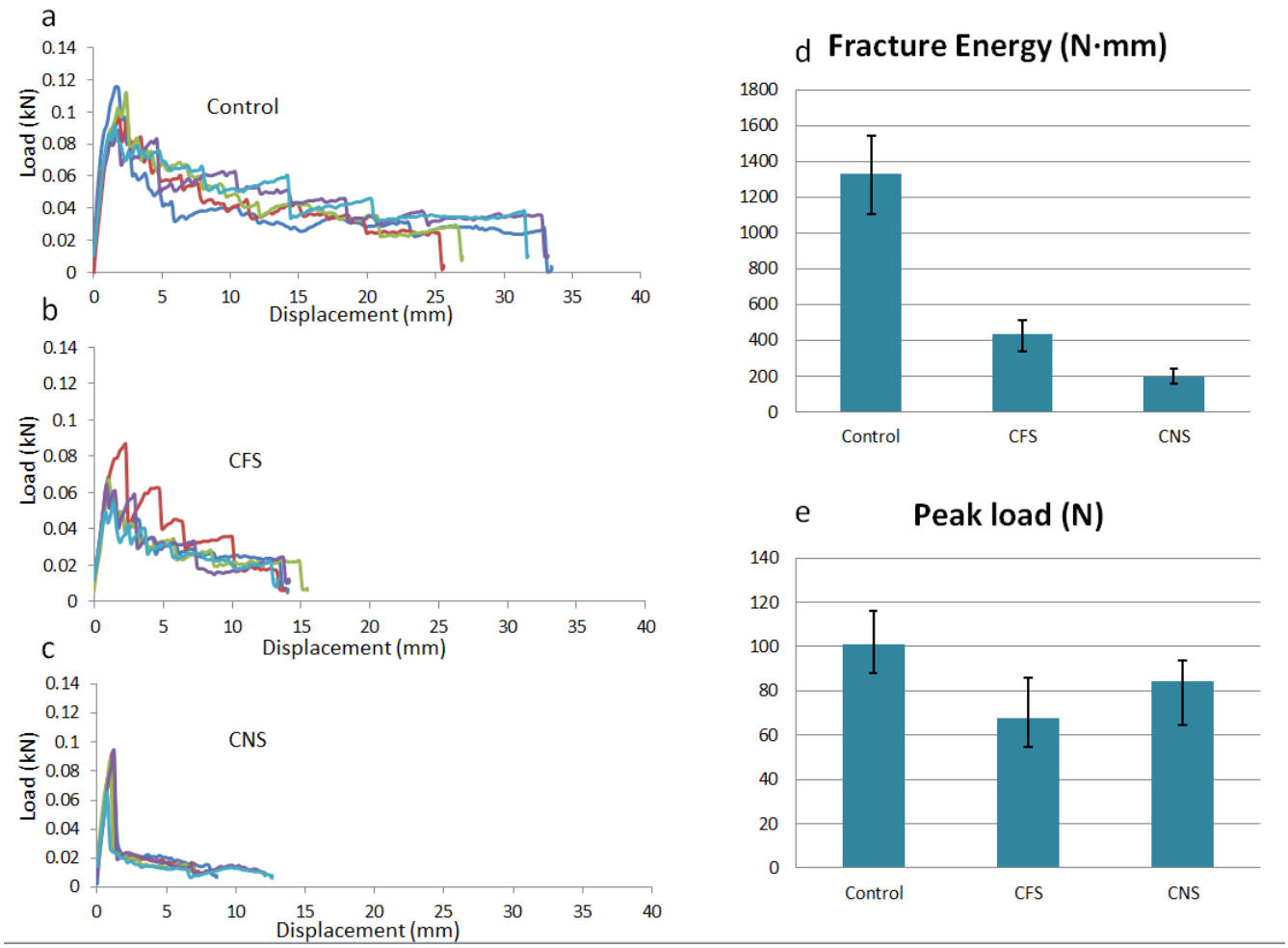

Figure 4.8. Mode I load vs. displacement curve for the laminates with (a) no embedment, (b) a copper foam sheet and (c) a carbon nanotube sheet. Results of DCB testing: (d) fracture energy and (e) peak load.

4.3.4. Effects of carbon nanotube sheets on tensile properties

The tensile properties of composites with and without the carbon nanotube sheets are shown in **Fig. 4.9**. The experimental results indicate that CNTs can significantly improve the tensile strength of polymer composites without much affecting their elasticity modulus. For cotton fibre composites, failure happened with fracture of both the CNT sheet and the surrounding material and there was no obvious delamination. Considering that the CNT sheet was the primary loading component in cotton fibre composites, it can be expected

that they failed once the sheet had reached its ultimate strain and ruptured. Unlike in cotton fibre composites, failure in carbon fibre composites was the result of a combination of rupture of the sheet, breaking of reinforcement fibres and delamination, as shown in **Fig. 4.10**. However, in a carbon fibre composite material, delamination always needs to propagate through the matrix between two adjacent carbon fibre layers. When a layer of carbon nanotubes is present, a crack would need to penetrate it before reaching the next carbon fibre layer and this provides extra resistance to crack propagation and delamination. This could be the reason why the introduction of carbon nanotube sheets improved the tensile properties of carbon fibre composites.

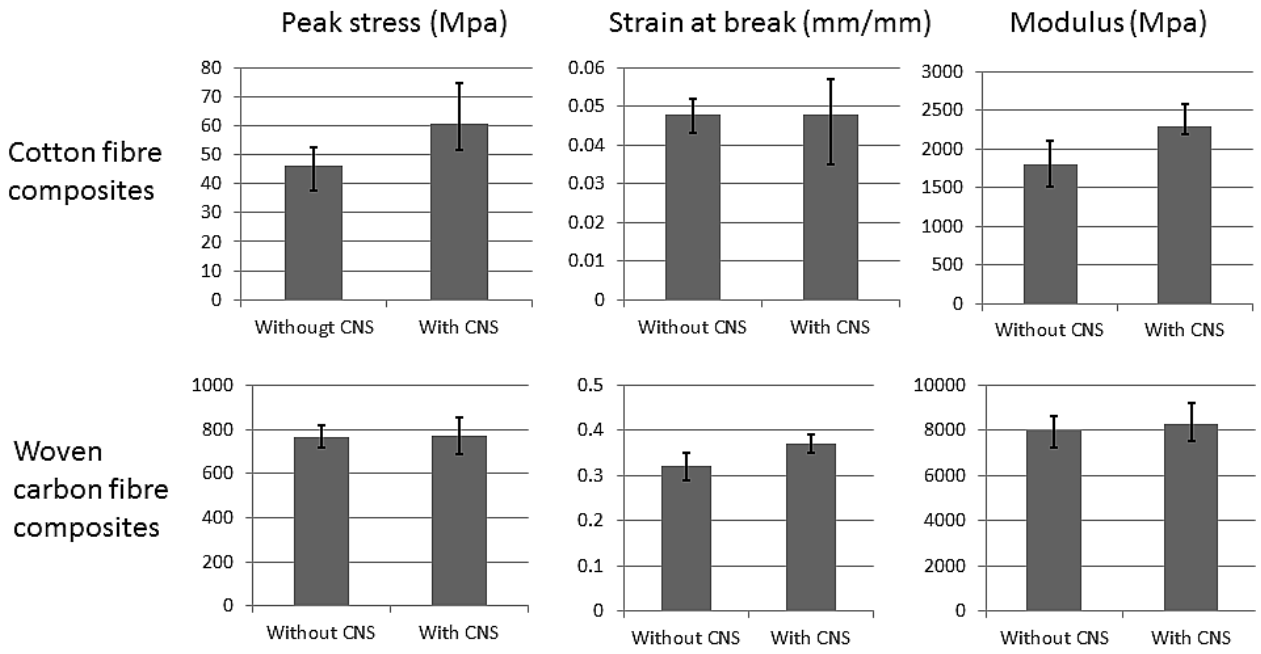

Figure 4.9. Tensile properties of composites with and without carbon nanotube sheets.

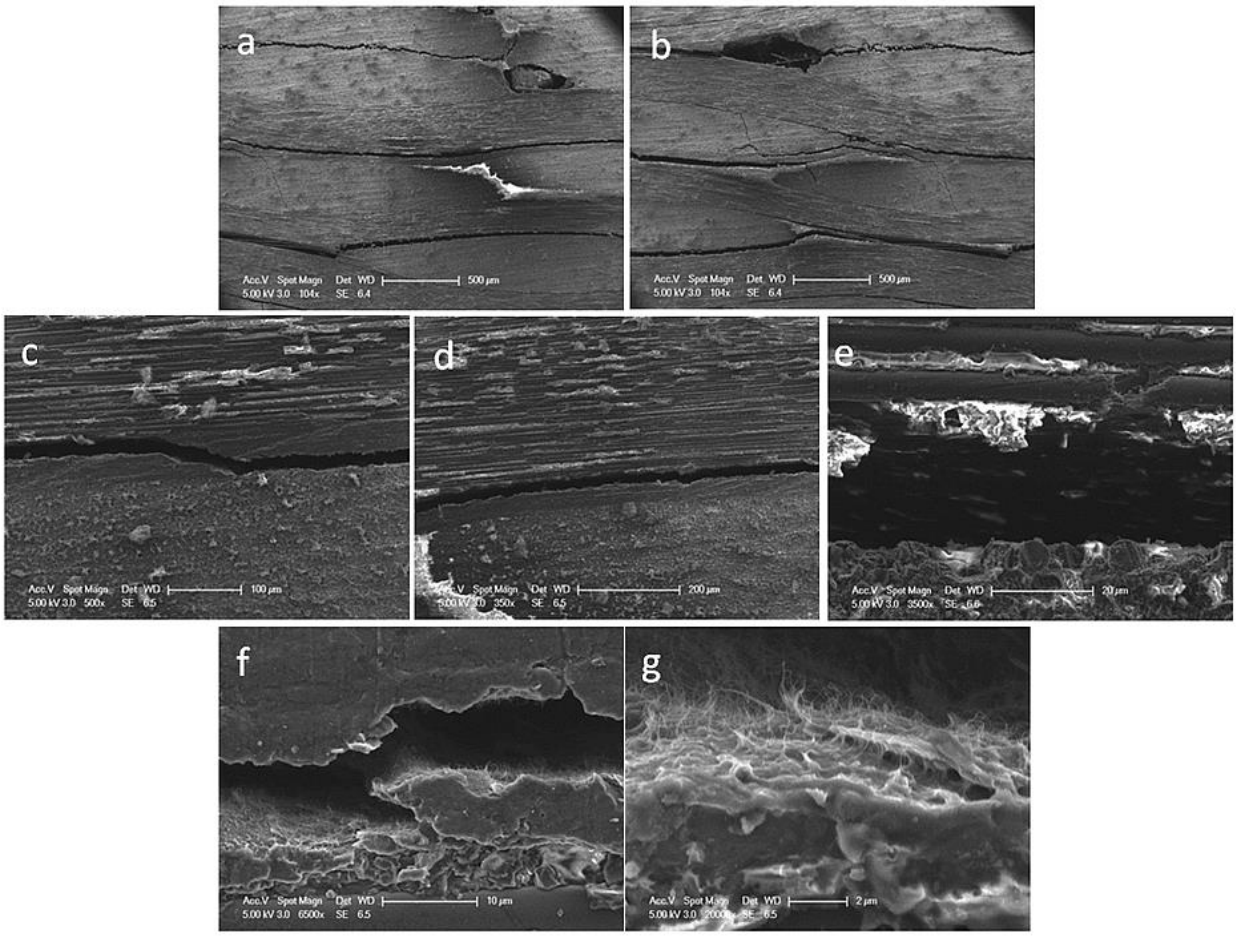

Figure 4.10. SEM images of carbon fibre composite incorporating carbon nanotube sheets after tensile tests. SEM image of crack in carbon fibre-reinforced composite incorporating carbon nanotube sheet. a,b) Cross section of a damaged sample; c-e) Delamination of carbon fibres and matrix; f,g) Delamination of carbon nanotube sheet and matrix

4.4. Summary

The chapter shows that self-healing at ultra-low temperatures can be implemented by adding vessels and a porous conductive layer into a composite material. Healing agents were continuously injected into the vessels and were released after the host material was damaged. The conductive layer increased the temperature of the composites through

electrical heating to assist the flow and curing of healing agents. Both the copper foam sheet and the carbon nanotube sheet were able to act as a conductive layer. However, the composite with the carbon nanotube sheet was able to self-heal more effectively and stably. As a result, healing in fibre-reinforced composites at a temperature around -60 C was achieved with an average recovery of 108% in fracture energy and 96% in peak load. The effects of the conductive sheet on interlaminar properties and tensile properties were experimentally investigated. It was found that the introduction of a carbon nanotube sheet increased the tensile strength of polymer composites, but had negative effects on interlaminar properties.

Chapter 5 - Towards autonomous restoration of structural carbon fibres in polymer composites using vascular systems and electric alignment

5.1. Preliminaries

The chapter reports a carbon fibre-reinforced composite that can repair its structural fibres and restore its mechanical properties after damage by using an embedded vascular self-healing system. The healing agents in the vessels contain short carbon fibres (SCFs) which could be aligned in an *in situ* electric field produced by charging the broken structural carbon fibres. The aligned SCFs reconnect the broken carbon fibres, resulting in recovered structural properties. Various variables and parameters were investigated to observe their effects on the healing performance and determine the optimum healing agent composition and conditions. This chapter also presents a model that can be used to analyse healing performances. Under optimum conditions, the healing efficiency and performance increased by 3788% and 153% respectively compared to an unprocessed epoxy resin used in conventional self-healing materials, and as much as 45% of the original strength could be restored. The role of the chapter in the thesis is shown in **Fig. 5.1**.

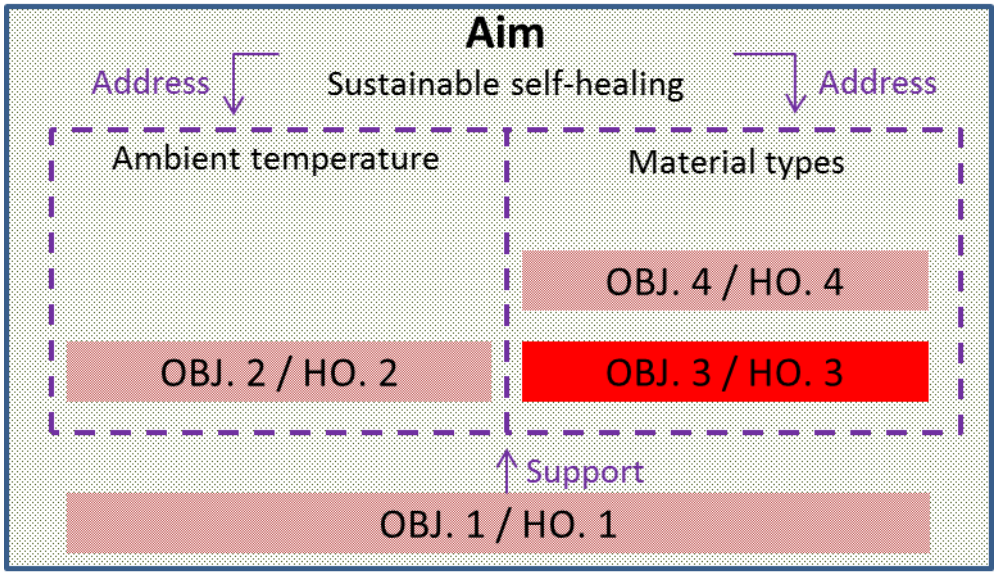

Figure 5.1. Role of Chapter 5 in the thesis (red area)

5.2. Methodology

5.2.1. Healing mechanism

When CFRCs are embedded with hollow vessels, a healing agent mixed with SCFs can be injected into the materials. As structural carbon fibres in CFRCs are damaged, they are disconnected by a gap which causes the vessels to release the liquid. Meanwhile, the short fibres are released into the gap along with the liquid. As the carbon fibres are electrically conductive, when CFRCs are connected to a power supply, the fractured carbon fibres produce an *in situ* electric field in the gap which can drive the short fibres to align and form head-to-head contacts to reconnect the fractured carbon fibres. At the meantime, the epoxy resin in the gap starts to cure and solidify. After curing, the aligned SCFs are fixed in the resin and the reconnection complete. The concept enabling the recovery of the structural carbon fibre can be seen in **Fig. 5.2**.

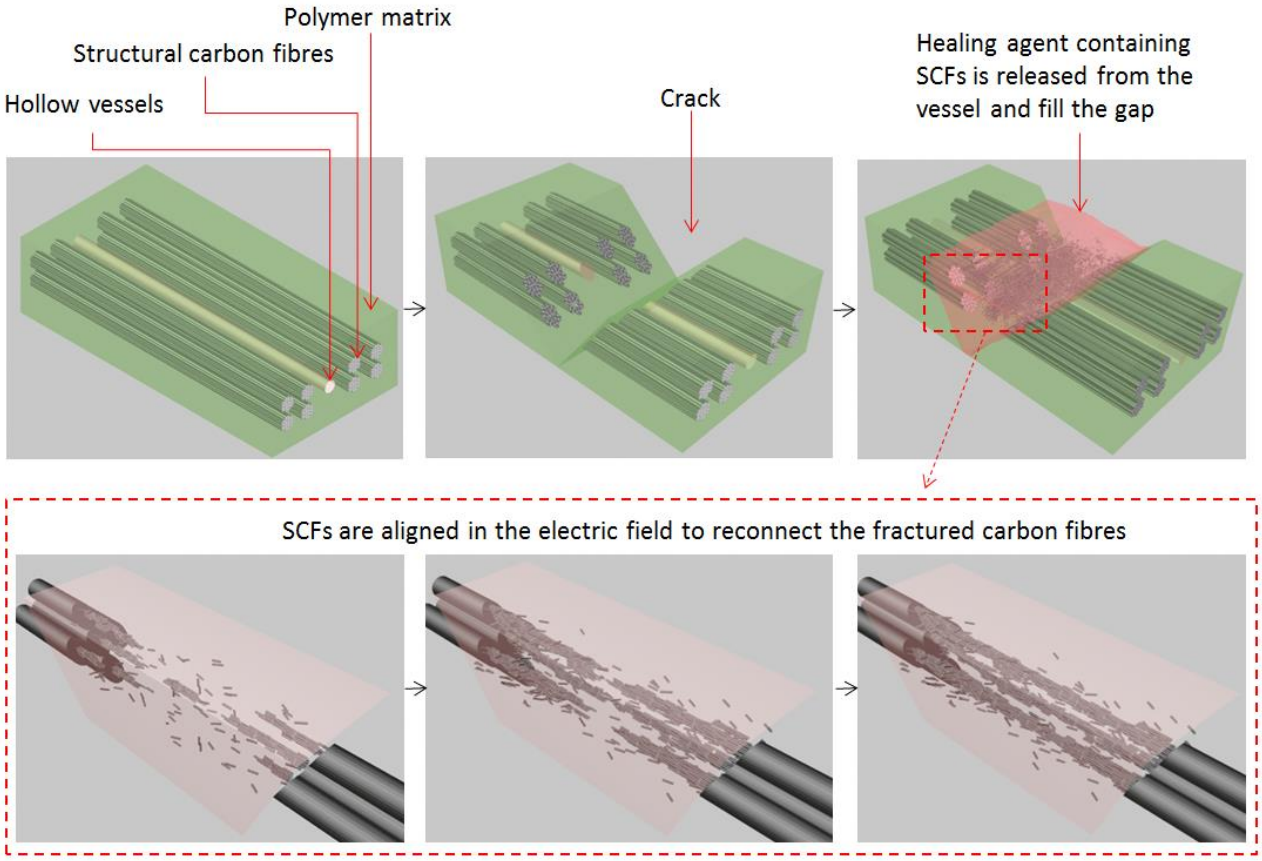

Figure 5.2. Schematic of the recovery of structural carbon fibres

Fig. 5.2 shows how the procedure starts with an undamaged CFRC sample incorporating hollow vessels. The sample is then damaged producing a visible gap which breaks the structural carbon fibres and the vessel, resulting in the healing agent being released to the crack. When the CFRC is connected to a power supply, the voltage produces an electric field in the gap, resulting in the alignment of the SCFs in the healing agent to reconnect the broken carbon fibres. After the healing agent is fully cured, the aligned SCFs are fixed in the gap, and the CFRC recovers as a result.

5.2.2. Investigated variables and parameters

An investigation of various variables was conducted to observe their effects on the healing performance. Experimentation started with comparing the effect of healing the specimens within an electric field. At the same time as this, the effect of introducing milled SCFs into the healing agent was also tested. Once a conclusion was reached, the effect of the short carbon fibre weight content of the healing agent, expressed as '%wt.', was explored so that a trend of SCFs effect can be established.

The effect of increasing the strength of the electric field was investigated. This was done by altering the voltage producing the electric field, comparing the alignment strength of the healed specimens in electric fields caused by 0V, 25V and 50V piecewise constant voltage supplies. A custom circuit was created to avoid burn damage to specimens caused by electrical heating, subjecting specimens to a rapid spike of high voltage (+/-50V) that decayed to 0V over a period of 2 seconds.

Healing agents containing carbon fibres of differing length were tested to reveal the effects of fibre length on self-healing performance. The healing performance of healing agents made from 150 μm (avg.) length short fibres was compared to a different batch/brand of 100 μm (avg.) to see if fibre length/type had an effect on the final healing performance.

Finally, the addition of dispersant was tested to see if it had a positive effect on the resultant healing performance. It was tested against a healing agent which didn't contain the additive, in an attempt to pinpoint its contribution to (or deduction from) the overall healing performance.

5.2.3. Fabrication of samples

The method to fabricate CFRC samples incorporating hollow vessels is shown in **Fig. 5.3**. A polypropylene table was covered with PVA releasing agent to prevent damage during removal. The releasing agent became completely dry in 30 min at room temperature. Epoxy resin and hardener (Very High Temperature Epoxy Laminating Resin, EasyComposites Ltd.) were mixed at a ratio of 100:35 parts by weight and degassed at 35 ^{0}C for 30 minutes in a vacuum chamber. Nylon fishing line 2 mm in diameter was fixed on table by using a sealant tape which were also used to construct a rectangular barrier to contain liquid. The uncured resin was poured onto the table and immersed the fishing lines, followed by curing at room temperature for 24h. After curing, the nylon lines were pulled out manually, leaving hollow vessels inside the material. Carbon fibre cloth fabrics (CF-PL-200-100, EasyComposites Ltd.) were laminated onto the material using the same uncured resin and a soft brush. After another 24 hours for curing at room temperature, post-cure heating cycles were applied as instructed by the supplier. The fully cured composite which had a thickness of 2 mm was cut into identical pieces 22 mm $\times$ 6 mm each containing a hollow vessel and a carbon fibre reinforced layer on top, using a grit saw and polished with sand paper. The cutting and polishing followed a high-speed-low-force strategy to avoid damage.

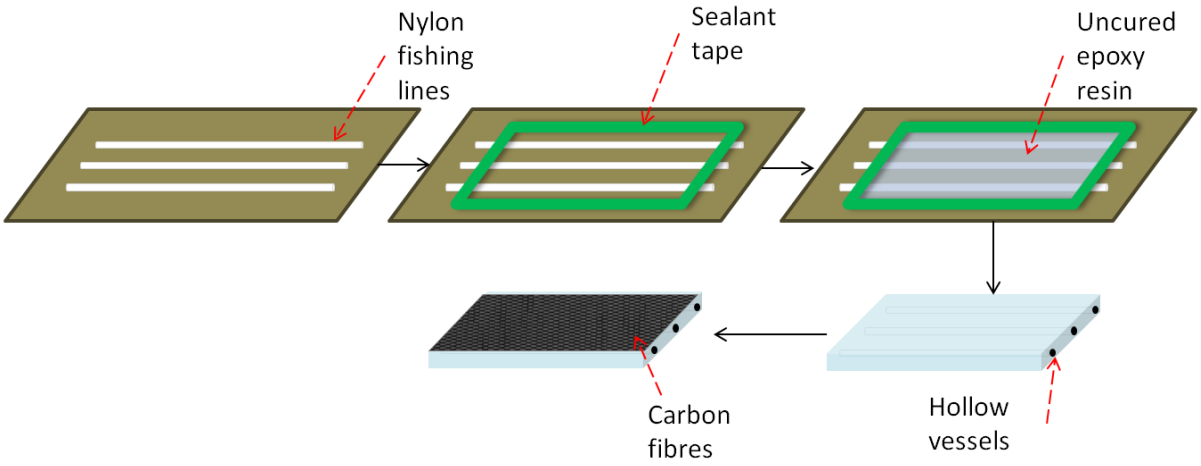

Figure 5.3. Fabrication procedure

5.2.4. Healing agent composition and synthesis

The healing agent used during experimentation, is made up from an epoxy resin base (RT151, Resintech Ltd.), short carbon fibres (Carbiso Milled Carbon Fibre, EasyComposites Ltd. and AGM 99-150, Asbury Graphite Mills, Inc.), depending on the %wt. of the desired healing agent, and dispersant (DISPERBYK-191, BYK-Chemie GmbH) that are to be tested. Throughout this project, the range of healing agents used are as follows; 0 wt%, 15 wt%, 18 wt%, and 20 wt% short carbon fibre content, 1 wt%, 2 wt% and 3 wt% and 3% dispersant. Resin, short fibres and any other additives were mixed in a magnetic stirrer for 1h, followed by adding the hardener and mixing for another ten minutes.

5.2.5. Experimental procedure

The general test format was split into four phases/stages. First was the preparation phase in which the specimens were purposefully damaged using an air grinder to fully cut

through the carbon fibre layer, to simulate a crack, and prepared for healing. Secondly was the alignment phase in which healing agent was applied to the specimens, after which they were connected to a power supply for 24 hours in which an electric field is produced in the gap to manipulate SCFs. The third phase was the curing phase, where the healed specimens spent another 24 hours in an oven (40^{o}C) to ensure the healing agent was fully cured. The final phase was the tensile test phase, where the specimens were destructively tested to find out the overall healing recovery of its original mechanical properties by measuring the load required to fracture each specimen. A MTS Criterion testing machine (MTS Criterion Model 43 Electromechanical Universal Test System) was used to collect data. Loading rate was 0.05 mm/s. Conclusions were then arrived at, as the fracture loads can be compared to the results for different variables or reference (undamaged) specimens. **Fig. 5.4** shows an undamaged, a damaged and a healed specimen for clarity.

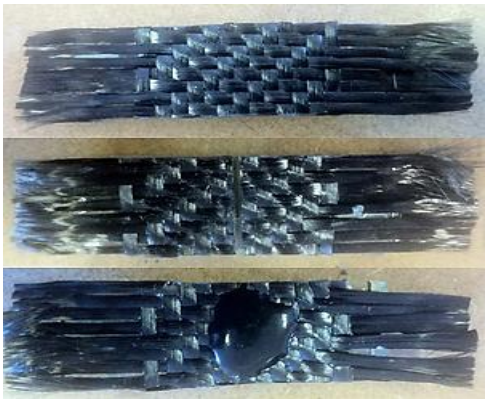

Figure 5.4. Topside view of an undamaged (top), damaged (middle) and healed (bottom) specimen.

To conclude the experimentation, once the optimum healing agent composition and conditions for self-healing were found, they were used to heal a specimen by injecting from the vessel by using a liquid dispenser to show that comparable levels of self-healing can

be achieved, shown in **Fig. 5.5**, which replicates a real-world system, to prove this research's validity and potential commercial and industrial applicability.

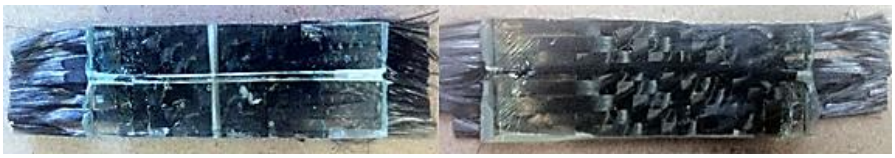

Figure 5.5. An underside view of a damaged (left) and a healed (right) vessel specimen.

5.2.6. Healing performance/efficiency

Healing performance and efficiency are defined below:

$$HP = \frac{F_H}{F_{UD}}, \quad HE = \frac{F_H - F_D}{F_{UD} - F_D} \tag{5.1}$$

Where HP and HE are the healing performance and efficiency respectively, F_H is the Force required to fracture a healed specimen, F_D is the force required to fracture a damaged specimen after cutting through the carbon fibre layer (no healing agent applied), and F_{UD} is the force required to fracture an undamaged specimen. Both indexes indicate the performance of recovery but with different focuses. Healing performance focuses on what would be the percentage of the original strength that can be restored. Healing efficiency considers how much the lost strength caused by the damage that can be recovered.

5.3. Results and discussion

5.3.1. 3.1 Parameters tested

The reconnection of a bundle of fractured carbon fibres immersed in healing agents containing 5 wt% SCFs took place in a piecewise constant electric field produced by connecting the two ends of the fractured carbon fibres to a 20V piecewise constant power source. As shown in **Fig. 5.6**, where reconnection was accomplished in 1 h.

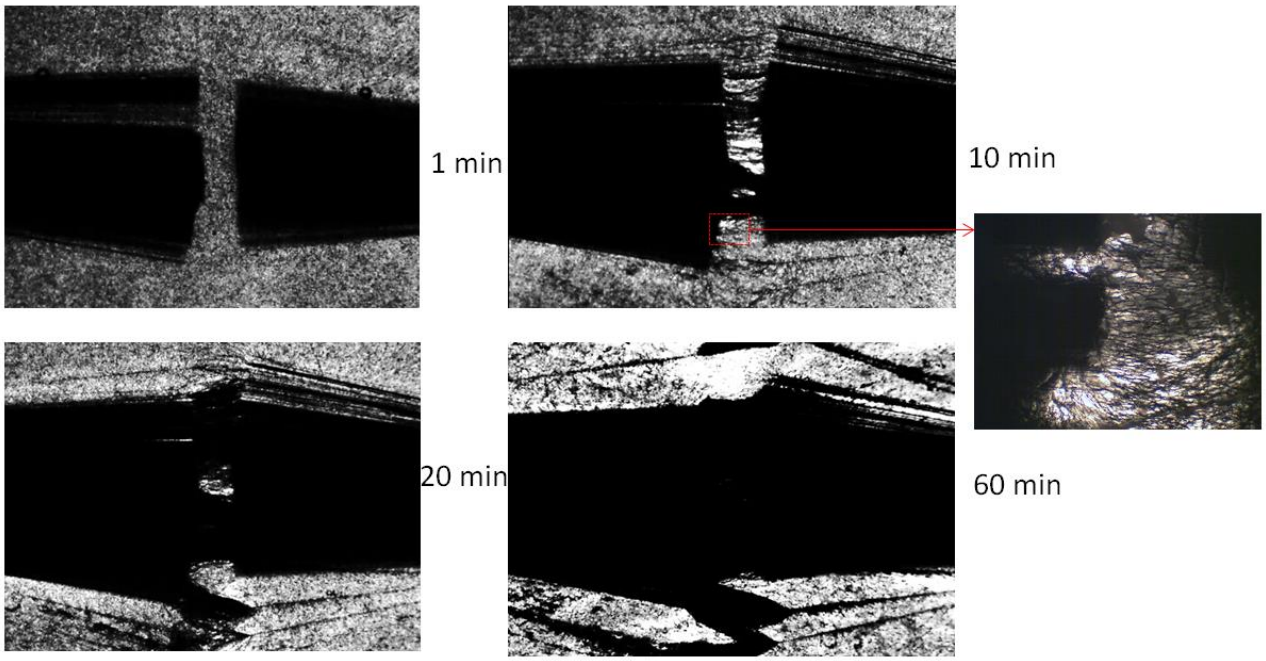

Figure 5.6. Reconnection of a bundle of fractured carbon fibres

Based on the observed phenomenon, variables/parameters were tested in the order below with respect to the healed specimens efficiency/performance achieved:

- Investigation of the effect of SCF addition to the healing agent and effect of alignment
- Investigation to see whether altering electric field intensity affects the recovery strength

- Investigation of the effect of SCF %wt. content within the healing agent
- Investigation of the effect of SCF length/type within the healing agent
- Investigation into the addition of dispersant to see the effect on healing agent application and ease of alignment

The rest of this section discusses the results of conducted experiments and their respective conclusions.

5.3.2. Modelling and verifying the effect of electric alignment and additive short fibres on restored strength

The aim of this study was to model and verify the effects of the introduction of milled SCFs into the healing agent on the healing efficiency of the specimen. Alongside this, the effect of the alignment of the SCFs (100 μm in length) on the healing performance will be investigated by using an electric field produced to align the SCFs in the longitudinal direction to improve its tensile strength.

The Rule of Mixtures is often used to model the strength of fibre reinforced composites. For unidirectional continuous fibre composites under the isostrain conditions, the rule of mixture is as follows [175]:

$$\sigma_{cd} = \sigma_{fu} V_f + \sigma'_m (1 - V_f) \tag{5.2}$$

Where σ_{cd} and σ_{fu} are the ultimate tensile strength of the compostie and structural fibres respectively. V_f is volume fraction of structural fibres and σ'_m is the stress of matrix at failure. In the case of uni-directional short fibre composites, **Eq. 5.3** is modified in order to become [175]:

$$\sigma_{cd} = \sigma_{fu} V_f F\left(\frac{l_c}{l}\right) + \sigma'_m(1 - V_f) \tag{5.3}$$

Where the factor $F\left(\frac{l_c}{l}\right)$ models the effect of the fibre length changes the resulting solution and l_c and l denote fibre critical length and average length, respectively.

If the fibre length is uniform then the $F\left(\frac{l_c}{l}\right)$ is equal to

$$\begin{gathered} 1\text{-}\left(\frac{l_c}{2l}\right) \text{ when } l > l_c \\ \text{And } \left(\frac{l}{2l_c}\right) \text{ when } l < l_c \end{gathered} \tag{5.4}$$

The critical fibre length is calculated using **Eq. 5.5** [175]:

$$l_c > {\sigma_f d}\Big/{2\tau_c} \tag{5.5}$$

Where σ_f denotes the tensile strength of the fibre, *d* is the diameter of the short fibres and τ_c is the greater value out of shear strength of the fibre-matrix interface and the matrix tensile strength. In manufacturedunc short fibre composites, there are variations not only in fibre length but also in fibre orientation. Therefore, **Eq. 5.3** is further modified to [175]:

$$\sigma_{cd} = \sigma_{fu} V_f F\left(\frac{l_c}{l}\right) C_o + \sigma'_m(1 - V_f) \tag{5.6}$$

where C_o is the fibre orientation factor that can be calculated by using the Krenchel equation [176]. The calculated result can be seen in **Table 5.1**.

Table 5.1. Fibre orientation factors corresponding to orientation

Orientation of fibres	C_o
Unidirectional parallel	1
Biaxial parallel	0.5
Biaxial on the bias angle (at ±45º to the fibres)	0.25
Random (in-plane)	0.375
Random (3D)	0.2
Unidirectional perpendicular	0

When the healing agent containing SCFs is released into the gap, it forms a healed space reinforced by short fibres. The strength of the healed space could be calculated by using the **Eq. 5.6**. The tensile property of matrix σ'_m are in the range of 55-68 MPa and the V_f is 20 vol%. The data provided by the supplier showed that σ_f = 3150 MPa, d = 7 μm and τ_c = ~75 Mpa. Therefore, l_c is calculated to be equal to be approximately 147 μm. According to **Eq. 5.6**, the calculated strength of the sample healed by using the healing agent containing SCFs should be about 48% higher than that using the conventional healing agent without SCFs. When electric field was adopted, the alignment caused by the field should increase the value of fibre orientation factor which results in higher healing performance.

Hence, it is expected that similar results will be observed in the experiment. During this experiment, healing agents containing aligned and unaligned SCFs were compared to a pure epoxy resin to observe whether the addition of SCFs to the healing agent or the alignment process has an effect on healing performance. The test results and calculation results are shown in **Fig. 5.7**.

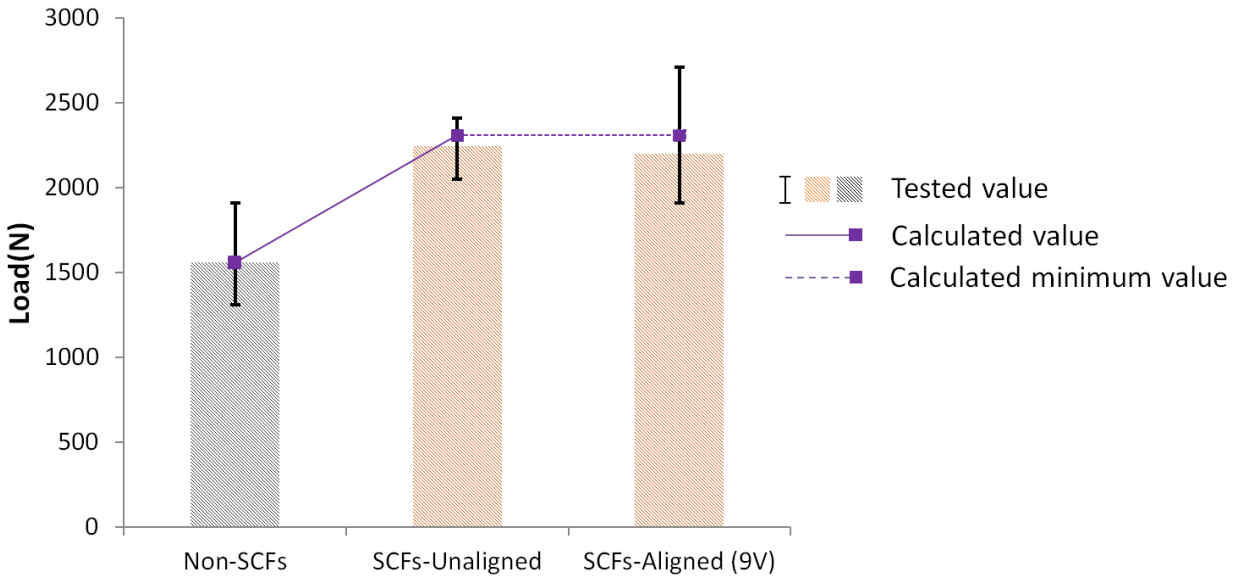

Figure 5.7. The effect of SCF addition & alignment

Test Summary:

As it can be seen from **Fig. 5.7**, the specimens healed with a healing agent containing short fibres have a much greater restored strength, 42.6%, than the specimens that were healed with a healing agent not containing SCFs. The calculated minimum value, based on the assumption that C_o did not improve at all, is the minimum strength calculated. The result is in accordance with the calculated result using the model presented. However, it is worth noting that the results for the aligned and unaligned specimens are inconclusive, as the voltage used in this experiment (9V) was not high enough to promote consistent alignment of the SCFs. As a result of this, further experimentation is required to investigate whether SCF alignment has an effect on healing performance.

5.3.3. Effects of electric field intensity on restored strength

Building on the previous test, this experiment aimed to find out whether voltage affects the healing performance. The theory behind this experiment is that increasing the voltage should increase the intensity of the electric field producing stronger force for alignments, resulting in a higher C_o value and better healing performance. Similar experiments have already demonstrated that the aligned carbon nanotubes [177] and multilayer graphene flakes [178] in electric fields can improve mechanical properties of polymer composites. During this test, 3 different voltages, 0V (unaligned), 25V and 50V, were connected to the CFRC specimens to observe their effects on alignment. The test results are shown in **Fig. 5.8**.

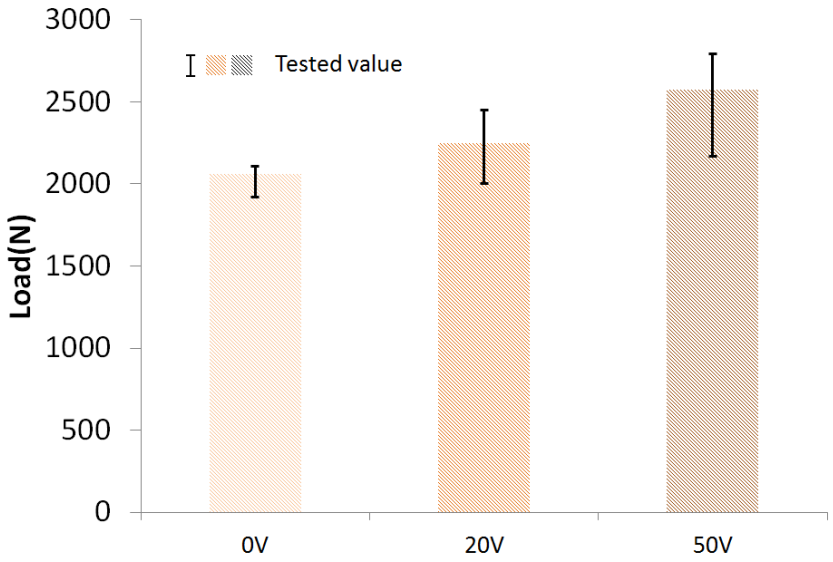

Figure 5.8. The effect of voltage on alignment

Test Summary:

Fig. 5.8 clearly shows that there is a strong trend between increasing the voltage during the alignment process and a higher respective healing performance, due to the theory previously mentioned, with average loads for 50V aligned specimens being 25.1% and

14.7% higher than 0V and 25V aligned specimens respectively. When the voltage is 0V, no electric field was produced to align short fibres so that the fibres in the crack were dispersed randomly. Hence, its C_o should be 0.2, as shown in **Table 5.1**. When the voltage was raised to 50V, the 25.1% growth in healing strength indicated that the C_o was increased to near 0.31. The calculation was based on **Eq. 5.6** and true values of all parameters given previously.

It is worth noting that alignment at a higher voltage, 80V, was originally attempted in this experiment but at this voltage specimens were subject to moderate burn damage which reduced their mechanical strength significantly. Therefore it was found that there is a limit to the intensity of the electric field. Alternatively, a capacitor could be connected in series to the samples and power supplies to change the pattern of the electric field from piecewise constant to periodic impulse. Therefore, the force manipulating SCFs produced by high voltage could be strong enough for alignment, and the resting time in each period could allow the samples to dissipate heat fully to avoid thermal damage. The test result also demonstrated similar healing levels.

5.3.4. Investigating the effect of short carbon fibre %wt. on restored strength

The goal of this experiment was to investigate the effect that increasing the weight fraction of SCFs, within the healing agent, has on the resultant healing performance of the specimens. By increasing the %wt. of SCFs within the healing agent, or increasing V_f, the alignment achieved during the electric field stage (50V) will be stronger due to more fibres being aligned within the cured healing agent. As a result of this, the cured healing agent can be stronger. During the test, three different wt%. (15 wt%, 18 wt%, 20 wt%) were

tested and compared to one another. The results of the experiment and calculated value using the model are shown in **Fig. 5.9**.

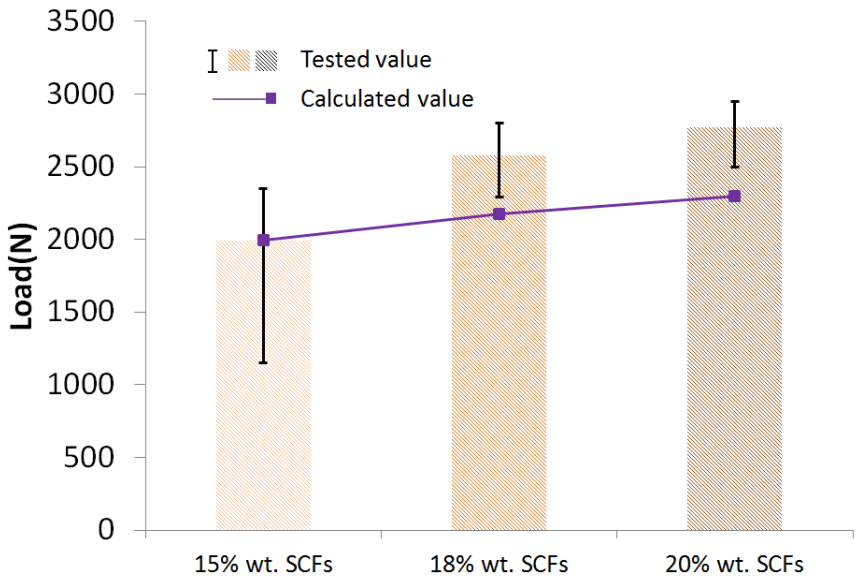

Figure 5.9. The effect of SCF %wt

Test Summary:

Fig. 5.9 clearly shows that increasing the SCF content in the healing agent increases its healing performance by a significant margin. The average load result for 20 wt% SCF content was 39.1% higher than the respective load for 15 wt%. The average load results for 18 wt% were in between the two tested specimen types. This confirms that there is a trend present between a higher SCF content in the healing agent and an increase in healing performance.

However, it is worth noting that as the SCF %wt. increases the viscosity of the healing agent also increases, which can lead to some issues while pumping the healing agent onto the specimen as the vessels, and injection tools such as syringes can get blocked. Therefore there is a limit to how high the SCF %wt. can be achieved before

adverse consequences are experienced. A healing agent with a SCF content of 25 wt% was originally planned to be used in this experiment, alongside 20 wt%, 18 wt% and 15 wt%, but the healing agent produced was deemed too viscous to be applied and could not be used.

5.3.5. Investigating the effect of short carbon fibre length/quality on restored strength

The aim of this experiment is to validate whether or not fibre length and quality has an effect on the healing performance. As σ_{fu} and $F\left(\frac{l_c}{l}\right)$ in **Eq. 5.6** are related to fibre quality and length respectively, altering their values could lead to different healing performances.

During this test, healing agent made from 100 μm and 150 μm length fibres, manufactured by Asbury Graphite Mills (AGM), were compared to healing agent made from 100 μm length fibres, manufactured by Easy Composites Ltd. (EC), to see if a trend between fibre length, or fibre quality and healing performance could be established. For EC carbon fibres, the σ_{fu} is 3150 MPa which is higher than 2800 Mpa, that for AGM fibres. The calculated results and tests results are shown in **Fig. 5.10**.

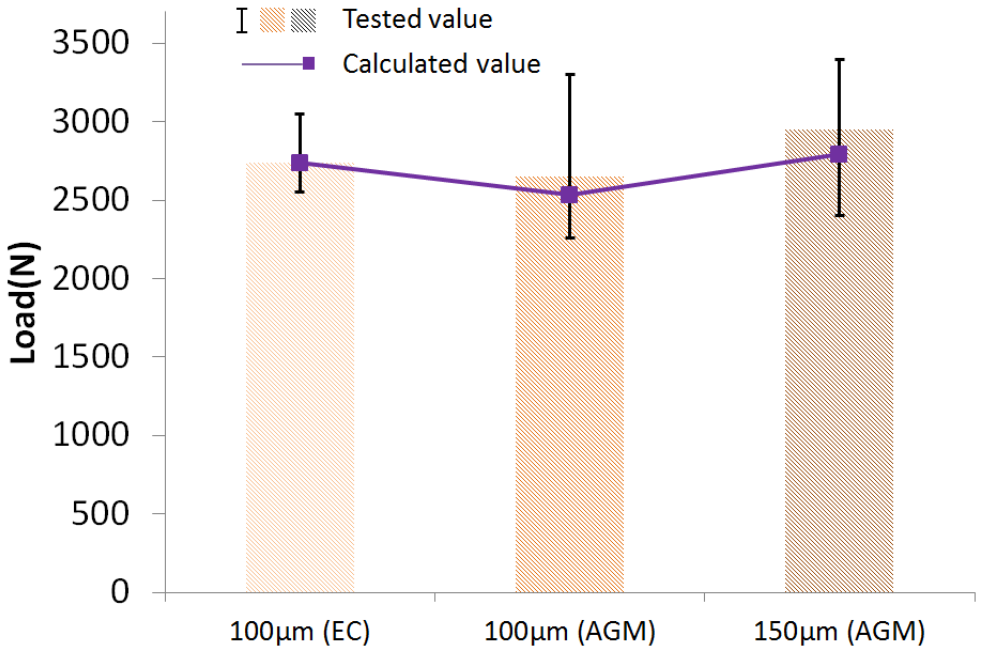

Figure 5.10. The effect of changing fibre length/quality

Test Summary:

Fig. 5.10 shows that the average load for 150 µm length specimens is higher than that for 100 µm AGM and 100 µm EC specimens by 11.3% and 7.8% respectively. It also appears that the 100 µm EC specimens have more consistent load values. All experiment results are in accordance with the calculated results. The result proves that the adoption of stronger and/or higher carbon fibres could lead to higher recovery strength.

5.3.6. Investigating the effect of adding dispersant to the healing agent

The goal of this experiment was to examine whether adding a dispersant to the healing agent mixture would improve its healing performance. The dispersant, BYK-191, was used in an established study regarding the alignment of carbon nanofibers [179]. The motivation

of the study comes from the theory based on **Eq. 5.6** that further increasing the key factor C_o, which has been raised to 0.31, could lead to higher healing performances. The addition of dispersant could reduce viscous resistance during rotation and forming head-to-head contacts. During the test, specimens healed with a healing agent containing 3 wt% BYK-191, 20 wt% SCF, were tested against specimens healed with a healing agent not containing dispersant, so that the effect of dispersant on healing performance could be ascertained. The results are shown in **Fig. 5.11.**

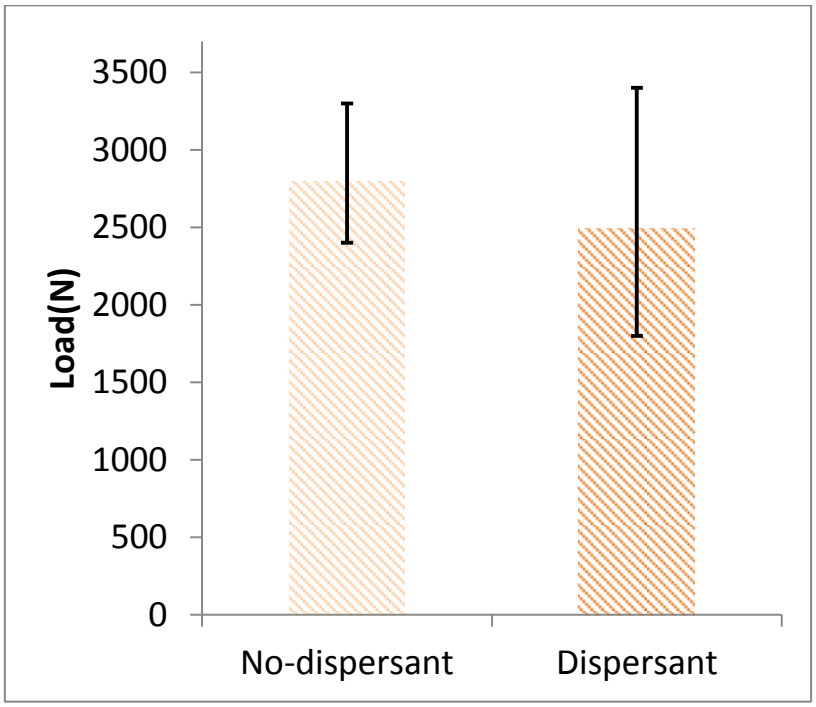

Figure 5.11. The effect of adding dispersant to the healing agent

Test Summary:

Based on the results shown in **Fig. 5.11**, a conclusion can be reached that adding dispersant to the healing agent does not improve the healing performance of cured specimens, as the average load required to fracture for the 'No-Dispersant' specimen

group was 12.3% higher than for the average specimens healed with healing agent containing BYK-191. The results were not as expected due to the possible reason that although the viscous resistance could be reduced, the modified mixture could also reduce shear strength of fibre-matrix interface, τ_c in **Eq. 5.5**, which cause the factor $F\left(\frac{l_c}{l}\right)$ to decrease. Therefore, dispersant may raise the orientation factor C_o, but could also reduce the factor $F\left(\frac{l_c}{l}\right)$, and the overal healing performance depends on the propotion of the two.

5.3.7. Implementation of a vascular self-healing system

By adopting the new mechanism based on the electric alignment of short structural fibres, the improvement in the restored strength is shown in **Fig. 5.12**, which indicates that the maximum healing performance of the healed specimens is 45.4%, and the maximum healing efficiency is 23.0%.

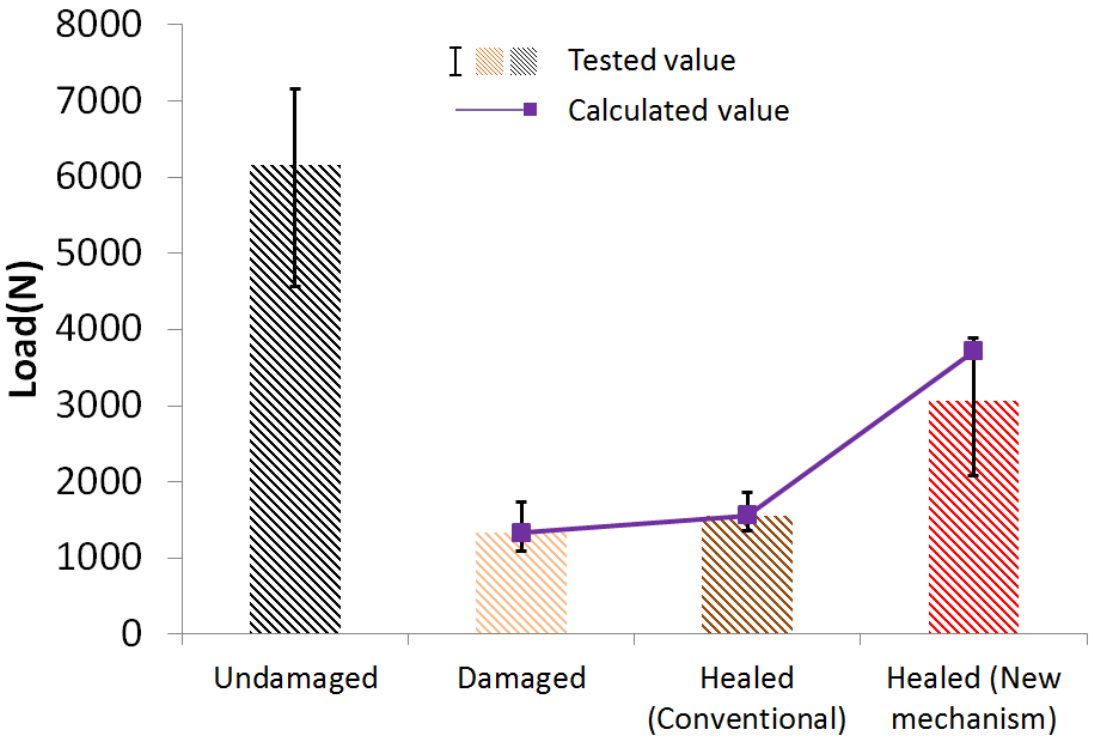

Figure 5.12. Comparison of the restored strength of samples with and without using the new healing mechanism

The test results also demonstrate that the model presented in **Section 3.2** could be used to analyse key factors limiting recovery strength and even to predict healing performance. Based on the model, many other works could further improve the healing performance as long as they can increase the values of Fibre strength σ_{fu}, Volume fraction of structural fibres V_f, Fibre length factor $F\left(\frac{l_c}{l}\right)$ and Orientation factor C_o. In the study, the healing performance reached 45.4% when $\sigma_{fu} = 2800MPa$, $V_f = 0.267, F\left(\frac{l_c}{l}\right) = 0.5$ and $C_o = 0.31$. If high-strength carbon fibres were used, the σ_{fu} can be raised to near 6000Mpa. And $F\left(\frac{l_c}{l}\right)$ can be increased to 0.6 by using slightly longer fibres or modify the surface of the carbon fibre to reduce the critical length l_c. C_o can be raised to 0.5 by adopting more advanced charging strategy. If the modification mentioned above were

successful, the healing performance would be over 100%, suggesting that a healed sample could be even stronger than an undamaged sample.

5.4. Summary

Significant improvements in the automatic recovery of fibre-reinforced composites have been made through the introduction of SCFs, optimising the electric field alignment process and using suitable additives. A healing agent made with pure epoxy resin was compared to a healing agent containing epoxy resin, 20 wt% short carbon fibres (150 μm in length) aligned in an electric field. This increased healing efficiency by 3788% and healing performance by 153%. As much as 45% of the original tensile strength could be restored after the structural carbon fibres were completely ruptured. This chapter has also demonstrated that the healing performance could be analysed and predicted by using a theory based on the Rule of Mixture, which suggests that further improving the alignment process and using stronger short fibres to promote recovery are promising research directions.

Chapter 6 - Towards autonomous restoration of the electrical conductivity of a polymer composite incorporating a carbon nanotube sheet

6.1. Preliminaries

The focus of some research on self-healing composites has recently moved onto restoring other properties such as electrical conductivity [180], [181], driven by the need for multifunctional materials and structures that can simultaneously perform combined structural and non-structural functions [182]. For example, conductive composite materials are used in aircraft structures, where lightning strikes may damage non-conducting structures. Structural composites can incorporate piezoelectric micro-electromechanical systems (MEMS) for sensing and actuation [183]. Piezoelectric materials can be used to make energy storage or harvesting materials by converting mechanical deformations from vibrating structures such as beams and plates to electrical power [184]. Some composites could be used to build electromagnetic interference shielding materials [185]. All the above multifunctional materials contain conductive component inside. Though research into the area of self-healing conductive materials is not as popular as the aforementioned activities on restoring mechanical properties in self-healing materials, there has still been some notable research for example Williams *et al.* [186], Guo *et al*. [187] and Odom *et al*. [188] who show different possible methods of achieving materials with the ability to restore their electrical conductivity.

Due to the extensive list of possible applications for a self-healing conductive material, this chapter aims to produce a method to restore the electrical conductivity to a carbon nanotube sheet (CNS) embedded inside a polymer composite after it has

sustained damage. As seen in **Chapter 4**, CNS could be used as a heating component to defrost [151] or to facilitate healing at low temperatures [189]. It could also be used as sensing component with very high sensitivity [190], [191].

This chapter demonstrates that the composite and the sheet can self-heal using aligned short carbon fibres (SCFs) as a nanofiller after it has sustained damage. The SCFs will be mixed into the healing agent and alignment will take place using an electric field during curing. The use of SCFs to improve the mechanical and electrical properties of an epoxy nanocomposite has been demonstrated by Ladani *et al*. [179]. Therefore, it is expected they can be used to restore electrical conductivity to a CNS. Various factors, including the voltage of the electric field used for alignment and the weight percent of SCFs, will be investigated to identify the effect they have on the alignment and the conductivity of the healed samples. A conclusion will then be reached regarding the composition of the best healing agent for restoring the electrical conductivity to the CNS. The role of the chapter in the thesis is shown in **Fig. 6.1**.

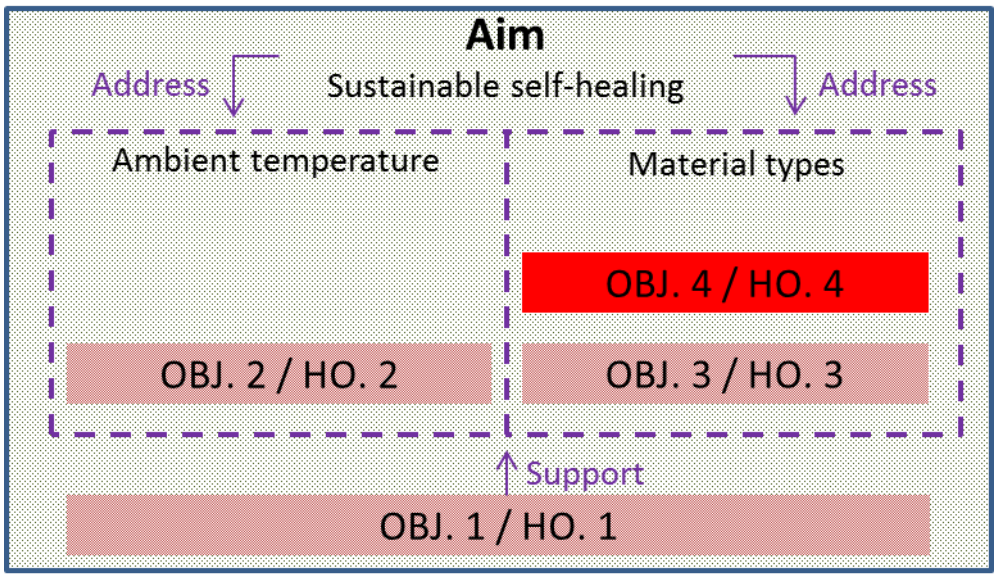

Figure 6.1. Role of Chapter 6 in the thesis (red area)

6.2. Methodology

6.2.1. Healing mechanism

The basic concept used to enable recovery of the conductivity can be seen in **Fig. 6.2**.

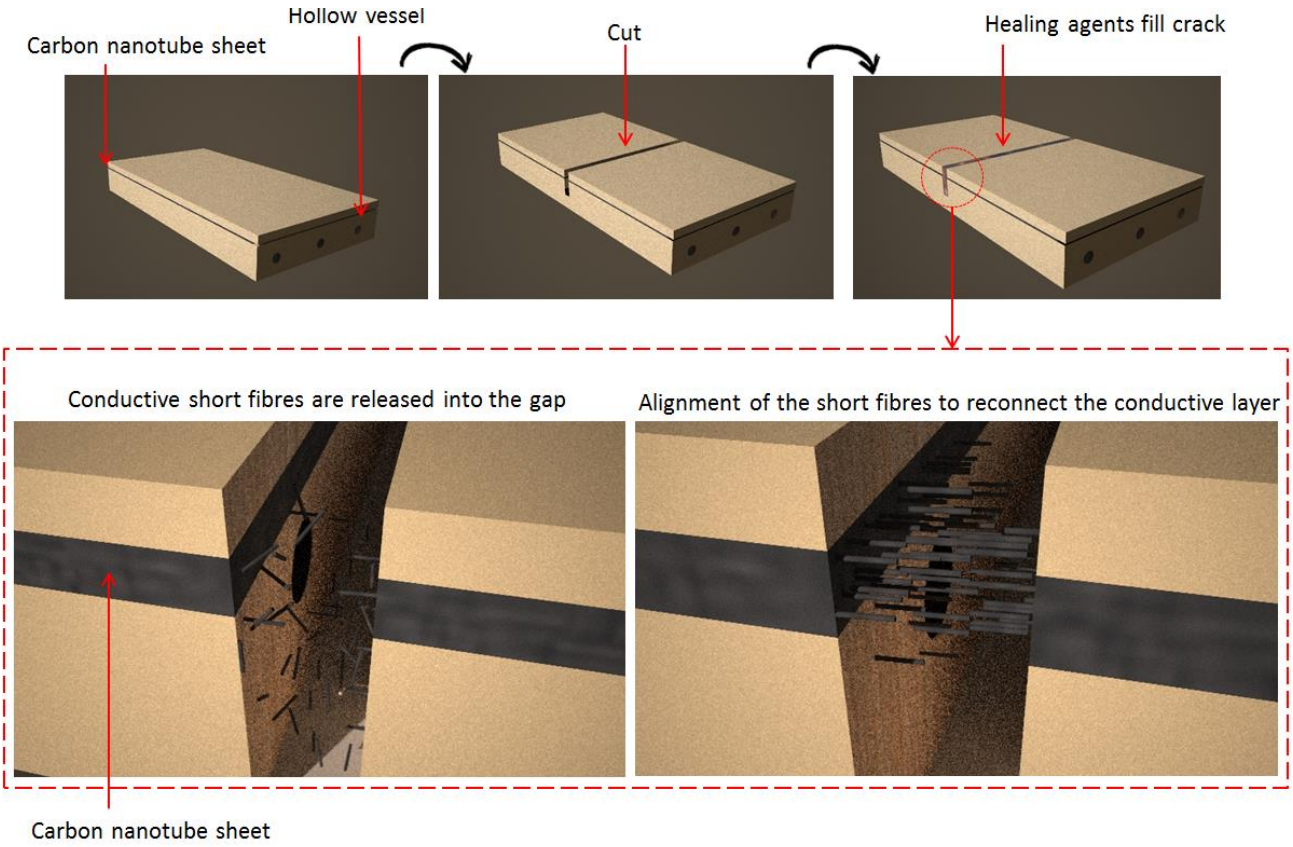

Figure 6.2. Schematic of the restoration of a carbon nanotube sheet

Fig. 6.2 shows how the procedure starts with an undamaged sample, consisting of a CNS. The CNS is then damaged producing a visible gap which ensures there is no conductivity. The HA is then delivered to the damaged area through the hollow vessels. As the CNS is conductive, when it is connected to an external power supply, the broken CNS produces an electrical field in the gap, causing the SCFs to gather and form head-to-head

contacts. As a result, the alignment of the SCFs in the HA restore the electrical conductivity. This experiment is repeated, each time changing different variables (e.g. composition of HA and electric field, *etc*.) to improve the recovery.

6.2.2. Sample fabrication

The samples are glass fibre laminates embedded with hollow vessels and carbon nanotube sheets. The sheet can be connected to a power supply through carbon fibres which were attached to the sheet. The samples were made as follows (**Fig. 6.3**):

1. Fabrication of carbon nanotube sheets. The carbon nanotube sheet was fabricated by multiple steps of single-wall carbon nanotubes (SWCNTs) dispersion and suspension filtration [151].
2. Connect a carbon nanotube sheet to carbon fibres. Carbon nanotubes were connected to carbon fibres by using a silver paste (Paint Conductive Adhesive, RS components), followed by a heating treatment at 40 ^{o}C for 6h for the adhesive to fully cure.
3. Fabrication of glass fibre laminates incorporating hollow vessels. A polypropylene table ready for resin infusion was covered with PVA releasing agent to prevent damage during de-moulding. The releasing agent became completely dry in 30 min at room temperature. Epoxy resin and hardener (Very High-Temperature Epoxy, Easy Composites Ltd.) were mixed at a ratio of 100:35 parts by weight and degassed at 35 ^{0}C for 30 minutes in a vacuum chamber. Eight layers of woven glass fibres (area density of 290 g/m2 for each layer) were laminated manually using the mixed resin and a soft brush. Nylon fishing line 2 mm in diameter was

fixed on the laminate. Eight more layers of woven glass fibres were laminated again above the nylon line. Resin infusion technique was adopted and the laminate incorporating nylon lines cured in 24h. Post-cure heating cycles were applied before pulling out the nylon lines manually, leaving hollow vessels inside the glass fibre laminate.

4. Attach the carbon nanotube sheet to the laminate. The sheet with the attached carbon fibres was placed onto the laminate, covered by another layer of glass fibres. More uncured resin was applied to soak the carbon nanotube sheet and the new glass fibre layer, followed by a repeated curing procedure in Step 3.
5. Cutting. The fully cured composite which had a thickness of 6 mm was cut into identical pieces each containing a small carbon nanotube sheet using a grit saw and polished with sand paper. The cutting and polishing followed a high-speed-low-force strategy to avoid damage. **Fig. 6.4** shows a fabricated specimen.

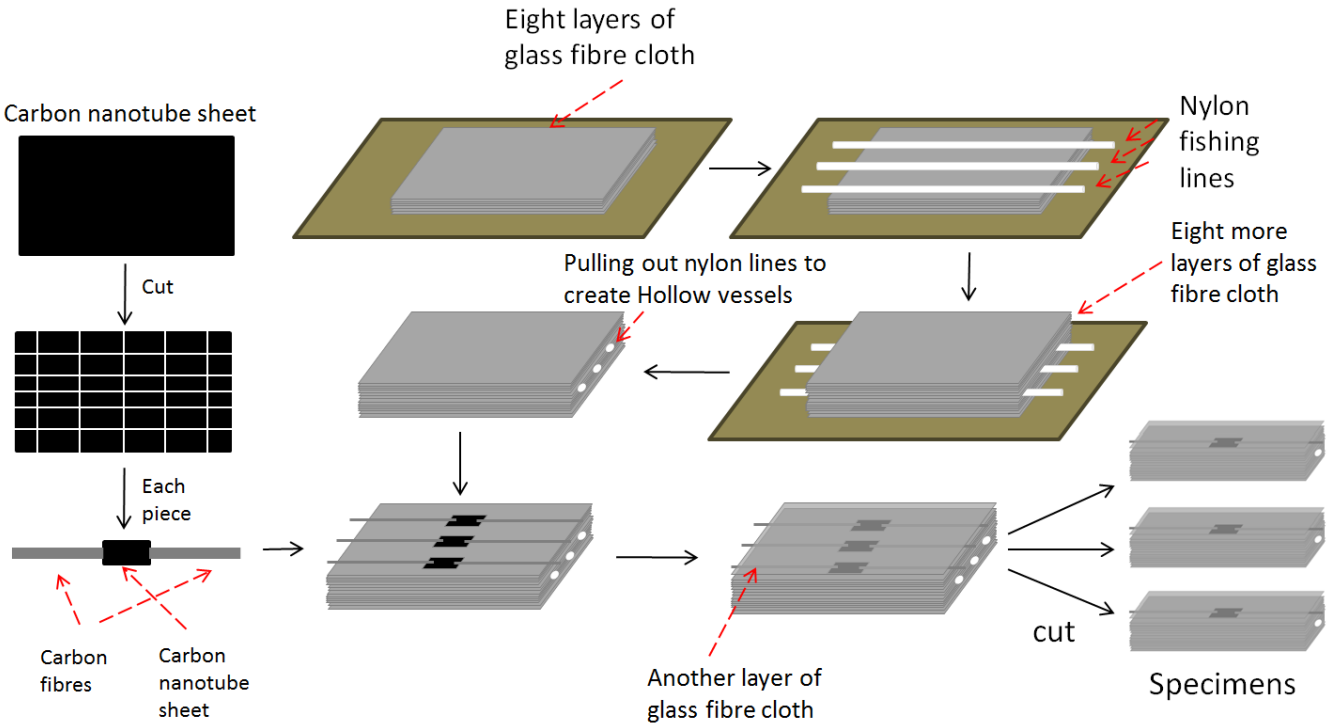

Figure 6.3. Fabrication process

a b

Figure 6.4. (a) Top view of a specimen; (b) Bottom view of a specimen

6.2.3. Testing method and procedure

A brief experimental procedure can be seen in **Fig. 6.5**.

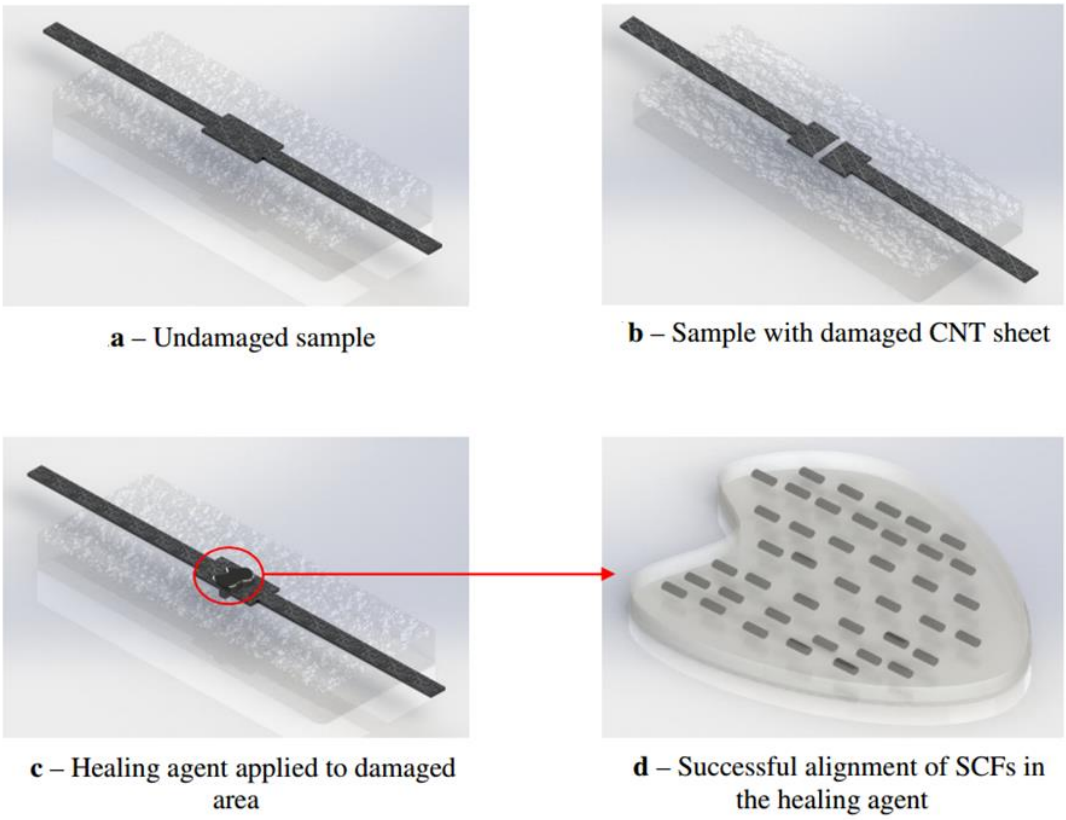

Figure 6.5. Experimental procedure

The procedure for the experiment is:

1. Using sticky gum secure three undamaged samples to a wooden fixture, and place a crocodile clip on the soft carbon fibre ends, then label each sample. It is important not to remove the samples from the wooden fixture, or remove the clips until the end of the healing process.
2. Measure the conductivity of the undamaged samples using a voltmeter and Wheatstone bridge circuit to measure the voltage across each sample.
3. An air grinder is used to cut the carbon nanotube sheet completely. It is necessary for the carbon nanotube sheet and the vascular tunnels to be fully cut.
4. The samples are then connected to a power supply, and voltage readings are checked to ensure the carbon nanotube sheet has been fully disconnected.
5. The healing agent is then collected into a syringe and applied to the damaged area directly or through the vessel while the sample is connected to the power supply. Samples were be connected to the power supply as this is used for the alignment of the short carbon fibres present in the healing agent. A new syringe is used for each application of HA.
6. The desired time is then given for healing (e.g. 24 hours, 48 hours, *etc*.).
7. After the desired time has been given, each sample is again tested with the voltage across each sample recorded.
8. The samples may then be placed in an oven for curing for another period depending on the variable being tested (e.g. 24 hours, 48 hours, etc.) The voltage across each sample would then again be measured and recorded.

Results are then shown as a recovery % (healing performance) by using **Eq. 6.1** below:

$$\text{Recovery}\ (\%) = \frac{3.32 - \text{Voltage reading after healing}}{3.32 - \text{Voltage reading before healing}} \tag{6.1}$$

Note the value of 3.32 in **Eq. 6.1** is used due to a 3.32V power supply being used to apply the electric field to the samples. This report also uses healing efficiency which can be seen in **Eq. 6.2**.

$$\eta = \frac{f_{\text{healed}} - f_{\text{damaged}}}{f_{\text{virgin}} - f_{\text{damaged}}} \times 100\% \tag{6.2}$$

where f is the property being evaluated (in this case the voltage across the sample) [30].

6.3. Results and discussion

Section 6.3.1 gives results from the tests on different SCF content in the healing agent. **Section 6.3.2** looks into the effects of voltage on the recovery; **Section 6.3.3** discusses the use of a new circuit for the alignment process. **Section 6.3.4** looks into how the vascular networks affect the recovery. **Section 6.3.5** discusses the addition of silver paste, and finally, **Section 6.3.6** shows the results of adding a dispersant to the healing agent.

6.3.1. Effect of SCF content on healing performance

This test was designed to discover the effect, if any, that the SCF wt% (weight percent) has on the recovery of the samples. The theory behind this experiment is that increasing the SCF content in the healing agent will increase the amount of SCFs that are delivered to the damaged areas. As a result of the increased SCFs alignment the recovery of the

samples increases. It was predicted that the results would show that the higher the SCF content (wt%) the better the recovery seen.

This test consisted of three different SCF content, 15 wt%, 18 wt% and 20 wt%. Nine samples were used in total, three for each wt%. This was to ensure accurate and reliable data was gathered and appropriate conclusions could be drawn from the results (all samples used did not have the microvascular tunnels). **Table 6.1** gives the summary of the test results and **Fig. 6.6** shows the average results for each wt%.

Table 6.1. Test results for 15/18/20 wt.% SCF content

	Specimen 1	Specimen 2	Specimen 3
15 wt.%	109.09%	0%	0%
18 wt.%	95.02%	29.26%	0%
20 wt.%	77.29%	0%	57.92%

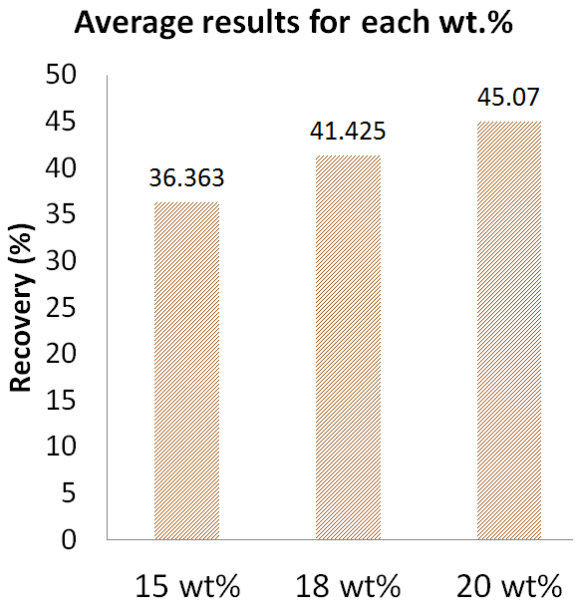

Figure 6.6. Average results for each wt.%

Fig. 6.6 shows that there is an obvious trend between the SCF content and the recovery seen. The results show as the SCF wt.% increases so does the recovery. It is interesting to note that although the average of the 15 wt.% is the lowest, it achieved the highest single recovery of a sample. This experiment has shown that the SCF wt.% has a large effect on the healing performance seen.

An important side note is that although there was a positive trend from the results for increasing SCF content, the results do not show a negative side effect of the higher SCF content. During the experiment, it was seen that as the wt.% of SCFs increased in the HA so did the viscosity. The higher the wt.% the more viscous the HA, therefore the 20 wt.% was considerably more viscous than the 15 wt.%. During the experiment applying the 18 wt.% and 20 wt.% HAs to the samples was particularly difficult, with the HA causing a blockage in the syringe preventing it from being applied. The experiments therefore showed that although higher wt% of SCF increased recovery, it also caused problems with application of the HA.

6.3.2. Effects of electric field intensity/type on healing performance

This experiment had the goal of determining whether there was a trend between the voltage of the electric field used for alignment and the recovery observed. The theory behind this experiment is that increasing the voltage increases electric field intensity, this in turn increases the alignment of the SCFs in the HA allowing for better recovery. This theory is supported by Park *et al.* [192], who show that electric field intensity has an effect on the alignment observed.

This set of experiments consisted of nine samples in total. The samples were split into groups of three and three experiments were done using the same procedure, with the HA having 15% SCF content. The difference between the experiments was the voltage of the electric field, 9V, 25V and 50V were all tested. **Table 6.2** gives the summary of the test results and **Fig. 6.7** shows the average sample results for each of the voltages.

Table 6.2. Test results for varying voltages

	Specimen 1	Specimen 2	Specimen 3
9V	109.09%	0%	0%
25V	100.38%	16.6%	0%
50V	35.97%	0%	87.32%

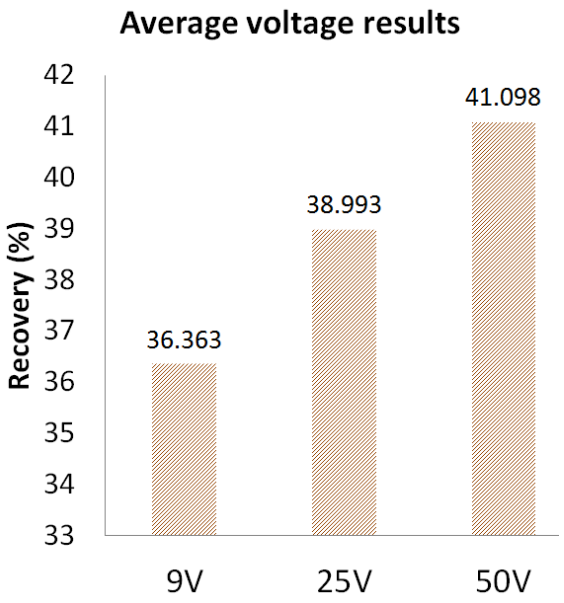

Figure 6.7. The averaged results for the samples tested at varying voltages

Fig. 6.7 shows a very clear trend between the increasing voltage and the recovery observed. The graph shows that as the voltage of the electric field has increased so too does the recovery of the samples. The averages from the 9V, 25V and 50V are 36.4%, 39.0% and 41.1% respectively.

Two things of note from this test are that the 50V samples produced small amounts of smoke when placed in the electric field. Secondly, higher voltages (75V and 100V) were tested initially, however when the HA was applied while the samples were in the electric field there was a large amount of smoking from the samples. As the conductivity recover, high voltage caused high electrical current in the material. The electrical heating could be high enough to damage samples. After 24 hours the samples showed visible burn damage and poor healing recovery. This experiment therefore showed that increasing voltage does increase the recovery up to a point where the growth in voltage starts to damage the samples.

6.3.3. Alternative circuit for alignment method

The tests into the effects of voltage in section 3.2 identified the occurrence of smoke and burned damage to the samples when using large voltages (75V and 100V) for alignment. Although lower voltages did not exhibit the obvious signs of damage observed with the higher voltages, a new circuit was produced with the purpose of preventing this burn damage from occurring in the samples as well as reducing the smoke produced. The original circuit used produced a piecewise constant voltage at the desired value. The new circuit instead produced a periodic pulse as in **Fig. 6.8**, so for a 50V test it would produce a voltage impulse every two seconds, thus giving the samples sufficient time to cool down

and prevent burn damage. As a side note, the change in the circuit was used to reduce smoke from samples and prevent burn damage, not to increase recovery.

The test used six samples in total. Three samples used were tested at 50V on the old circuit, and three samples were tested at 50V with the new circuit. All of the samples were applied with 15 wt% HA, and all the samples did not have vascular networks.

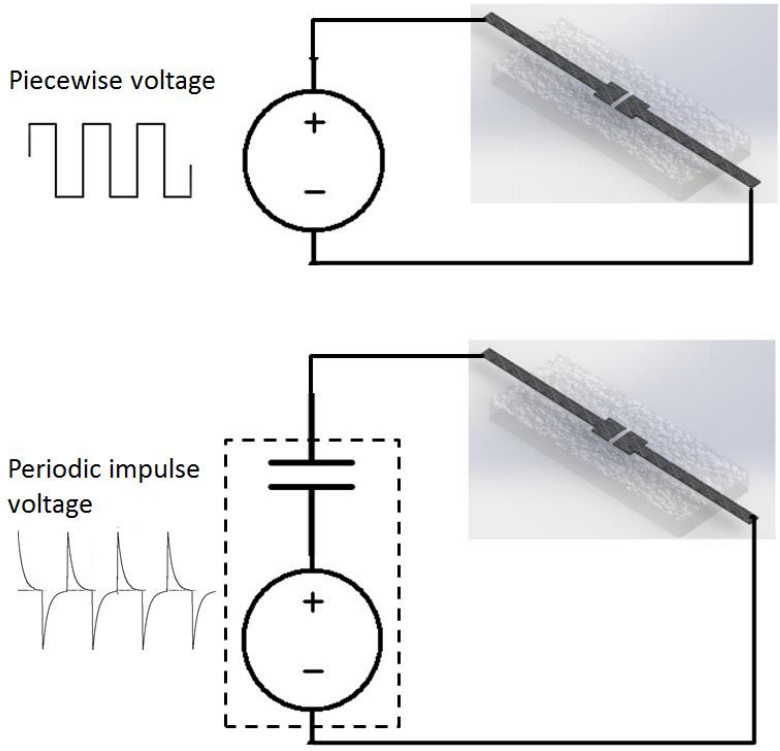

Figure 6.8. Alternative circuit adopted to avoid over heat

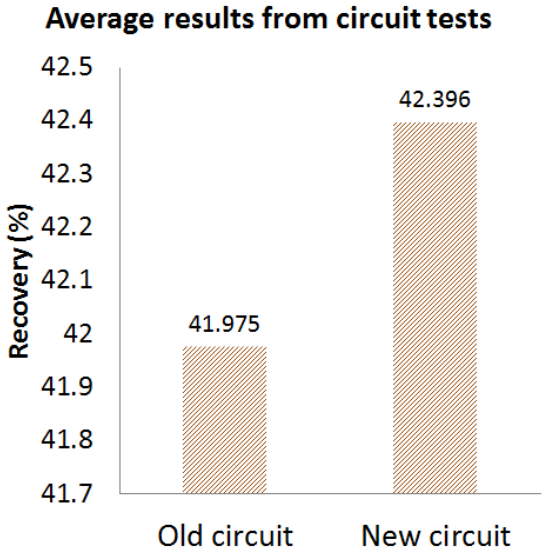

Figure 6.9. Average results for the two different circuits

Fig. 6.9 shows that the change of circuit did not affect the recovery in a negative way. The average for the new circuit was slightly higher, with the old circuit being 42.0% and the new circuit achieving 42.4%. However, this small increase was more to do with the individual samples rather than the change in circuit. The new circuit did not affect the recovery observed, but it did manage to reduce electrical heating caused by high voltage. Due to the use of the new circuit, no smoking of the samples was observed during the alignment process, hence justifying its use.

6.3.4. Investigating the effect of silver paste

This set of experiments was designed to investigate what effect the addition of silver paste to the HA has on the recovery of the samples. The theory behind the addition of silver paste is that the silver paste could act as another conductive path for the damaged area, mimicking the effect of the SCFs. As a side note silver paste was chosen due to silver

paste being lower cost and more available making it more suitable for widespread commercial use. Odom *et al.* [180] followed a similar experiment where they produced a self-healing conductive ink which consisted of silver particles. They produced silver particle ink lines, which they then damaged using a razor blade and healed.

This test consisted of nine samples with vascular structures, three samples for each experiment. All three experiments used 15 wt% SCFs, 50V electric field and pumping from one side of samples. The difference between the experiments was one used 1 wt% silver paste added into the HA, one used 2 wt% silver paste and the last used 3 wt% silver paste. **Table 6.3** gives the summary of the test results and **Fig. 6.10** shows the averaged results of the silver paste experiments.

Table 6.3. Test results for silver paste

	Specimen 1	**Specimen 2**	**Specimen 3**
1% Silver Paste	53.85%	53.36%	0.73%
2% Silver Paste	20.63%	92.72%	17.33%
3% Silver Paste	0.96%	2.28%	1.91%

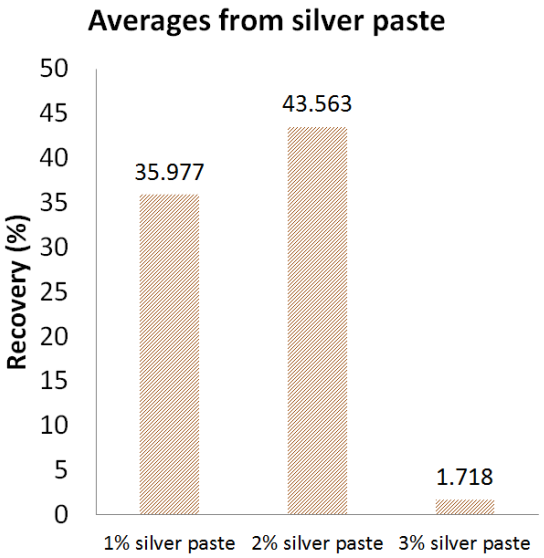

Figure 6.10. Results for the averages from silver paste experiments

Fig. 6.10 shows the addition of 1 wt% and 2 wt% silver paste allowed for good recovery of conductivity, with the 1% silver paste achieving 36% average and the 2% achieving 43.6%. The 3 wt% silver paste showed very poor recovery which was due to burn damage to the samples. During the experiment for the 3% silver paste when the HA was applied to the samples in the electric field there was a large amount of smoke produced within the first 30 minutes. After 30 minutes the smoking had ceased. However the samples were already damaged leading to the poor results. The results from these experiments therefore show that the addition of silver paste to the healing agent does increase the recovery. However there is a limit to how much silver paste can be added before it becomes detrimental to the recovery of the samples.

6.3.5. Addition of dispersant to the healing agent

The test described here was designed to investigate the effect adding a dispersant has on the HA and the recovery seen. The dispersant DISPERBYK-191 (BYK Additives & Instruments, GmbH) was chosen as its purpose was primarily for use with short fibres such as the SCFs used in this study. There are two reasons behind the introduction of the dispersant. The first is to help disperse the SCFs out more consistently in the HA. One problem with current results is the randomness of the healing, i.e one sample will recover well while the next will show poor recovery. The inconsistent diffusion of the SCFs in the HA, meaning each sample gets differing amounts of SCF for alignment. Ladani *et al*. [20] used this dispersant for the same reasons when improving the toughness of epoxy

nanocomposites. The second reason for using a dispersant is that it can make the alignment process easier. The addition of the dispersant can reduce the viscosity of the HA and therefore decrease the viscous forces on the SCFs when they are rotating during alignment, thus making alignment easier and more consistent throughout the damaged area of the sample.

This test used six samples in total, all of which contained vascular tunnels. One set of three samples were tested with HA consisting of 15 wt% SCF content along with 2 wt% silver paste and 3% dispersant. The next three samples were tested with HA consisting of 15 wt% SCF content and 2 wt% silver paste but without any dispersant. **Fig. 6.11a** and **6.11b** show the individual and averaged sample results for recovery respectively.

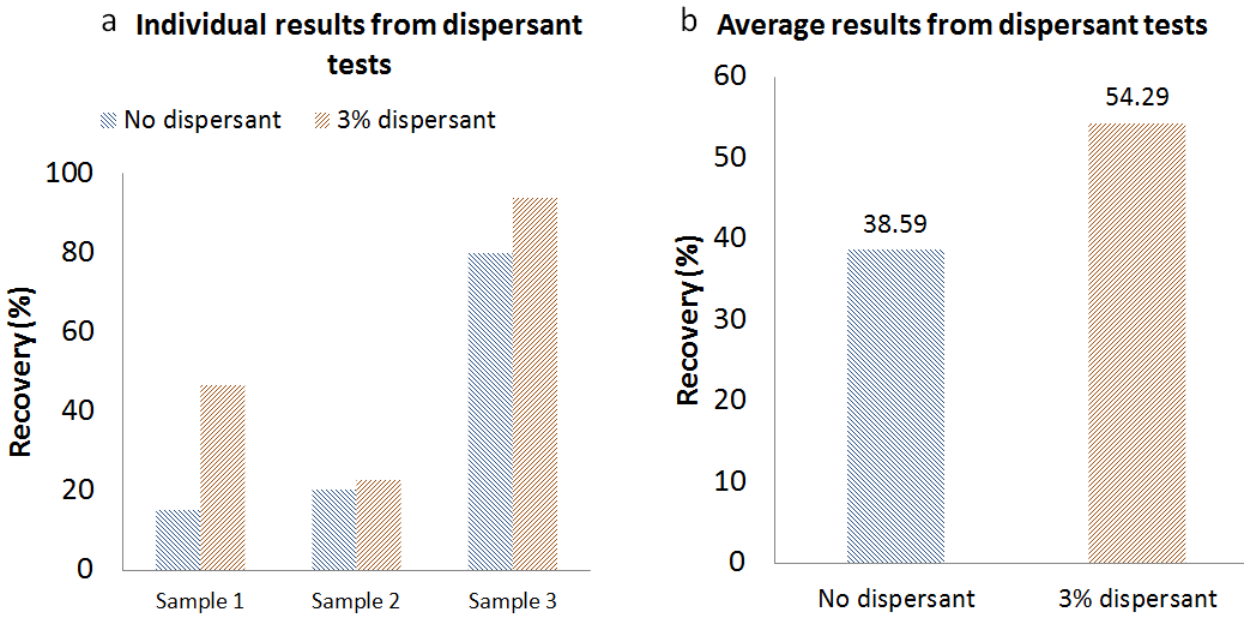

Figure 6.11. a) Individual recovery of samples; b) Averaged recovery results

Fig. 6.11 shows a clear increase in the recovery of the samples both individually and for the averages when dispersant is added into the HA. The average recovery for the

samples which did not have dispersant in the HA was 38.6% which increased to 54% in the samples which had HA with dispersant added in.

Fig. 6.12 shows a sample from the initial stage through to the final stage where it has been healed.

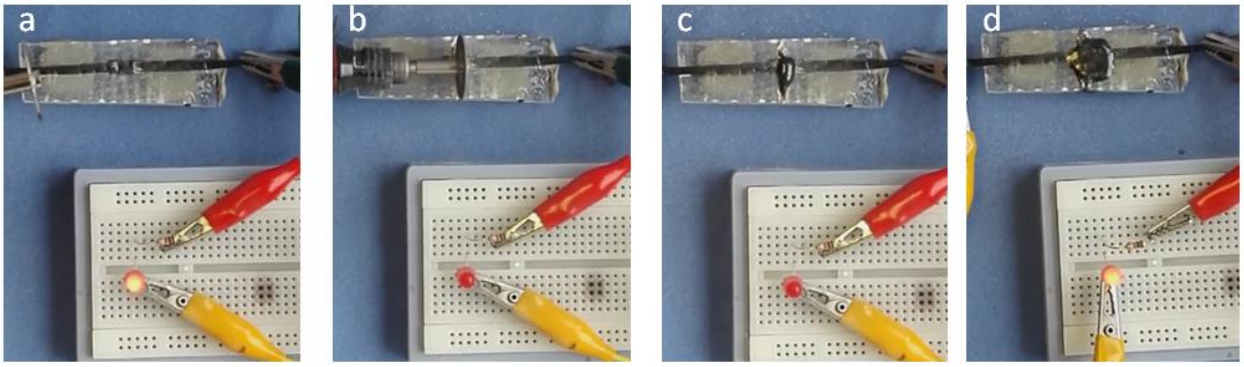

Figure 6.12. (a) shows the original undamaged sample, (b) shows the sample being cut, losing its conductivity, (c) shows the sample release HA from vessels, and (d) shows the sample restore its conductivity after 24 hours as SCFs being aligned in an electric field to reconnect the broken CNS.

6.4. Summary

This Chapter has described a healing agent composition and a healing mechanism that can restore the conductivity to a carbon nanotube sheet embedded inside polymer composites. The results reveal that the main parameters affecting the recovery are the voltage of the electric field, the addition of silver paste and the inclusion of a dispersant in the healing agent. This chapter has also shown that increasing the SCF content in the HA has a positive effect on the recovery exhibited by the samples. However, this also negatively affects the viscosity of the healing agent, making its application difficult.

Overall, the results from the experiments have allowed the optimum HA composition to be formulated. The final composition which gives the best results was found to contain 15 wt% SCF content with the addition of 2 wt% silver paste and 3 wt% dispersant. The average recovery was 54%, and the best healing performance could reach 100%.

Chapter 7 - Conclusions, contributions and future work

7.1. Conclusions

This research has presented various techniques to enhance the sustainability of healing capacity. To appreciate previous development in self-healing composites and reveal key barriers in practice, the thesis provides an overview of the various self-healing concepts proposed over the past decades, and a comparative analysis of healing mechanisms and fabrication techniques for building capsules and vascular networks. Based on the analysis, factors that influence healing performance are presented to highlight the importance of developing sustainable self-healing capability to allow materials to recover regardless of ambient temperatures and material types.

The first part of the research was to experimentally investigate the effects of vessel configurations on the healing performance and flexural properties of fibre-reinforced composites. It also analysed the crack behaviour caused by bending and healing processes in laminates. Experimental results indicate that vessels should be placed in the core of the laminates instead of under the surface. The vessels should penetrate multiple layers and have wide in-plane coverage so that large-scale delamination could be cured. When the damage is minor, mainly consisting of debonding and delamination, the composites are able to achieve a high healing efficiency, even a full recovery. However, the fractured structural fibres becoming the primary crack site should be avoided. When the composites are designed using a correct vessel configuration, the vessels can have a minor effect on the flexural properties, and a healing efficiency higher than 100% is achievable. Otherwise, the healing efficiency can be very poor. The results also indicate the importance of developing new healing agents that can repair not only the matrix but

also the structural fibres. In this part of the study, **Objective 1** was accomplished and **Hypothesis 1** was verified.

The aim of the second part of the research was to enable sustainable self-healing at very low ambient temperatures. The thesis has presented a structural composite able to maintain its temperature to provide a sustainable self-healing capability – similar to that in the natural world where some animals keep a constant body temperature to allow enzymes to stay active. The composite incorporates three-dimensional hollow vessels with the purpose of delivering and releasing healing agents, and a porous conductive element to provide heat internally to defrost and promote healing reactions. Healing in fibre-reinforced composites at a temperature around -60 C was achieved with an average recovery of 108% in fracture energy and 96% in peak load. The effects of the sheets on the interlaminar and tensile properties have been experimentally investigated. It was found that the introduction of a carbon nanotube sheet increased the tensile strength of polymer composites, but had negative effects on interlaminar properties. In this work, **Objective 2** was accomplished and **Hypothesis 2** was verified.

The third part of the research focussed on an approach to recover carbon fibres, a common material adopted in structural fibre-reinforced composites. The thesis reports the development of a carbon fibre composite that can repair its structural fibres and restore its mechanical properties after it has been subjected to damage, by using an embedded vascular self-healing system. Damage is healed through the application of an epoxy-based resin containing short carbon fibres that can reconnect the fractured carbon fibres upon electric alignment and curing. Different variables and parameters were investigated to observe their effects on the healing performance until the optimum healing agent composition and conditions were found. A model based on the Rule of Mixture can be

used to analyse and predict healing performances. The optimum conditions demonstrate that the healing efficiency and performance were increased by 3788% and 153% respectively compared to an unprocessed epoxy resin used in conventional self-healing materials, and as high as 45% of the original strength could be restored. In this study, **Objective 3** was accomplished and **Hypothesis 3** was verified.

The final part of the research dealt with another type of materials, conductive porous elements, which can be automatically repaired by using a modified mechanism based on the third part. Conductive elements are popular in the development of multifunctional composite materials. The composite incorporated hollow vessels which could deliver a healing agent containing short carbon fibres to the damaged areas to repair broken carbon nanotube sheets. The recovery process took place in an electric field to aid the alignment of the short carbon fibres. The healing agent composition was changed as well as parameters such as the electric field intensity and short carbon fibre content to determine their effects on the recovery of the carbon nanotube sheet. The results show that the intensity of the electric field, the addition of silver paste to the healing agent, and the addition of dispersant to the healing agent lead to optimum recovery. Experimental results demonstrate that an average recovery of 54% is achievable, and recovery as high as 100% has been observed. Thus, **Objective 4** was accomplished and **Hypothesis 4** was verified.

The work presented in the thesis has demonstrated new techniques and a novel design enabling structural composites to recover regardless of ambient conditions and material types. Therefore, the aim of the research has been achieved.

7.2. Contributions

The following are the key contributions of this study:

- For the first time, it has been demonstrated that vessel configurations can have significant negative effects on the mechanical properties and healing performances of fibre-reinforced composites. This research has identified vessel configurations that are suitable for self-healing composites.
- This research has resulted in a practical method to enable materials, commonly used in aircraft and satellites, to self-heal cracks at temperatures well below freezing. No self-healing has been reported for materials operating under such severe conditions until now.
- The research has proposed and verified a design enabling the healing of structural carbon fibres. Carbon fibre composites are used for their light weight and high strength. Previous research efforts had focused on the recovery of the matrix of the material. However, until the present work, structural carbon fibres could not be autonomously mended.
- The thesis has presented a new method allowing the recovery of the electrical conductivity of conductive components in a composite material. Multifunctional composites incorporating sensors or actuators often contain conductive components. However, research on self-healing composites had previously been focusing just on mechanical properties. This research has enabled not only the structural component but also the functional or conductive component to be repaired.

7.3. Future work

The experimental results presented in **Chapter 4** indicate that the introduction of carbon nanotube sheets could cause a reduction in interlaminar strength. A potential solution might be to include patterns on the sheet surface to preserve interlaminar properties without significantly affecting heating performance.

Chapter 5 reported that 45% of the original strength of a carbon fibre composite could be restored. As discussed in **Section 5.3.7**, the healing performance might further improve if the values of Fibre strength σ_{fu}, Volume fraction of structural fibres V_f, Fibre length factor $F\left(\frac{l_c}{l}\right)$ and Orientation factor C_o could be increased. This should be tested in the future.

As reported in **Chapter 6,** research into the restoration of conductivity has successfully achieved an average healing over all samples of 54%. Raising this to 100% recovery is a possible avenue of enquiry. Another area of research is consistent healing performance. This research has found that healing efficiency can be as high as 100% for some samples. However, other samples may demonstrate very poor recovery, resulting in a much lower average recovery. An important research topic would therefore be how to obtain similar healing results across multiple samples. The last area of further investigation related to the restoration of conductivity is a phenomenon observed during this study where the conductivity of the samples started to decrease 24 hours after healing. It was found that the healing would finish (full conductivity was achieved) after around 2-3 hours. Then, after the samples were removed from the electric field, the conductivity would reduce by around 1-2%. Research into this phenomenon would be of interest.

References

[1] B. J. Blaiszik, S. L. B. Kramer, S. C. Olugebefola, J. S. Moore, N. R. Sottos, and S. R. White, “Self-Healing Polymers and Composites,” *Annu. Rev. Mater. Res.*, vol. 40, no. 1, pp. 179–211, 2010.

[2] S. R. White, N. R. Sottos, P. H. Geubelle, J. S. Moore, M. R. Kessler, S. R. Sriram, E. N. Brown, and S. Viswanathan, “Autonomic healing of polymer composites,” *Nature*, vol. 409, no. 6822, pp. 794–797, 2001.

[3] Y. Wang, D. T. Pham, and C. Ji, “Self-healing composites: A review,” *Cogent Eng.*, vol. 2, no. 1, p. 1075686, 2015.

[4] D. Y. Zhu, M. Z. Rong, and M. Q. Zhang, “Self-healing polymeric materials based on microencapsulated healing agents: From design to preparation,” *Prog. Polym. Sci.*, vol. 49–50, pp. 175–220, 2015.

[5] X. J. Ye, J. L. Zhang, Y. Zhu, M. Z. Rong, M. Q. Zhang, Y. X. Song, and H. X. Zhang, “Ultrafast Self-Healing of Polymer toward Strength Restoration,” *ACS Appl. Mater. Interfaces*, vol. 6, no. 5, pp. 3661–3670, 2014.

[6] S. R. White, J. S. Moore, N. R. Sottos, B. P. Krull, W. A. S. Cruz, and R. C. R. Gergely, “Restoration of Large Damage Volumes in Polymers,” *Science,* vol. 344, Issue 6184, pp. 620-623, 2014.

[7] J. F. Patrick, K. R. Hart, B. P. Krull, C. E. Diesendruck, J. S. Moore, S. R. White, and N. R. Sottos, “Continuous Self-Healing Life Cycle in Vascularized Structural Composites,” *Adv. Mater.*, vol. 26, no. 25, pp. 4302–4308, 2014.

[8] “Autonomous materials systems.” [Online]. Available: http://autonomic.beckman.illinois.edu/.

[9] “Self-Healing Plastics Make a Major Breakthrough.” [Online]. Available: http://www.engineering.com/DesignerEdge/DesignerEdgeArticles/ArticleID/7595/Self-Healing-Plastics-Make-a-Major-Breakthrough.aspx.

[10] B. J. Blaiszik, S. L. B. Kramer, S. C. Olugebefola, J. S. Moore, N. R. Sottos, and S. R. White, “Self-Healing Polymers and Composites,” *Annu. Rev. Mater. Res.*, vol. 40, no. 1, pp. 179–211, 2010.

[11] X. X. Chen, F. Wudl, A. K. Mal, H. B. Shen, and S. R. Nutt, “New thermally remendable highly cross-linked polymeric materials,” *Macromolecules*, vol. 36, no. 6, pp. 1802–1807, 2003.

[12] D. Habault, H. Zhang, and Y. Zhao, “Light-triggered self-healing and shape-memory polymers,” *Chem Soc Rev*, vol. 42, no. 17, pp. 7244–7256, 2013.

[13] E. Selver, P. Potluri, C. Soutis, and P. Hogg, “Healing potential of hybrid materials for structural composites,” *Compos. Struct.*, 2014.

[14] C. Zheng and Z. Huang, “Microgel reinforced composite hydrogels with pH-

responsive, self-healing properties," *Colloids Surfaces A Physicochem. Eng. Asp.*, vol. 468, no. 0, pp. 327–332, 2015.

[15] M. R. Kessler, "Self-healing: a new paradigm in materials design," *Proc. Inst. Mech. Eng. Part G J. Aerosp. Eng.*, vol. 221, no. 4, pp. 479–495, 2007.

[16] B. Aïssa, D. Therriault, E. Haddad, and W. Jamroz, "Self-Healing Materials Systems: Overview of Major Approaches and Recent Developed Technologies," *Adv. Mater. Sci. Eng.*, vol. 2012, pp. 1–17, 2012.

[17] R. Frei, R. McWilliam, B. Derrick, A. Purvis, A. Tiwari, and G. Di Marzo Serugendo, "Self-healing and self-repairing technologies," *Int. J. Adv. Manuf. Technol.*, vol. 69, no. 5–8, pp. 1033–1061, 2013.

[18] N. K. Guimard, K. K. Oehlenschlaeger, J. Zhou, S. Hilf, F. G. Schmidt, and C. Barner-Kowollik, "Current Trends in the Field of Self-Healing Materials," *Macromol. Chem. Phys.*, vol. 213, no. 2, pp. 131–143, 2012.

[19] C. Norris, I. Bond, and R. Trask, "Bioinspired Vasculatures for Self-Healing Fibre Reinforced Polymer Composites," *Proc. Asme Conf. Smart Mater. Adapt. Struct. Intell. Syst. (Smasis 2011), Vol 2*, pp. 599–606, 2012.

[20] T. J. Swait, A. Rauf, R. Grainger, P. B. S. Bailey, A. D. Lafferty, E. J. Fleet, R. J. Hand, and S. A. Hayes, "Smart composite materials for self-sensing and self-healing," *Plast. Rubber Compos.*, vol. 41, no. 4–5, pp. 215–224, 2012.

[21] R. S. Trask, H. R. Williams, and I. P. Bond, "Self-healing polymer composites: mimicking nature to enhance performance," *Bioinspir Biomim*, vol. 2, no. 1, pp. P1–9, 2007.

[22] R. P. Wool, "Self-healing materials: a review," *Soft Matter*, vol. 4, no. 3, p. 400, 2008.

[23] D. Y. Wu, S. Meure, and D. Solomon, "Self-healing polymeric materials: A review of recent developments," *Prog. Polym. Sci.*, vol. 33, no. 5, pp. 479–522, 2008.

[24] Y. Yang and M. W. Urban, "Self-healing polymeric materials," *Chem Soc Rev*, vol. 42, no. 17, pp. 7446–7467, 2013.

[25] Y. C. Yuan, "Self healing in polymers and polymer composites. Concepts, realization and outlook: A review," *eXPRESS Polym. Lett.*, vol. 2, no. 4, pp. 238–250, 2008.

[26] M. Zhang and M. Rong, "Design and synthesis of self-healing polymers," *Sci. China Chem.*, vol. 55, no. 5, pp. 648–676, 2012.

[27] M. R. Kessler, N. R. Sottos, and S. R. White, "Self-healing structural composite materials," *Compos. Part a-Applied Sci. Manuf.*, vol. 34, no. 8, pp. 743–753, 2003.

[28] M. R. Kessler and S. R. White, "Self-activated healing of delamination damage in woven composites," *Compos. Part a-Applied Sci. Manuf.*, vol. 32, no. 5, pp. 683–699, 2001.

[29] E. N. Brown, S. R. White, and N. R. Sottos, "Retardation and repair of fatigue cracks

in a microcapsule toughened epoxy composite - Part 1: Manual infiltration," *Compos. Sci. Technol.*, vol. 65, no. 15–16, pp. 2466–2473, 2005.

[30] B. J. Blaiszik, M. Baginska, S. R. White, and N. R. Sottos, "Autonomic Recovery of Fiber/Matrix Interfacial Bond Strength in a Model Composite," *Adv. Funct. Mater.*, vol. 20, no. 20, pp. 3547–3554, 2010.

[31] A. R. Jones, B. J. Blaiszik, S. R. White, and N. R. Sottos, "Full recovery of fiber/matrix interfacial bond strength using a microencapsulated solvent-based healing system," *Compos. Sci. Technol.*, vol. 79, pp. 1–7, 2013.

[32] A. R. Jones, A. Cintora, S. R. White, and N. R. Sottos, "Autonomic Healing of Carbon Fiber/Epoxy Interfaces," *ACS Appl. Mater. Interfaces*, vol. 6, no. 9, pp. 6033–6039, 2014.

[33] J. M. Kamphaus, J. D. Rule, J. S. Moore, N. R. Sottos, and S. R. White, "A new self-healing epoxy with tungsten (VI) chloride catalyst," *J. R. Soc. Interface*, vol. 5, no. 18, pp. 95–103, 2008.

[34] T. S. Coope, U. F. J. Mayer, D. F. Wass, R. S. Trask, and I. P. Bond, "Self-Healing of an Epoxy Resin Using Scandium(III) Triflate as a Catalytic Curing Agent," *Adv. Funct. Mater.*, vol. 21, no. 24, pp. 4624–4631, 2011.

[35] S. Billiet, W. Van Camp, X. K. D. Hillewaere, H. Rahier, and F. E. Du Prez, "Development of optimized autonomous self-healing systems for epoxy materials based on maleimide chemistry," *Polymer (Guildf).*, vol. 53, no. 12, pp. 2320–2326, 2012.

[36] B. Aïssa, K. Tagziria, E. Haddad, W. Jamroz, J. Loiseau, A. Higgins, M. Asgar-Khan, S. V Hoa, P. G. Merle, D. Therriault, and F. Rosei, "The Self-Healing Capability of Carbon Fibre Composite Structures Subjected to Hypervelocity Impacts Simulating Orbital Space Debris," *ISRN Nanomater.*, vol. 2012, pp. 1–16, 2012.

[37] J. K. Lee, S. J. Hong, X. Liu, and S. H. Yoon, "Characterization of dicyclopentadiene and 5-ethylidene-2-norbornene as self-healing agents for polymer composite and its microcapsules," *Macromol. Res.*, vol. 12, no. 5, pp. 478–483, 2004.

[38] X. Liu, J. K. Lee, S. H. Yoon, and M. R. Kessler, "Characterization of diene monomers as healing agents for autonomic damage repair," *J. Appl. Polym. Sci.*, vol. 101, no. 3, pp. 1266–1272, 2006.

[39] G. C. Huang, J. K. Lee, and M. R. Kessler, "Evaluation of Norbornene-Based Adhesives to Amine-Cured Epoxy for Self-Healing Applications," *Macromol. Mater. Eng.*, vol. 296, no. 10, pp. 965–972, 2011.

[40] M. Raimondo and L. Guadagno, "Healing efficiency of epoxy-based materials for structural applications," *Polym. Compos.*, vol. 34, no. 9, pp. 1525–1532, 2013.

[41] S. H. Cho, H. M. Andersson, S. R. White, N. R. Sottos, and P. V. Braun, "Polydimethylsiloxane-Based Self-Healing Materials," *Adv. Mater.*, vol. 18, no. 8, pp. 997–1000, 2006.

[42] S. H. Cho, S. R. White, and P. V Braun, “Self-Healing Polymer Coatings,” *Adv. Mater.*, vol. 21, no. 6, pp. 645–649, 2009.

[43] J. L. Moll, H. Jin, C. L. Mangun, S. R. White, and N. R. Sottos, “Self-sealing of mechanical damage in a fully cured structural composite,” *Compos. Sci. Technol.*, vol. 79, pp. 15–20, 2013.

[44] T. Yin, M. Z. Rong, M. Q. Zhang, and G. C. Yang, “Self-healing epoxy composites – Preparation and effect of the healant consisting of microencapsulated epoxy and latent curing agent,” *Compos. Sci. Technol.*, vol. 67, no. 2, pp. 201–212, 2007.

[45] L. Yuan, G. Z. Liang, J. Q. Xie, L. Li, and J. Guo, “Preparation and characterization of poly(urea-formaldehyde) microcapsules filled with epoxy resins,” *Polymer (Guildf).*, vol. 47, no. 15, pp. 5338–5349, 2006.

[46] Y. C. Yuan, M. Z. Rong, M. Q. Zhang, J. Chen, G. C. Yang, and X. M. Li, “Self-healing polymeric materials using epoxy/mercaptan as the healant,” *Macromolecules*, vol. 41, no. 14, pp. 5197–5202, 2008.

[47] Y. C. Yuan, M. Z. Rong, M. Q. Zhang, G. C. Yang, and J. Q. Zhao, “Self-healing of fatigue crack in epoxy materials with epoxy/mercaptan system,” *eXPRESS Polym. Lett.*, vol. 5, no. 1, pp. 47–59, 2011.

[48] B. J. Blaiszik, M. M. Caruso, D. A. McIlroy, J. S. Moore, S. R. White, and N. R. Sottos, “Microcapsules filled with reactive solutions for self-healing materials,” *Polymer (Guildf).*, vol. 50, no. 4, pp. 990–997, 2009.

[49] M. M. Caruso, B. J. Blaiszik, S. R. White, N. R. Sottos, and J. S. Moore, “Full recovery of fracture toughness using a nontoxic solvent-based self-healing system,” *Adv. Funct. Mater.*, vol. 18, no. 13, pp. 1898–1904, 2008.

[50] M. M. Caruso, D. A. Delafuente, V. Ho, N. R. Sottos, J. S. Moore, and S. R. White, “Solvent-promoted self-healing epoxy materials,” *Macromolecules*, vol. 40, no. 25, pp. 8830–8832, 2007.

[51] H. Choi, K. Y. Kim, and J. M. Park, “Encapsulation of aliphatic amines into nanoparticles for self-healing corrosion protection of steel sheets,” *Prog. Org. Coatings*, vol. 76, no. 10, pp. 1316–1324, 2013.

[52] L. Liao, W. Zhang, Y. Xin, H. Wang, Y. Zhao, and W. Li, “Preparation and characterization of microcapsule containing epoxy resin and its self-healing performance of anticorrosion covering material,” *Chinese Sci. Bull.*, vol. 56, no. 4–5, pp. 439–443, 2011.

[53] X. X. Liu, H. R. Zhang, J. X. Wang, Z. Wang, and S. C. Wang, “Preparation of epoxy microcapsule based self-healing coatings and their behavior,” *Surf. Coat. Technol.*, vol. 206, no. 23, pp. 4976–4980, 2012.

[54] H. Zhang and J. L. Yang, “Development of self-healing polymers via amine-epoxy chemistry: II. Systematic evaluation of self-healing performance,” *Smart Mater. Struct.*, vol. 23, no. 6, 2014.

[55] H. Zhang and J. L. Yang, “Development of self-healing polymers via amine-epoxy chemistry: I. Properties of healing agent carriers and the modelling of a two-part self-healing system,” *Smart Mater. Struct.*, vol. 23, no. 6, 2014.

[56] W. T. Li, Z. W. Jiang, Z. H. Yang, N. Zhao, and W. Z. Yuan, “Self-Healing Efficiency of Cementitious Materials Containing Microcapsules Filled with Healing Adhesive: Mechanical Restoration and Healing Process Monitored by Water Absorption,” *PLoS One*, vol. 8, no. 11, 2013.

[57] D. Snoeck, K. Van Tittelboom, S. Steuperaert, P. Dubruel, and N. De Belie, “Self-healing cementitious materials by the combination of microfibres and superabsorbent polymers,” *J. Intell. Mater. Syst. Struct.*, vol. 25, no. 1, pp. 13–24, 2014.

[58] C. M. Dry, “Three designs for the internal release of sealants, adhesives, and waterproofing chemicals into concrete to reduce permeability,” *Cem. Concr. Res.*, vol. 30, no. 12, pp. 1969–1977, 2000.

[59] F. Xing, Z. Ni, N. X. Han, B. Q. Dong, X. X. Du, Z. Huang, and M. Zhang, “Self-Healing Mechanism of a Novel Cementitious Composite Using Microcapsules,” *Adv. Concr. Struct. Durability, Proc. Icdcs2008, Vols 1 2*, pp. 195–204, 2008.

[60] J.-F. Su, J. Qiu, and E. Schlangen, “Stability investigation of self-healing microcapsules containing rejuvenator for bitumen,” *Polym. Degrad. Stab.*, vol. 98, no. 6, pp. 1205–1215, 2013.

[61] K. Van Tittelboom and N. De Belie, “Self-Healing in Cementitious Materials-A Review,” *Materials (Basel).*, vol. 6, no. 6, pp. 2182–2217, 2013.

[62] E. N. Brown, M. R. Kessler, N. R. Sottos, and S. R. White, “In situ poly(urea-formaldehyde) microencapsulation of dicyclopentadiene,” *J Microencapsul*, vol. 20, no. 6, pp. 719–730, 2003.

[63] X. Liu, X. Sheng, J. K. Lee, and M. R. Kessler, “Synthesis and Characterization of Melamine-Urea-Formaldehyde Microcapsules Containing ENB-Based Self-Healing Agents,” *Macromol. Mater. Eng.*, vol. 294, no. 6–7, pp. 389–395, 2009.

[64] Q. Li, A. K. Mishra, N. H. Kim, T. Kuila, K. Lau, and J. H. Lee, “Effects of processing conditions of poly(methylmethacrylate) encapsulated liquid curing agent on the properties of self-healing composites,” *Compos. Part B Eng.*, vol. 49, pp. 6–15, 2013.

[65] Q. Li, Siddaramaiah, N. H. Kim, D. Hui, and J. H. Lee, “Effects of dual component microcapsules of resin and curing agent on the self-healing efficiency of epoxy,” *Compos. Part B-Engineering*, vol. 55, pp. 79–85, 2013.

[66] V. V Zuev, J. Lee, S. V Kostromin, S. V Bronnikov, and D. Bhattacharyya, “Statistical analysis of the self-healing epoxy-loaded microcapsules across their synthesis,” *Mater. Lett.*, vol. 94, pp. 79–82, 2013.

[67] B. J. Blaiszik, N. R. Sottos, and S. R. White, “Nanocapsules for self-healing materials,” *Compos. Sci. Technol.*, vol. 68, no. 3–4, pp. 978–986, 2008.

[68] A. Fereidoon, M. Ghorbanzadeh Ahangari, and M. Jahanshahi, “Effect of nanoparticles on the morphology and thermal properties of self-healing poly(urea-formaldehyde) microcapsules,” *J. Polym. Res.*, vol. 20, no. 6, 2013.

[69] Y. Yang, Z. Wei, C. Wang, and Z. Tong, “Versatile Fabrication of Nanocomposite Microcapsules with Controlled Shell Thickness and Low Permeability,” *ACS Appl. Mater. Interfaces*, vol. 5, no. 7, pp. 2495–2502, 2013.

[70] J. D. Rule, E. N. Brown, N. R. Sottos, S. R. White, and J. S. Moore, “Wax-protected catalyst microspheres for efficient self-healing materials,” *Adv. Mater.*, vol. 17, no. 2, p. 205–+, 2005.

[71] D. A. McIlroy, B. J. Blaiszik, M. M. Caruso, S. R. White, J. S. Moore, and N. R. Sottos, “Microencapsulation of a Reactive Liquid-Phase Amine for Self-Healing Epoxy Composites,” *Macromolecules*, vol. 43, no. 4, pp. 1855–1859, 2010.

[72] Y. L. Chen and Z. B. Guan, “Self-assembly of core-shell nanoparticles for self-healing materials,” *Polym. Chem.*, vol. 4, no. 18, pp. 4885–4889, 2013.

[73] H. Zhang, P. F. Wang, and J. L. Yang, “Self-healing epoxy via epoxy-amine chemistry in dual hollow glass bubbles,” *Compos. Sci. Technol.*, vol. 94, pp. 23–29, 2014.

[74] H. Zhang and J. L. Yang, “Etched glass bubbles as robust micro-containers for self-healing materials,” *J. Mater. Chem. A*, vol. 1, no. 41, pp. 12715–12720, 2013.

[75] H. H. Jin, C. L. Mangun, A. S. Griffin, J. S. Moore, N. R. Sottos, and S. R. White, “Thermally Stable Autonomic Healing in Epoxy using a Dual-Microcapsule System,” *Adv. Mater.*, vol. 26, no. 2, pp. 282–287, 2014.

[76] N. V Jyothi, P. M. Prasanna, S. N. Sakarkar, K. S. Prabha, P. S. Ramaiah, and G. Y. Srawan, “Microencapsulation techniques, factors influencing encapsulation efficiency,” *J Microencapsul*, vol. 27, no. 3, pp. 187–197, 2010.

[77] L. Zhang, X. P. Dong, and H. Chen, “Study on the Effects of the Self-healing Microcapsules on the Tensile Properties of Polymer Composite,” *Mater. Manuf. Pts 1 2*, vol. 299–300, pp. 460–465, 2011.

[78] E. N. Brown, S. R. White, and N. R. Sottos, “Microcapsule induced toughening in a self-healing polymer composite,” *J. Mater. Sci.*, vol. 39, no. 5, pp. 1703–1710, 2004.

[79] J. Zhang, C. H. Wang, H. Niu, A. Gestos, T. Lin, and X. Wang, “Thermally mendable epoxy resin strengthened with carbon nanofibres,” *Compos. Part A Appl. Sci. Manuf.*, vol. 55, pp. 45–52, 2013.

[80] C. Uchijo, Y. Kuroda, K. Kemmochi, and L. M. Bao, “Research on FRP composite structures with self-healing function - Effect of Filler on FRP interlaminar fracture toughness -,” *Adv. Text. Mater. Pts 1-3*, vol. 332–334, pp. 31–34, 2011.

[81] C. Chen, H. W. Ji, and H. W. Wang, “Damage Properties Simulations of Self-Healing Composites,” *J. Nanosci. Nanotechnol.*, vol. 13, no. 10, pp. 6679–6686, 2013.

[82] M. Tripathi, Rahamtullah, D. Kumar, C. Rajagopal, and P. K. Roy, “Influence of Microcapsule Shell Material on the Mechanical Behavior of Epoxy Composites for Self-Healing Applications,” *J. Appl. Polym. Sci.*, vol. 131, no. 15, 2014.

[83] E. N. Brown, N. R. Sottos, and S. R. White, “Fracture testing of a self-healing polymer composite,” *Exp. Mech.*, vol. 42, no. 4, pp. 372–379, 2002.

[84] E. N. Brown, S. R. White, and N. R. Sottos, “Fatigue crack propagation in microcapsule-toughened epoxy,” *J. Mater. Sci.*, vol. 41, no. 19, pp. 6266–6273, 2006.

[85] J. D. Rule, N. R. Sottos, and S. R. White, “Effect of microcapsule size on the performance of self-healing polymers,” *Polymer (Guildf).*, vol. 48, no. 12, pp. 3520–3529, 2007.

[86] G. O. Wilson, J. S. Moore, S. R. White, N. R. Sottos, and H. M. Andersson, “Autonomic healing of epoxy vinyl esters via ring opening metathesis polymerization,” *Adv. Funct. Mater.*, vol. 18, no. 1, pp. 44–52, 2008.

[87] J. L. Moll, S. R. White, and N. R. Sottos, “A Self-sealing Fiber-reinforced Composite,” *J. Compos. Mater.*, vol. 44, no. 22, pp. 2573–2585, 2010.

[88] A. J. Patel, N. R. Sottos, E. D. Wetzel, and S. R. White, “Autonomic healing of low-velocity impact damage in fiber-reinforced composites,” *Compos. Part a-Applied Sci. Manuf.*, vol. 41, no. 3, pp. 360–368, 2010.

[89] H. Y. Li, R. G. Wang, and W. B. Liu, “Preparation and self-healing performance of epoxy composites with microcapsules and tungsten (VI) chloride catalyst,” *J. Reinf. Plast. Compos.*, vol. 31, no. 13, pp. 924–932, 2012.

[90] T. Yin, M. Z. Rong, and M. Q. Zhang, “Self-healing of cracks in epoxy composites,” *Multi-Functional Mater. Struct. Pts 1 2*, vol. 47–50, pp. 282–285, 2008.

[91] S. C. Li, P. Han, and H. P. Xu, “Self-Healing Polymeric Materials,” *Prog. Chem.*, vol. 24, no. 7, pp. 1346–1352, 2012.

[92] C. Dry, “Procedures developed for self-repair of polymer matrix composite materials,” *Compos. Struct.*, vol. 35, no. 3, pp. 263–269, 1996.

[93] C. Dry and W. McMillan, “Three-part methylmethacrylate adhesive system as an internal delivery system for smart responsive concrete,” *Smart Mater. Struct.*, vol. 5, no. 3, pp. 297–300, 1996.

[94] C. Dry and N. R. Sottos, “Passive Smart Self-Repair in Polymer Matrix Composite-Materials,” *Smart Mater.*, vol. 1916, pp. 438–444, 1993.

[95] S. M. Bleay, C. B. Loader, V. J. Hawyes, L. Humberstone, and P. T. Curtis, “A smart repair system for polymer matrix composites,” *Compos. Part a-Applied Sci. Manuf.*, vol. 32, no. 12, pp. 1767–1776, 2001.

[96] J. W. C. Pang and I. P. Bond, “A hollow fibre reinforced polymer composite encompassing self-healing and enhanced damage visibility,” *Compos. Sci. Technol.*, vol. 65, no. 11–12, pp. 1791–1799, 2005.

[97] J. W. C. Pang and I. P. Bond, "'Bleeding composites'—damage detection and self-repair using a biomimetic approach," *Compos. Part A Appl. Sci. Manuf.*, vol. 36, no. 2, pp. 183–188, 2005.

[98] K. S. Toohey, N. R. Sottos, J. A. Lewis, J. S. Moore, and S. R. White, "Self-healing materials with microvascular networks," *Nat Mater*, vol. 6, no. 8, pp. 581–585, 2007.

[99] R. S. Trask and I. P. Bond, "Biomimetic self-healing of advanced composite structures using hollow glass fibres," *Smart Mater. Struct.*, vol. 15, no. 3, pp. 704–710, 2006.

[100] H. R. Williams, R. S. Trask, and I. P. Bond, "Self-healing composite sandwich structures," *Smart Mater. Struct.*, vol. 16, no. 4, pp. 1198–1207, 2007.

[101] K. S. Toohey, C. J. Hansen, J. A. Lewis, S. R. White, and N. R. Sottos, "Delivery of Two-Part Self-Healing Chemistry via Microvascular Networks," *Adv. Funct. Mater.*, vol. 19, no. 9, pp. 1399–1405, 2009.

[102] H. R. Williams, R. S. Trask, and I. P. Bond, "Self-healing sandwich panels: Restoration of compressive strength after impact," *Compos. Sci. Technol.*, vol. 68, no. 15–16, pp. 3171–3177, 2008.

[103] M. Nademi, A. Mozaffari, and A. Farrokhabadi, "A New Self Healing Method in Composite Laminates Using the Hollow Glass Fiber," *Compos. Sci. Technol. Pts 1 2*, vol. 471–472, pp. 548–551, 2011.

[104] C. Chen, K. Peters, and Y. Li, "Self-healing sandwich structures incorporating an interfacial layer with vascular network," *Smart Mater. Struct.*, vol. 22, no. 2, p. 25031, 2013.

[105] J. F. Patrick, N. R. Sottos, and S. R. White, "Microvascular based self-healing polymeric foam," *Polymer (Guildf).*, vol. 53, no. 19, pp. 4231–4240, 2012.

[106] A. R. Hamilton, N. R. Sottos, and S. R. White, "Mitigation of fatigue damage in self-healing vascular materials," *Polymer (Guildf).*, vol. 53, no. 24, pp. 5575–5581, 2012.

[107] K. S. Toohey, N. R. Sottos, and S. R. White, "Characterization of Microvascular-Based Self-healing Coatings," *Exp. Mech.*, vol. 49, no. 5, pp. 707–717, 2009.

[108] C. Joseph, A. D. Jefferson, B. Isaacs, R. Lark, and D. Gardner, "Experimental investigation of adhesive-based self-healing of cementitious materials," *Mag. Concr. Res.*, vol. 62, no. 11, pp. 831–843, 2010.

[109] V. C. Li, Y. M. Lim, and Y. W. Chan, "Feasibility study of a passive smart self-healing cementitious composite," *Compos. Part B-Engineering*, vol. 29, no. 6, pp. 819–827, 1998.

[110] C. J. Norris, I. P. Bond, and R. S. Trask, "Healing of low-velocity impact damage in vascularised composites," *Compos. Part a-Applied Sci. Manuf.*, vol. 44, pp. 78–85, 2013.

[111] A. R. Hamilton, N. R. Sottos, and S. R. White, "Pressurized vascular systems for

self- healing materials," *J. R. Soc. Interface*, vol. 9, no. 70, pp. 1020–1028, 2012.

[112] D. Therriault, S. R. White, and J. A. Lewis, "Chaotic mixing in three-dimensional microvascular networks fabricated by direct-write assembly," *Nat Mater*, vol. 2, no. 4, pp. 265–271, 2003.

[113] J. A. Lewis and G. M. Gratson, "Direct writing in three dimensions," *Mater. Today*, vol. 7, no. 7–8, pp. 32–39, 2004.

[114] S. Z. Guo, F. Gosselin, N. Guerin, A. M. Lanouette, M. C. Heuzey, and D. Therriault, "Solvent-Cast Three-Dimensional Printing of Multifunctional Microsystems," *Small*, vol. 9, no. 24, pp. 4118–4122, 2013.

[115] H. D. Dong, A. P. Esser-Kahn, P. R. Thakre, J. F. Patrick, N. R. Sottos, S. R. White, and J. S. Moore, "Chemical Treatment of Poly(lactic acid) Fibers to Enhance the Rate of Thermal Depolymerization," *ACS Appl. Mater. Interfaces*, vol. 4, no. 2, pp. 503–509, 2012.

[116] R. C. R. Gergely, S. J. Pety, B. P. Krull, J. F. Patrick, T. Q. Doan, A. M. Coppola, P. R. Thakre, N. R. Sottos, J. S. Moore, and S. R. White, "Multidimensional Vascularized Polymers using Degradable Sacrificial Templates," *Adv. Funct. Mater.*, p. n/a–n/a, 2014.

[117] W. Wu, A. DeConinck, and J. A. Lewis, "Omnidirectional Printing of 3D Microvascular Networks," *Adv. Mater.*, vol. 23, no. 24, pp. H178–H183, 2011.

[118] W. Wu, C. J. Hansen, A. M. Aragon, P. H. Geubelle, S. R. White, and J. A. Lewis, "Direct-write assembly of biomimetic microvascular networks for efficient fluid transport," *Soft Matter*, vol. 6, no. 4, pp. 739–742, 2010.

[119] C. J. Hansen, R. Saksena, D. B. Kolesky, J. J. Vericella, S. J. Kranz, G. P. Muldowney, K. T. Christensen, and J. A. Lewis, "High-Throughput Printing via Microvascular Multinozzle Arrays," *Adv. Mater.*, vol. 25, no. 1, pp. 96–102, 2013.

[120] S. C. Olugebefola, A. R. Hamilton, D. J. Fairfield, N. R. Sottos, and S. R. White, "Structural reinforcement of microvascular networks using electrostatic layer-by-layer assembly with halloysite nanotubes," *Soft Matter*, vol. 10, no. 4, pp. 544–548, 2014.

[121] A. J. Jacobsen, J. A. Kolodziejska, R. Doty, K. D. Fink, C. Zhou, C. S. Roper, and W. B. Carter, "Interconnected self-propagating photopolymer waveguides: An alternative to stereolithography for rapid formation of lattice-based open-cellular materials," *Twenty-First Annu. Int. Solid Free. Fabr. Symp. Austin, TX*, 2010.

[122] A. J. Jacobsen, W. Barvosa-Carter, and S. Nutt, "Micro-scale Truss Structures formed from Self-Propagating Photopolymer Waveguides," *Adv. Mater.*, vol. 19, no. 22, pp. 3892–3896, 2007.

[123] T. A. Schaedler, A. J. Jacobsen, A. Torrents, A. E. Sorensen, J. Lian, J. R. Greer, L. Valdevit, and W. B. Carter, "Ultralight metallic microlattices," *Science (80-.).*, vol. 334, no. 6058, pp. 962–965, 2011.

[124] C. S. Roper, R. C. Schubert, K. J. Maloney, D. Page, C. J. Ro, S. S. Yang, and A. J.

Jacobsen, “Scalable 3D Bicontinuous Fluid Networks: Polymer Heat Exchangers Toward Artificial Organs,” *Adv. Mater.*, p. n/a–n/a, 2015.

[125] L. M. Bellan, S. P. Singh, P. W. Henderson, T. J. Porri, H. G. Craighead, and J. A. Spector, “Fabrication of an artificial 3-dimensional vascular network using sacrificial sugar structures,” *Soft Matter*, vol. 5, no. 7, pp. 1354–1357, 2009.

[126] C. Gualandi, A. Zucchelli, M. F. Osorio, J. Belcari, and M. L. Focarete, “Nanovascularization of Polymer Matrix: Generation of Nanochannels and Nanotubes by Sacrificial Electrospun fibers,” *Nano Lett.*, vol. 13, no. 11, pp. 5385–5390, 2013.

[127] X. F. Wu, A. Rahman, Z. P. Zhou, D. D. Pelot, S. Sinha-Ray, B. Chen, S. Payne, and A. L. Yarin, “Electrospinning core-shell nanofibers for interfacial toughening and self-healing of carbon-fiber/epoxy composites,” *J. Appl. Polym. Sci.*, vol. 129, no. 3, pp. 1383–1393, 2013.

[128] A. M. Coppola, P. R. Thakre, N. R. Sottos, and S. R. White, “Tensile properties and damage evolution in vascular 3D woven glass/epoxy composites,” *Compos. Part a-Applied Sci. Manuf.*, vol. 59, pp. 9–17, 2014.

[129] L. M. Bellan, M. Pearsall, D. M. Cropek, and R. Langer, “A 3D Interconnected Microchannel Network Formed in Gelatin by Sacrificial Shellac Microfibers,” *Adv. Mater.*, vol. 24, no. 38, pp. 5187–5191, 2012.

[130] A. P. Esser-Kahn, P. R. Thakre, H. Dong, J. F. Patrick, V. K. Vlasko-Vlasov, N. R. Sottos, J. S. Moore, and S. R. White, “Three-dimensional microvascular fiber-reinforced composites,” *Adv Mater*, vol. 23, no. 32, pp. 3654–3658, 2011.

[131] N. W. Choi, M. Cabodi, B. Held, J. P. Gleghorn, L. J. Bonassar, and A. D. Stroock, “Microfluidic scaffolds for tissue engineering,” *Nat Mater*, vol. 6, no. 11, pp. 908–915, 2007.

[132] A. P. Golden and J. Tien, “Fabrication of microfluidic hydrogels using molded gelatin as a sacrificial element,” *Lab Chip*, vol. 7, no. 6, pp. 720–725, 2007.

[133] J. K. He, M. Mao, Y. X. Liu, J. Y. Shao, Z. M. Jin, and D. C. Li, “Fabrication of Nature-Inspired Microfluidic Network for Perfusable Tissue Constructs,” *Adv. Healthc. Mater.*, vol. 2, no. 8, pp. 1108–1113, 2013.

[134] L. M. Bellan, T. Kniazeva, E. S. Kim, A. A. Epshteyn, D. M. Cropek, R. Langer, and J. T. Borenstein, “Fabrication of a Hybrid Microfluidic System Incorporating both Lithographically Patterned Microchannels and a 3D Fiber-Formed Microfluidic Network,” *Adv. Healthc. Mater.*, vol. 1, no. 2, pp. 164–167, 2012.

[135] J.-H. Huang, J. Kim, N. Agrawal, A. P. Sudarsan, J. E. Maxim, A. Jayaraman, and V. M. Ugaz, “Rapid Fabrication of Bio-inspired 3D Microfluidic Vascular Networks,” *Adv. Mater.*, vol. 21, no. 35, pp. 3567–3571, 2009.

[136] D. Lim, Y. Kamotani, B. Cho, J. Mazumder, and S. Takayama, “Fabrication of microfluidic mixers and artificial vasculatures using a high-brightness diode-pumped

Nd : YAG laser direct write method," *Lab Chip*, vol. 3, no. 4, pp. 318–323, 2003.

[137] F. Zhou, C. H. Wang, and A. P. Mouritz, "Computational Analysis of the Structural Integrity of Self-Healing Composites," *Mater. Sci. Forum*, vol. 654–656, pp. 2576–2578, Jun. 2010.

[138] A. Kousourakis and A. P. Mouritz, "The effect of self-healing hollow fibres on the mechanical properties of polymer composites," *Smart Mater. Struct.*, vol. 19, no. 8, 2010.

[139] A. T. T. Nguyen and A. C. Orifici, "Structural assessment of microvascular self-healing laminates using progressive damage finite element analysis," *Compos. Part a-Applied Sci. Manuf.*, vol. 43, no. 11, pp. 1886–1894, 2012.

[140] C. J. Norris, I. P. Bond, and R. S. Trask, "Interactions between propagating cracks and bioinspired self-healing vascules embedded in glass fibre reinforced composites," *Compos. Sci. Technol.*, vol. 71, no. 6, pp. 847–853, 2011.

[141] C. Y. Huang, R. S. Trask, and I. P. Bond, "Characterization and analysis of carbon fibre-reinforced polymer composite laminates with embedded circular vasculature," *J. R. Soc. Interface*, vol. 7, no. 49, pp. 1229–1241, 2010.

[142] C. J. Hansen, W. Wu, K. S. Toohey, N. R. Sottos, S. R. White, and J. A. Lewis, "Self-Healing Materials with Interpenetrating Microvascular Networks," *Adv. Mater.*, vol. 21, no. 41, p. 4143–+, 2009.

[143] C. J. Hansen, S. R. White, N. R. Sottos, and J. A. Lewis, "Accelerated Self-Healing Via Ternary Interpenetrating Microvascular Networks," *Adv. Funct. Mater.*, vol. 21, no. 22, pp. 4320–4326, 2011.

[144] C. J. Norris, G. J. Meadway, M. J. O'Sullivan, I. P. Bond, and R. S. Trask, "Self-Healing Fibre Reinforced Composites via a Bioinspired Vasculature," *Adv. Funct. Mater.*, vol. 21, no. 19, pp. 3624–3633, 2011.

[145] C. J. Norris, J. A. P. White, G. McCombe, P. Chatterjee, I. P. Bond, and R. S. Trask, "Autonomous stimulus triggered self-healing in smart structural composites," *Smart Mater. Struct.*, vol. 21, no. 9, 2012.

[146] K. H. Cho, J. Lee, M. H. Kim, and A. Bejan, "Vascular design of constructal structures with low flow resistance and nonuniformity," *Int. J. Therm. Sci.*, vol. 49, no. 12, pp. 2309–2318, 2010.

[147] A. M. Aragón, R. Saksena, B. D. Kozola, P. H. Geubelle, K. T. Christensen, and S. R. White, "Multi-physics optimization of three-dimensional microvascular polymeric components," *J. Comput. Phys.*, vol. 233, pp. 132–147, 2013.

[148] A. Bejan and S. Lorente, "Vascularized multi-functional materials and structures," *Multi-Functional Mater. Struct. Pts 1 2*, vol. 47–50, pp. 511–514, 2008.

[149] A. Bejan, S. Lorente, and K. M. Wang, "Networks of channels for self-healing composite materials," *J. Appl. Phys.*, vol. 100, no. 3, p. 33528, 2006.

[150] S. Lorente and A. Bejan, “Vascularized smart materials: Designed porous media for self-healing and self-cooling,” *J. Porous Media*, vol. 12, no. 1, pp. 1–18, 2009.

[151] H. T. Chu, Z. C. Zhang, Y. J. Liu, and J. S. Leng, “Self-heating fiber reinforced polymer composite using meso/macropore carbon nanotube paper and its application in deicing,” *Carbon N. Y.*, vol. 66, pp. 154–163, 2014.

[152] B. C. Fehrman and U. A. Korde, “Targeted delivery of acoustic energy for self-healing,” *J. Intell. Mater. Syst. Struct.*, vol. 24, no. 15, pp. 1865–1887, 2013.

[153] C. A. Galindez-Jamioy and J. M. López-Higuera, “Brillouin Distributed Fiber Sensors: An Overview and Applications,” *J. Sensors*, vol. 2012, pp. 1–17, 2012.

[154] H. C.-S. Ju-Hyung Yun Joondong Kim, Jin-Won Song, Dong-Hun Shin, and Young-Geun Park, “Fabrication of Carbon Nanotube Sensor Device by Inkjet Printing ,” *Proc. 3rd IEEE Int. Conf. Nano/Micro Eng. Mol. Syst. January 6-9, 2008, Sanya, China*, 2014.

[155] E. T. Thostenson and T. W. Chou, “Carbon Nanotube Networks: Sensing of Distributed Strain and Damage for Life Prediction and Self Healing,” *Adv. Mater.*, vol. 18, no. 21, pp. 2837–2841, 2006.

[156] Z. Ranachowski, D. Jozwiak-Niedzwiedzka, A. M. Brandt, and T. Debowski, “Application of Acoustic Emission Method to Determine Critical Stress in Fibre Reinforced Mortar Beams,” *Arch. Acoust.*, vol. 37, no. 3, pp. 261–268, 2012.

[157] E. Kirkby, R. de Oliveira, V. Michaud, and J. A. Manson, “Impact localisation with FBG for a self-healing carbon fibre composite structure,” *Compos. Struct.*, vol. 94, no. 1, pp. 8–14, 2011.

[158] R. S. Trask, C. J. Norris, and I. P. Bond, “Stimuli-triggered self-healing functionality in advanced fibre-reinforced composites,” *J. Intell. Mater. Syst. Struct.*, vol. 25, no. 1, pp. 87–97, 2014.

[159] Y. Hong and M. Su, “Multifunctional Self-Healing and Self-Reporting Polymer Composite with Integrated Conductive Microwire Networks,” *ACS Appl. Mater. Interfaces*, vol. 4, no. 7, pp. 3759–3764, 2012.

[160] C. Knipprath, G. P. McCombe, R. S. Trask, and I. P. Bond, “Predicting self-healing strength recovery using a multi-objective genetic algorithm,” *Compos. Sci. Technol.*, vol. 72, no. 6, pp. 752–759, 2012.

[161] R. S. Trask, G. J. Williams, and I. P. Bond, “Bioinspired self-healing of advanced composite structures using hollow glass fibres,” *J. R. Soc. Interface*, vol. 4, no. 13, pp. 363–371, 2007.

[162] G. J. Williams, I. P. Bond, and R. S. Trask, “Compression after impact assessment of self-healing CFRP,” *Compos. Part a-Applied Sci. Manuf.*, vol. 40, no. 9, pp. 1399–1406, 2009.

[163] A. M. Coppola, A. S. Griffin, N. R. Sottos, and S. R. White, “Retention of mechanical performance of polymer matrix composites above the glass transition temperature

by vascular cooling," *Compos. Part A Appl. Sci. Manuf.*, vol. 78, pp. 412–423, 2015.

[164] M. Schunack, M. Gragert, D. Döhler, P. Michael, and W. H. Binder, "Low-Temperature Cu(I)-Catalyzed 'Click' Reactions for Self-Healing Polymers," *Macromol. Chem. Phys.*, vol. 213, no. 2, pp. 205–214, 2012.

[165] X. K. D. Hillewaere and F. E. Du Prez, "Fifteen Chemistries for Autonomous External Self-Healing Polymers and Composites," *Prog. Polym. Sci.*, no. 0, 2015.

[166] M. Raimondo, P. Longo, A. Mariconda, and L. Guadagno, "Healing agent for the activation of self-healing function at low temperature," *Adv. Compos. Mater.*, pp. 1–11, 2014.

[167] D. Liu, Z. Yang, P. Wang, F. Li, D. Wang, and D. He, "Preparation of 3D nanoporous copper-supported cuprous oxide for high-performance lithium ion battery anodes," *Nanoscale*, vol. 5, no. 5, pp. 1917–1921, 2013.

[168] J. Xu, X. Ji, W. Zhang, and G. Liu, "Pool boiling heat transfer of ultra-light copper foam with open cells," *Int. J. Multiph. Flow*, vol. 34, no. 11, pp. 1008–1022, 2008.

[169] Z. Xie, T. Ikeda, Y. Okuda, and H. Nakajima, "Sound absorption characteristics of lotus-type porous copper fabricated by unidirectional solidification," *Mater. Sci. Eng. A*, vol. 386, no. 1, pp. 390–395, 2004.

[170] W. Ding, S. Pengcheng, L. Changhong, W. Wei, and F. Shoushan, "Highly oriented carbon nanotube papers made of aligned carbon nanotubes," *Nanotechnology*, vol. 19, no. 7, p. 75609, 2008.

[171] S. Hashemi, A. J. Kinloch, and J. G. Williams, "Corrections needed in double-cantilever beam tests for assessing the interlaminar failure of fibre-composites," *J. Mater. Sci. Lett.*, vol. 8, no. 2, pp. 125–129, 1989.

[172] A. M. Aragon, C. J. Hansen, W. Wu, P. H. Geubelle, J. Lewis, and S. R. White, "Computational design and optimization of a biomimetic self-healing/cooling material - art. no. 65261G," *Behav. Mech. Multifunct. Compos. Mater. 2007*, vol. 6526, pp. G5261–G5261, 2007.

[173] S. Soghrati, A. M. Aragon, and P. H. Geubelle, "Design of actively-cooled microvascular materials: a genetic algorithm inspired network optimization," *Struct. Multidiscip. Optim.*, vol. 49, no. 4, pp. 643–655, 2014.

[174] E. Cetkin, S. Lorente, and A. Bejan, "Vascularization for cooling and mechanical strength," *Int. J. Heat Mass Transf.*, vol. 54, no. 13–14, pp. 2774–2781, 2011.

[175] H. Fukuda and T.-W. Chou, "A probabilistic theory of the strength of short-fibre composites with variable fibre length and orientation," *J. Mater. Sci.*, vol. 17, no. 4, pp. 1003–1011, 1982.

[176] J. A. Nairn, "Generalized Shear-Lag Analysis Including Imperfect Interfaces," *Adv. Comp. Letts*, 2005.

[177] S. U. Khan, J. R. Pothnis, and J.-K. Kim, "Effects of carbon nanotube alignment on

electrical and mechanical properties of epoxy nanocomposites," *Compos. Part A Appl. Sci. Manuf.*, vol. 49, pp. 26–34, 2013.

[178] S. Wu, R. B. Ladani, J. Zhang, E. Bafekrpour, K. Ghorbani, A. P. Mouritz, A. J. Kinloch, and C. H. Wang, "Aligning multilayer graphene flakes with an external electric field to improve multifunctional properties of epoxy nanocomposites," *Carbon N. Y.*, vol. 94, pp. 607–618, 2015.

[179] R. B. Ladani, S. Wu, A. J. Kinloch, K. Ghorbani, J. Zhang, A. P. Mouritz, and C. H. Wang, "Improving the toughness and electrical conductivity of epoxy nanocomposites by using aligned carbon nanofibres," *Compos. Sci. Technol.*, vol. 117, pp. 146–158, 2015.

[180] S. A. Odom, T. P. Tyler, M. M. Caruso, J. A. Ritchey, M. V Schulmerich, S. J. Robinson, R. Bhargava, N. R. Sottos, S. R. White, M. C. Hersam, and J. S. Moore, "Autonomic restoration of electrical conductivity using polymer-stabilized carbon nanotube and graphene microcapsules," *Appl. Phys. Lett.*, vol. 101, no. 4, p. 43106, 2012.

[181] B. J. Blaiszik, S. L. B. Kramer, M. E. Grady, D. A. McIlroy, J. S. Moore, N. R. Sottos, and S. R. White, "Autonomic Restoration of Electrical Conductivity," *Adv. Mater.*, vol. 24, no. 3, pp. 398–401, Jan. 2012.

[182] R. F. Gibson, "A review of recent research on mechanics of multifunctional composite materials and structures," *Compos. Struct.*, vol. 92, no. 12, pp. 2793–2810, 2010.

[183] S. Tadigadapa and K. Mateti, "Piezoelectric MEMS sensors: state-of-the-art and perspectives," *Meas. Sci. Technol.*, vol. 20, no. 9, p. 092001, Sep. 2009.

[184] Y. Lin and H. A. Sodano, "Fabrication and Electromechanical Characterization of a Piezoelectric Structural Fiber for Multifunctional Composites," *Adv. Funct. Mater.*, vol. 19, no. 4, pp. 592–598, Feb. 2009.

[185] D. D. . Chung, "Electromagnetic interference shielding effectiveness of carbon materials," *Carbon N. Y.*, vol. 39, no. 2, pp. 279–285, 2001.

[186] K. A. Williams, A. J. Boydston, and C. W. Bielawski, "Towards electrically conductive, self-healing materials.," *J. R. Soc. Interface*, vol. 4, no. 13, pp. 359–62, Apr. 2007.

[187] K. Guo, D.-L. Zhang, X.-M. Zhang, J. Zhang, L.-S. Ding, B.-J. Li, and S. Zhang, "Conductive Elastomers with Autonomic Self-Healing Properties," *Angew. Chemie*, p. n/a–n/a, 2015.

[188] S. A. Odom, S. Chayanupatkul, B. J. Blaiszik, O. Zhao, A. C. Jackson, P. V Braun, N. R. Sottos, S. R. White, and J. S. Moore, "A Self-healing Conductive Ink," *Adv. Mater.*, vol. 24, no. 19, pp. 2578–2581, 2012.

[189] Y. Wang, D. T. Pham, Z. Zhang, J. Li, C. Ji, Y. Liu, and J. Leng, "Sustainable Self-healing at Ultra-low Temperatures in Structural Composites Incorporating Hollow Vessels and Conductive Sheets," vol: 3, no. 9, pp.160488, 2016.

[190] Z. C. Zhang, H. T. Chu, K. W. Wang, Y. J. Liu, and J. S. Leng, “Multifunctional Carbon Nano-paper Composite,” *Fourth Int. Conf. Smart Mater. Nanotechnol. Eng.*, vol. 8793, 2013.

[191] Z. Zhang, H. Wei, Y. Liu, and J. Leng, “Self-sensing properties of smart composite based on embedded buckypaper layer,” *Struct. Heal. Monit.*, 2015.

[192] C. Park, J. Wilkinson, S. Banda, Z. Ounaies, K. E. Wise, G. Sauti, P. T. Lillehei, and J. S. Harrison, “Aligned single-wall carbon nanotube polymer composites using an electric field,” *J. Polym. Sci. Part B Polym. Phys.*, vol. 44, no. 12, pp. 1751–1762, Jun. 2006.